Spatial distribution of defects in ultra fine grained metals prepared by high pressure torsion

J. Čížek, O. Melikhova, I. Procházka, M. Janeček, P. Hruška

Faculty of Mathematics and Physics, Charles University Prague, Czech Republic

R. K. Islamgaliev

Institute of Physics of Advanced Materials, Ufa State Aviation Technical University, Ufa, Russia

S.V. Dobatkin

A. A. Baikov Institute of Metallurgy and Materials Science, Russian Academy of Sciences, Moscow, Russia

Ultra fine grained (UFG) materials

polycrystalline material

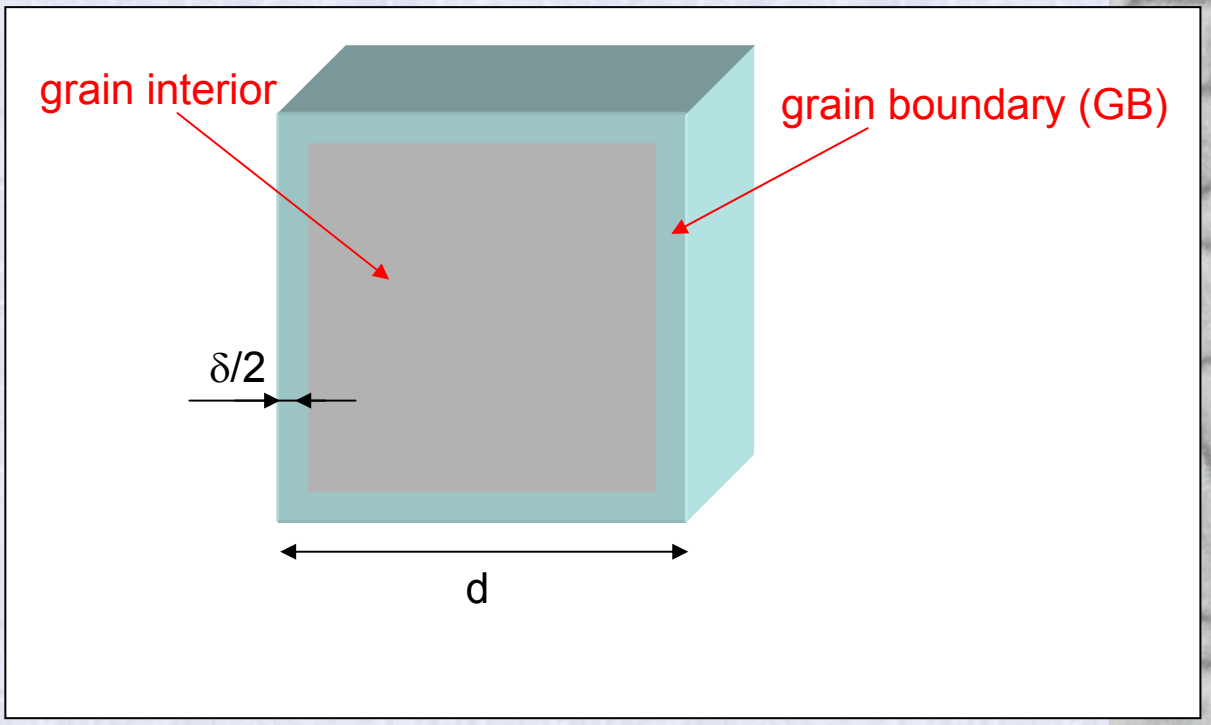

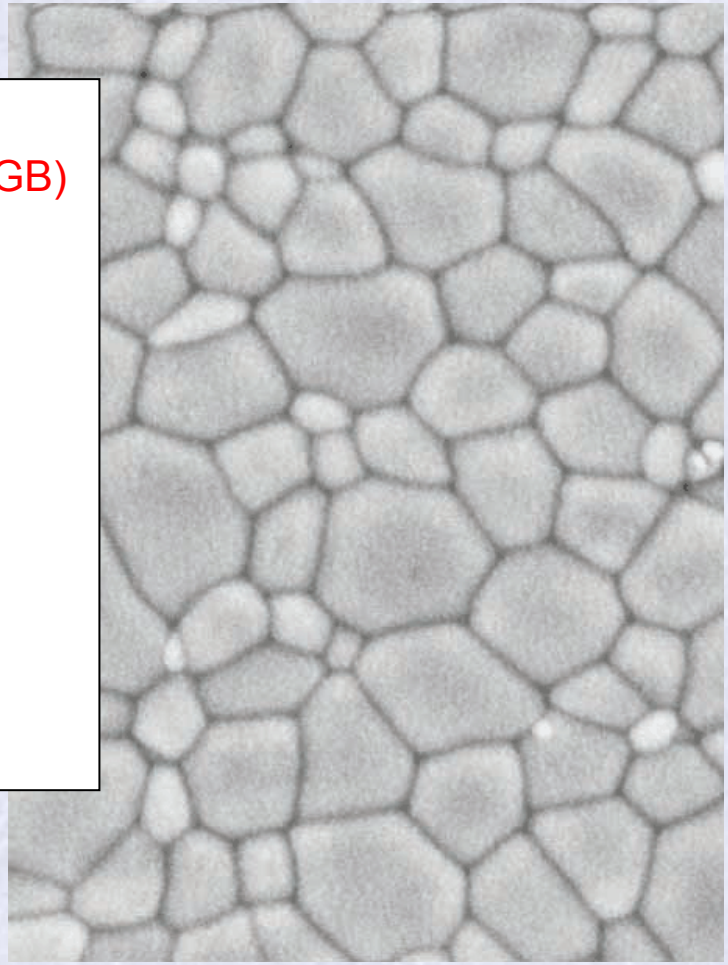

volume fraction of GB's

$$f_{GB} = 1 - \left(\frac{d - \delta}{d} \right)^3$$

Ultra fine grained (UFG) materials

polycrystalline material

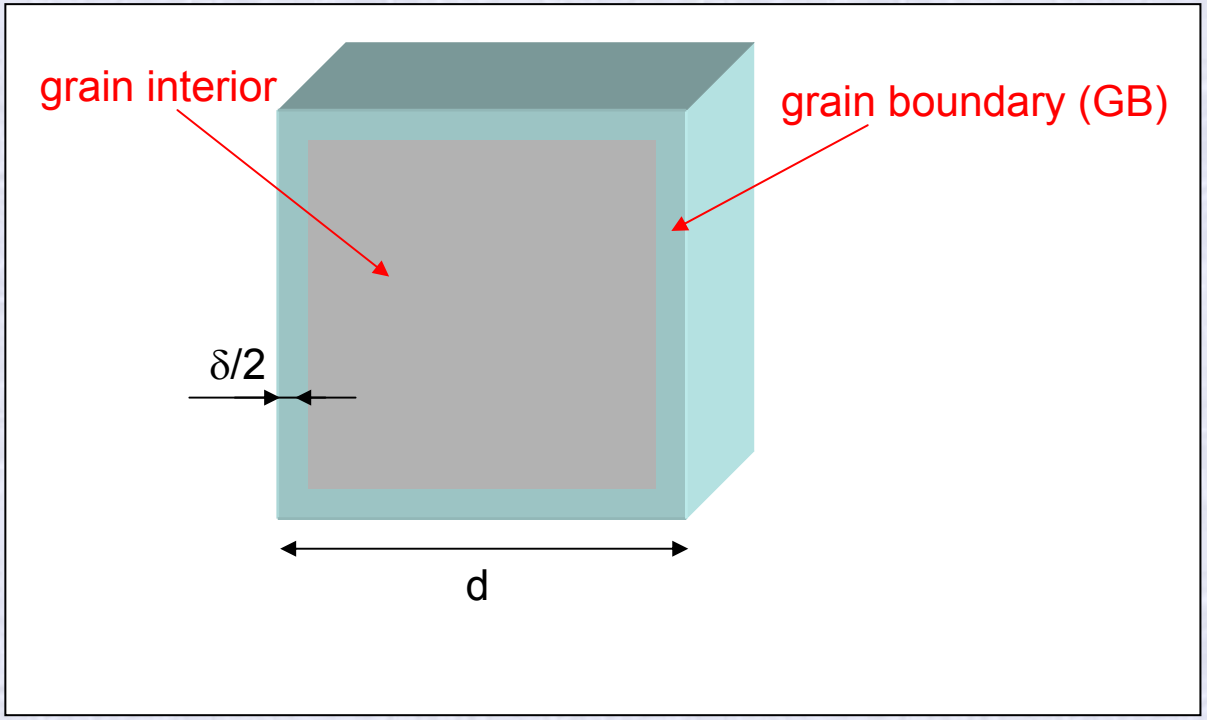

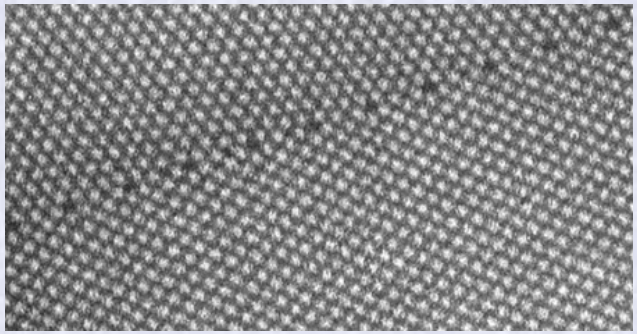

crystallographic width of GB's: $\delta \approx 1$ nm

volume fraction of GB's

$$f_{GB} = 1 - \left(\frac{d - \delta}{d} \right)^3$$

Ultra fine grained (UFG) materials

polycrystalline material

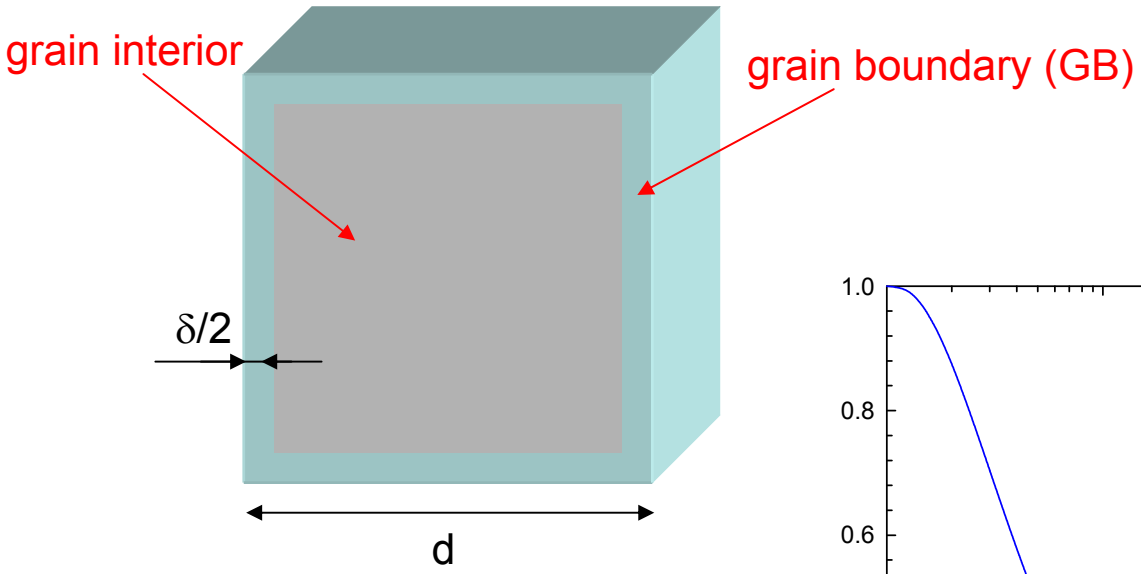

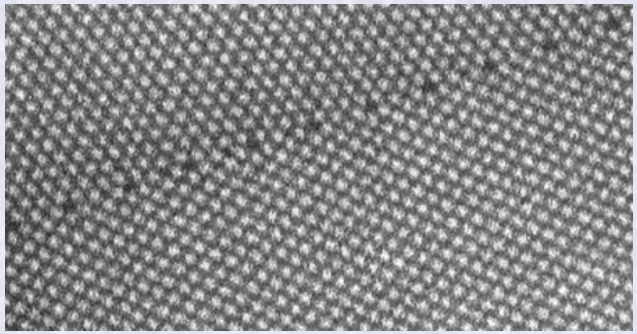

crystallographic width of GB's: $\delta \approx 1$ nm

volume fraction of GB's

$$f_{GB} = 1 - \left(\frac{d - \delta}{d} \right)^3$$

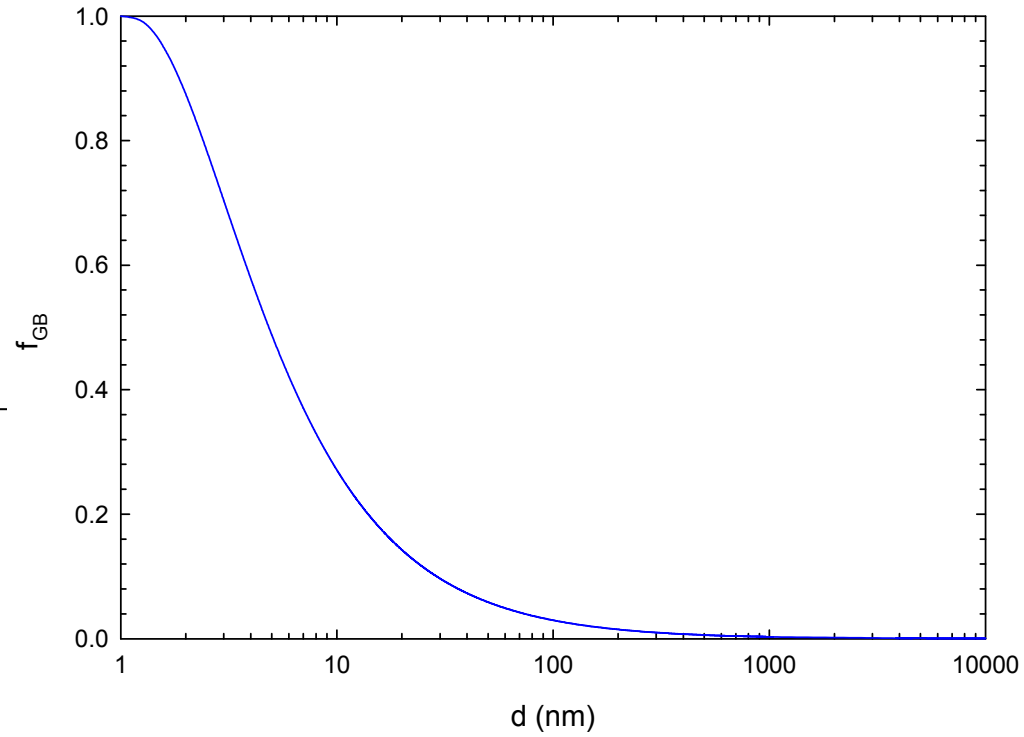

Ultra fine grained (UFG) materials

polycrystalline material

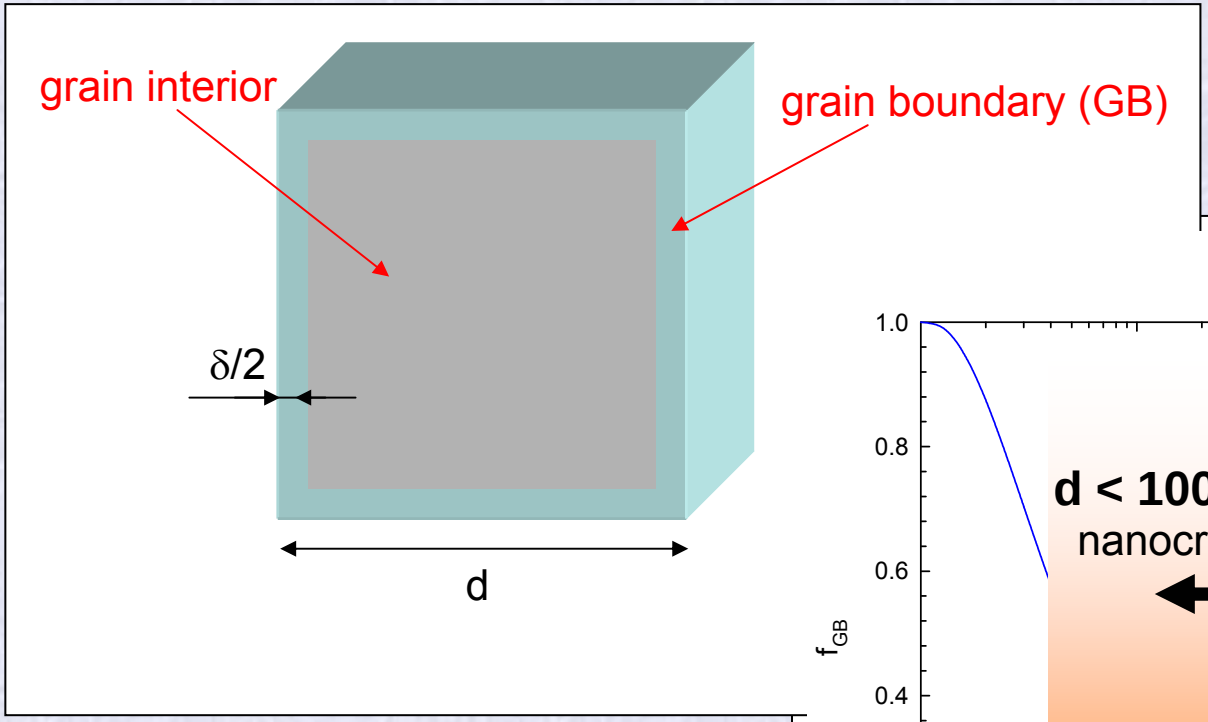

crystallographic width of GB's: $\delta \approx 1$ nm

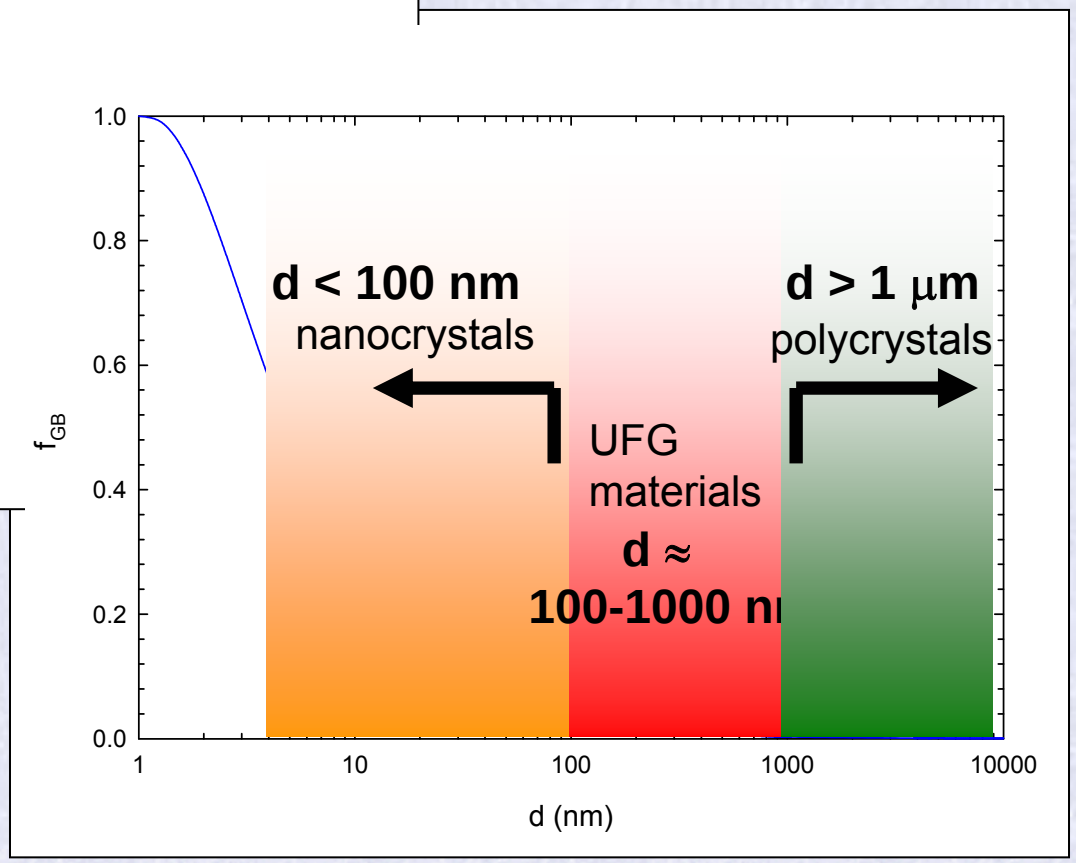

volume fraction of GB's

$$f_{GB} = 1 - \left(\frac{d - \delta}{d} \right)^3$$

Introduction

Severe plastic deformation

- very strong grain size reduction → down to nanoscale (~ 100 nm)
- conventional plastic deformation

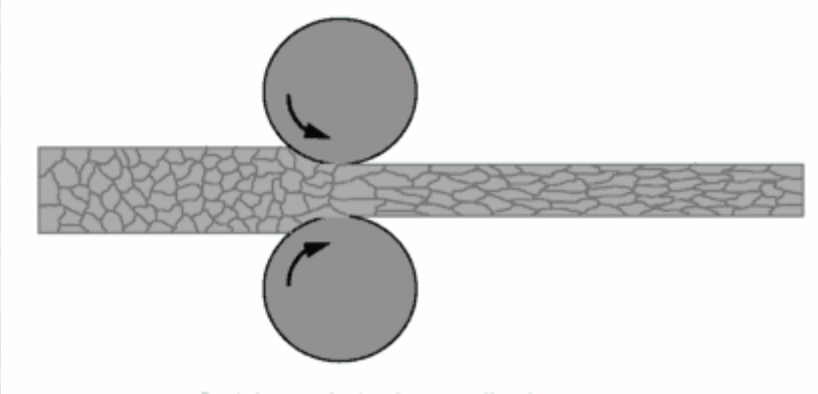

Introduction

Severe plastic deformation

- very strong grain size reduction → down to nanoscale (~ 100 nm)
- conventional plastic deformation → formation of cracks

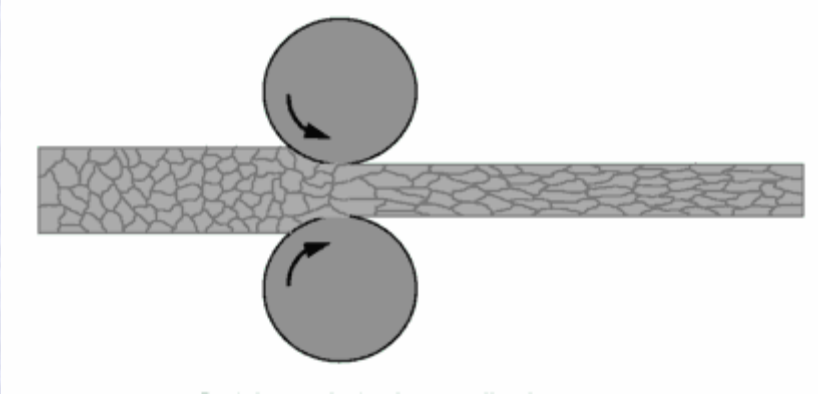

Introduction

Severe plastic deformation

- very strong grain size reduction → down to nanoscale (~ 100 nm)
- conventional plastic deformation → formation of cracks → material failure

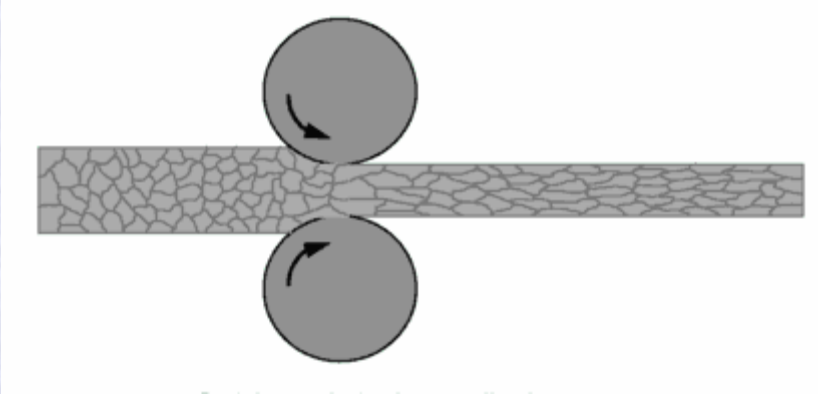

Introduction

Severe plastic deformation

- very strong grain size reduction → down to nanoscale (~ 100 nm)

- P.W. Bridgman, 1930 , Harvard University
  Large hydrostatic presure (10 GPa) + shear deformation
  Nobel prize in Physics 1946

- R.Z. Valiev, 1980 , Ufa State Aviation Technical University
  High pressure torsion (HPT)
  Equal channel angular pressing (ECAP)

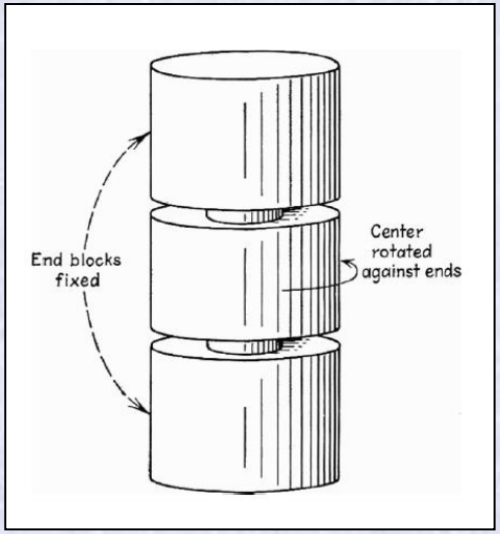

Introduction

High pressure torsion (HPT)

- the strongest grain refinement
- grain size 50 – 150 nm
- limited size: disk shaped samples
  diameter 10 – 20 mm, thickness 0.3 - 0.5 mm

UFG Cu sample prepared by HPT

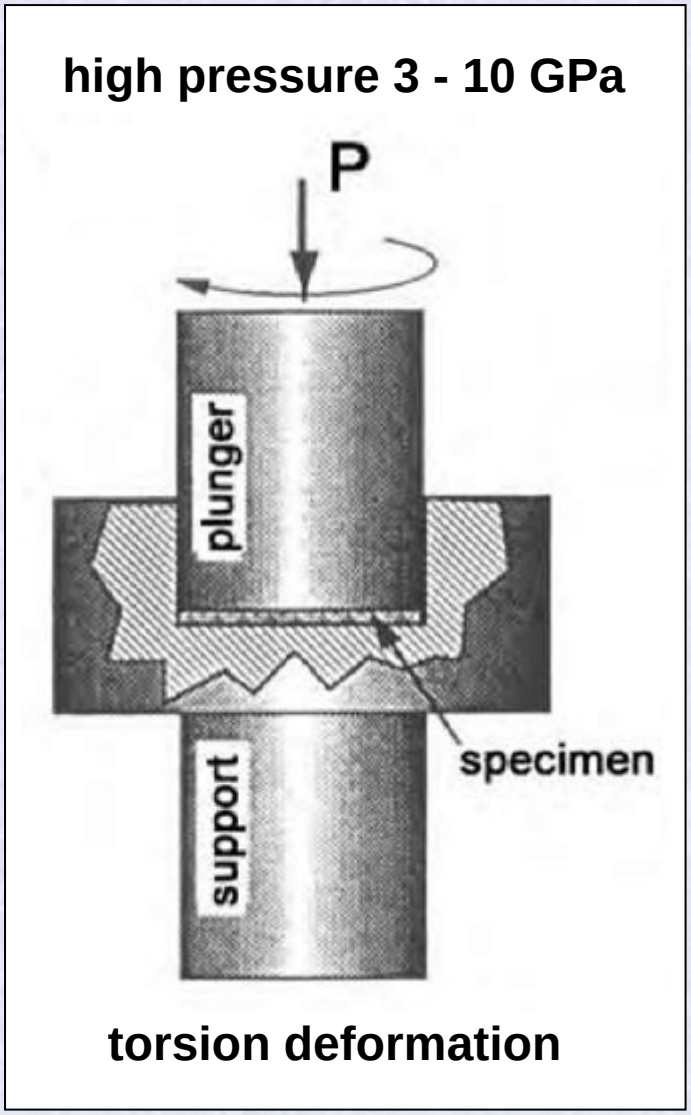

R.Z. Valiev, Nature Materials 3, 511-516 (2004)

Introduction

High pressure torsion (HPT)

- the strongest grain refinement
- grain size 50 – 150 nm

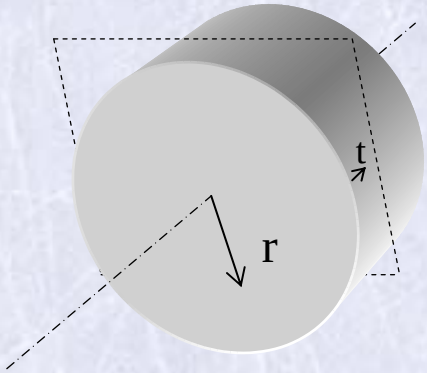

$$e = \frac{1}{\sqrt{3}} \frac{2\pi r N}{l}$$

- e - true strain
- N – number of rotations
- r - distance from center
- l - sample thickness

high pressure 3 - 10 GPa

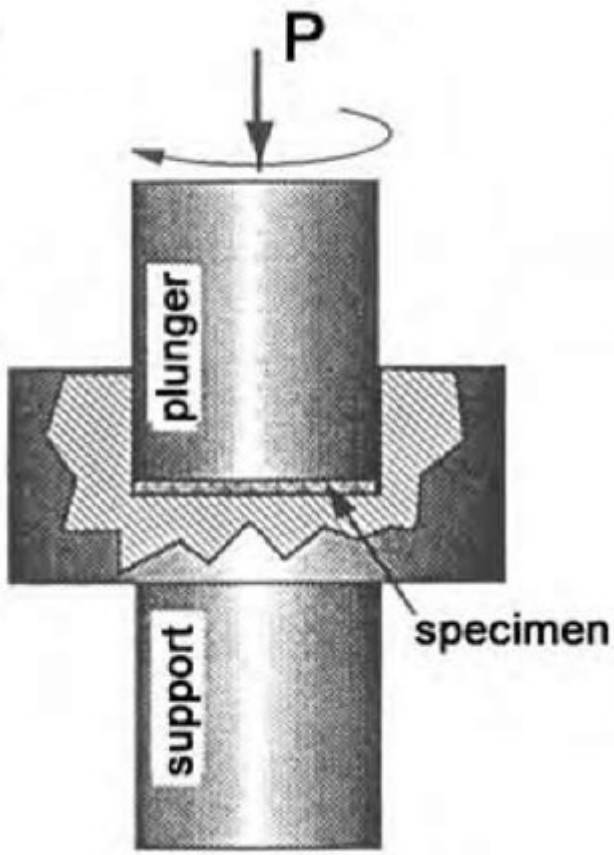

torsion deformation

R.Z. Valiev, Nature Materials 3, 511-516 (2004)

Equal Channel Angular Pressing (ECAP)

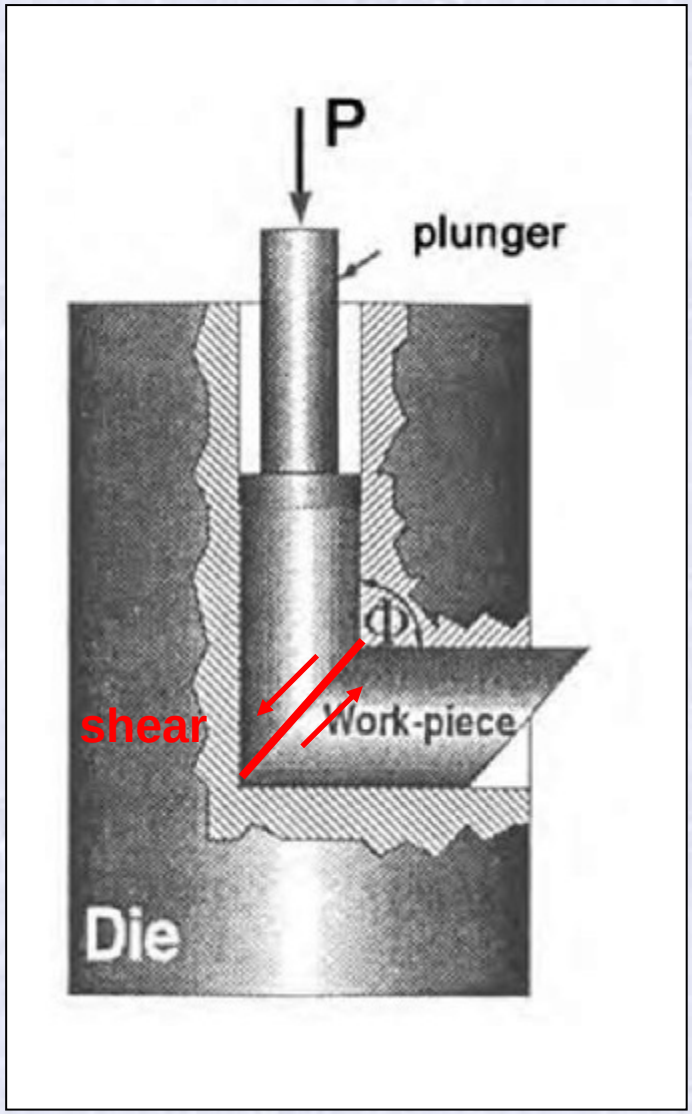

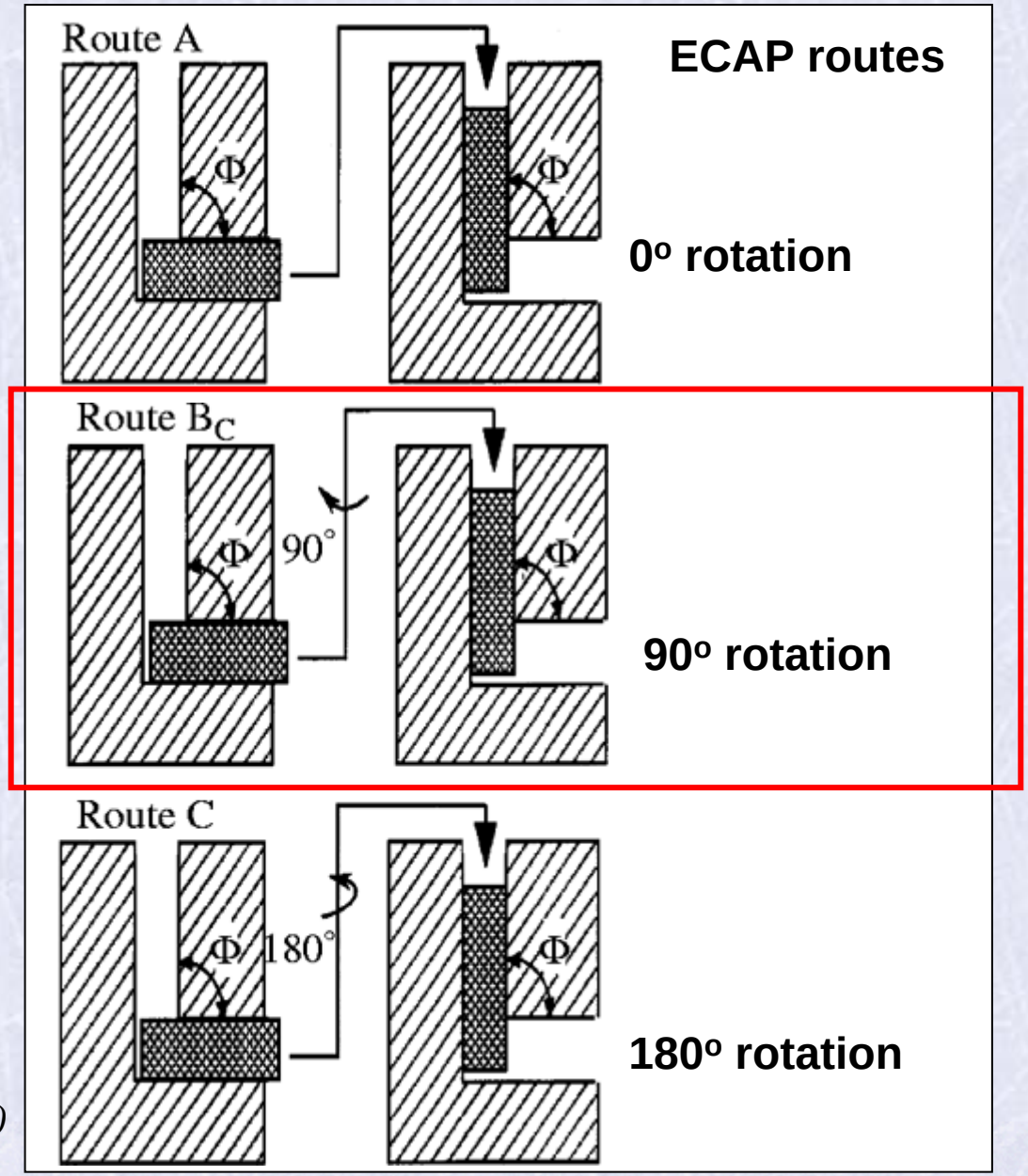

R.Z. Valiev et al., Prog. Mat. Sci. ***45*** *103 (2000)*

Equal Channel Angular Pressing (ECAP)

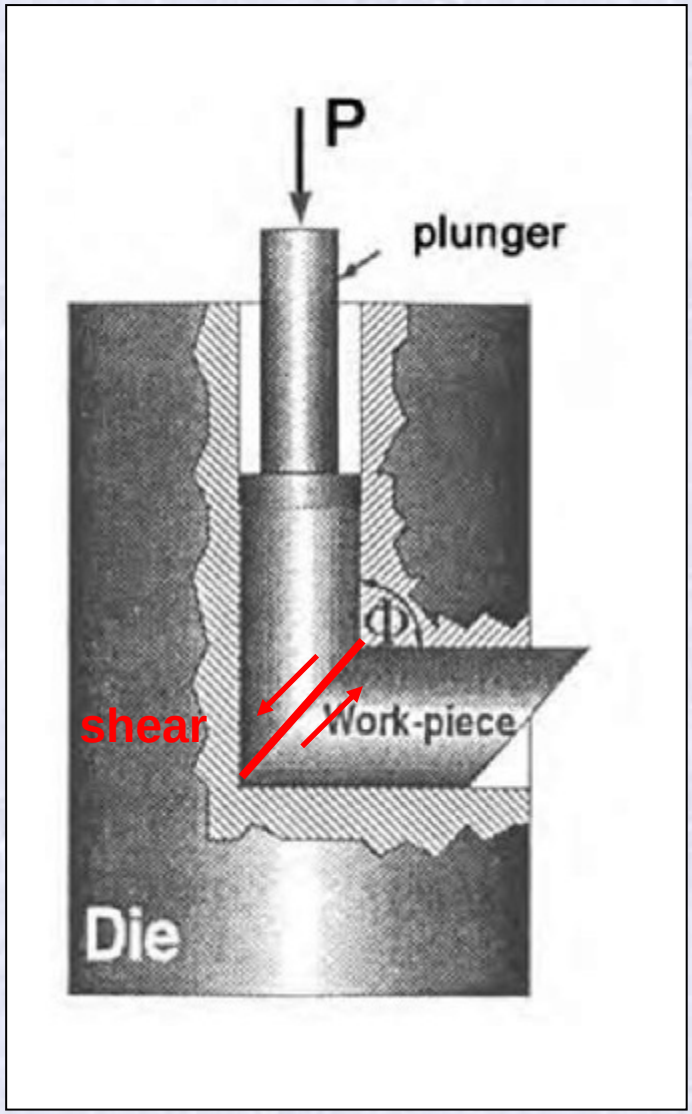

- grain size 100 - 500 nm
- no porosity
- high purity samples
- good reproducibility

- massive samples
  (diameter up to ≈ 100 mm,
  length up to ≈ 500 mm)

UFG Cu prepared by ECAP

R.Z. Valiev et al., Prog. Mat. Sci. ***45*** *103 (2000)*

Samples

High pressure torsion (HPT)

- Ufa State Aviation Technical University
- p = 6 GPa, 1-25 HPT revolutions
- Cu (99.99%)

Equal channel angular pressing (ECAP)

- Ufa State Aviation Technical University
- route B_c, 1-10 passes
- Cu (99.99%)

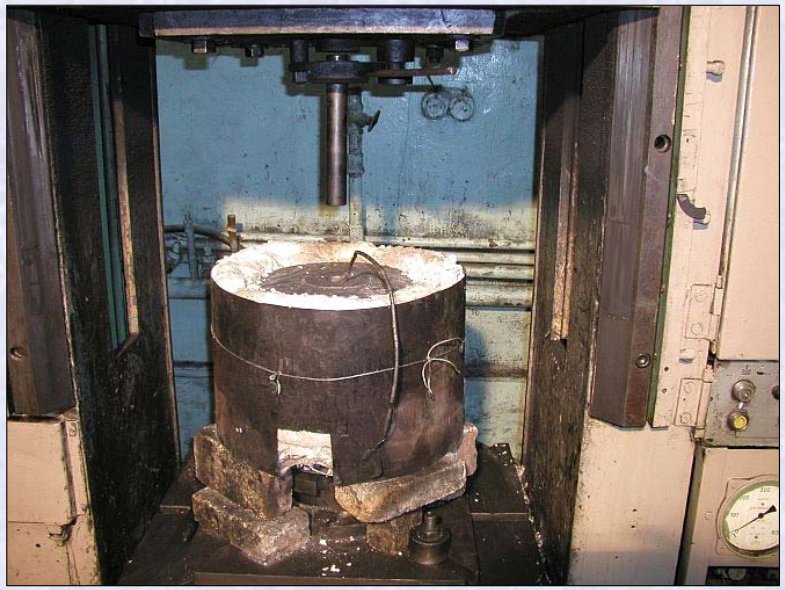

Mechanical properties of UFG metals prepared by SPD

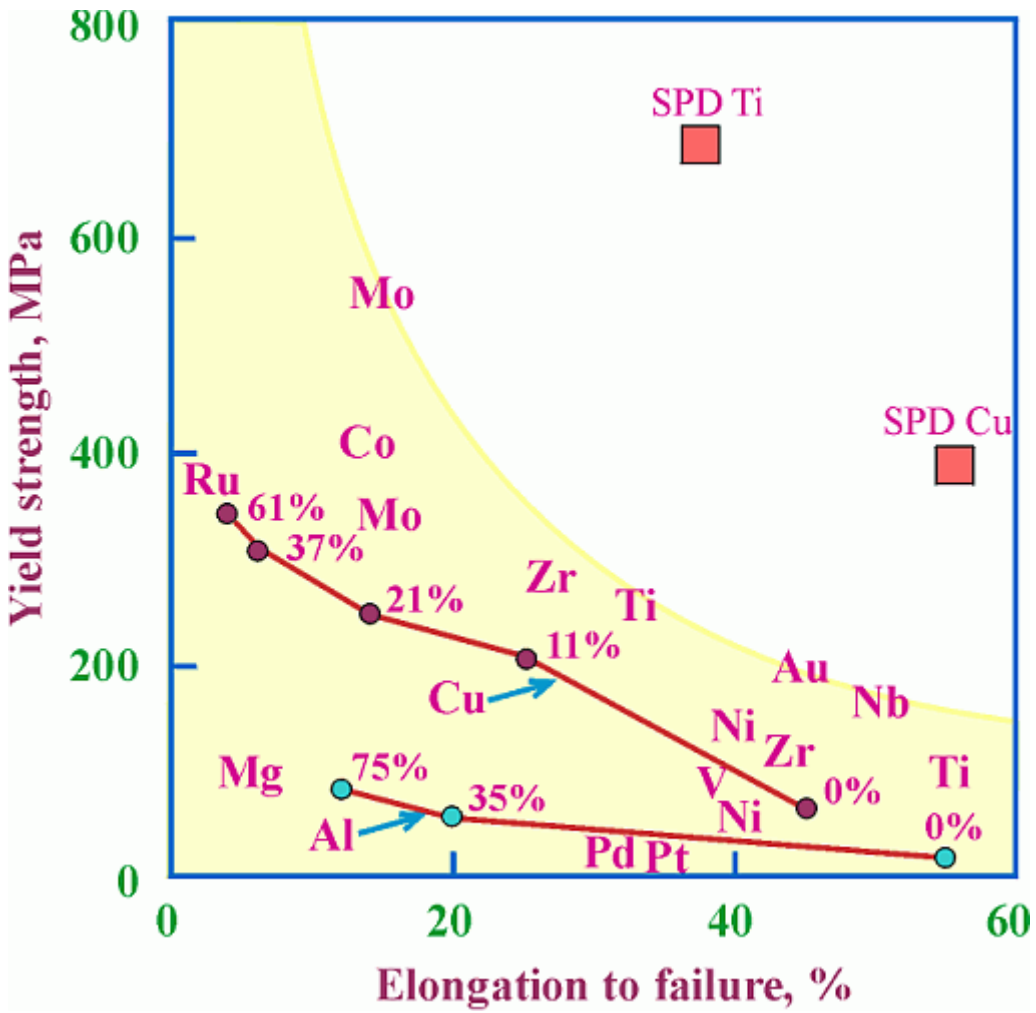

Y.T. Zhu et al., JOM, Oct. 58-63 (2004)
R.Z. Valiev et al., J. Mater. Res., 17, 5-10 (2002)

Hall-Petch relationship:

$$\sigma_y = \sigma_{y,0} + \frac{k}{\sqrt{d}}$$

UFG metals

$\Downarrow$

superior mechanical properties:

- high strength
- good ductility

Mechanical properties of UFG metals prepared by SPD

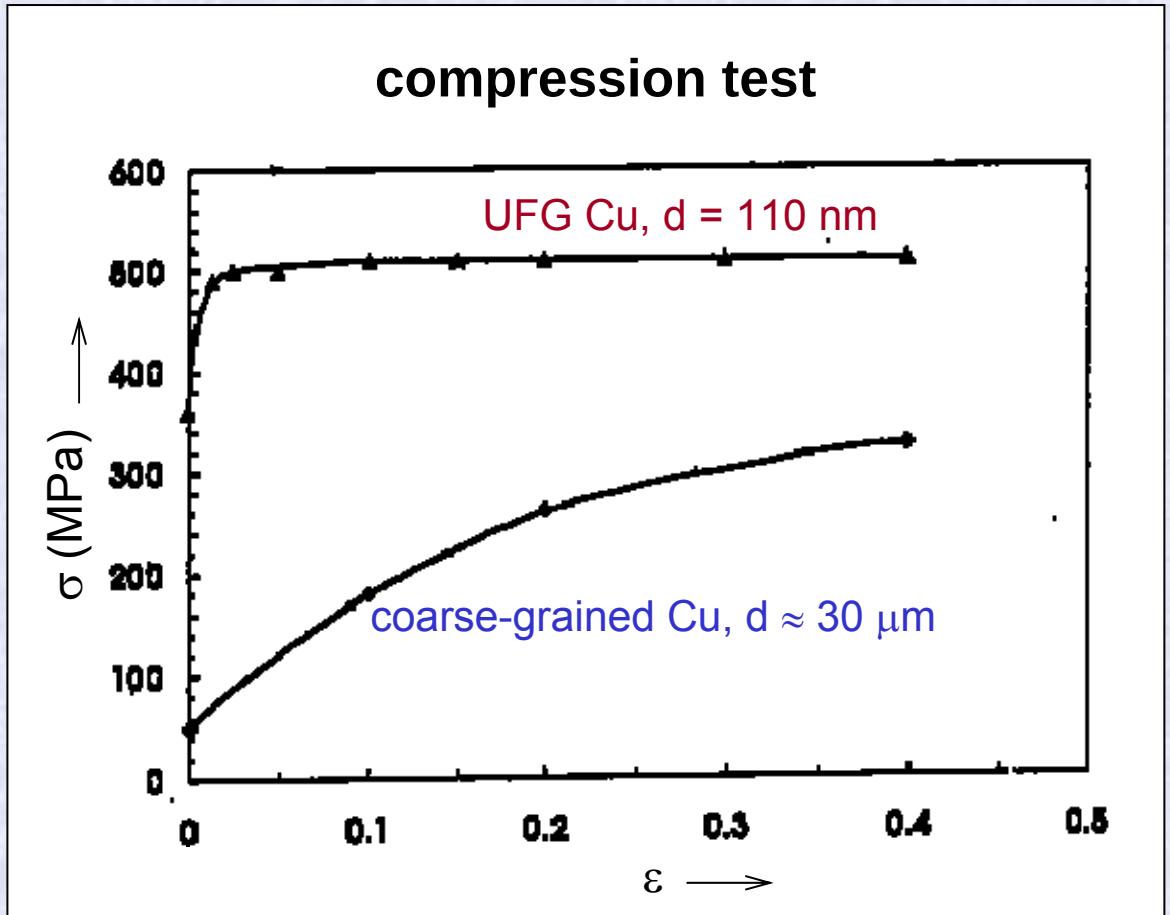

R.Z. Valiev, Mater. Sci. Eng. A ***234-236****, 59 (1997)*

UFG metals

⇓

superior mechanical properties:

- high strength
- good ductility

Microstructure of UFG metals prepared by SPD

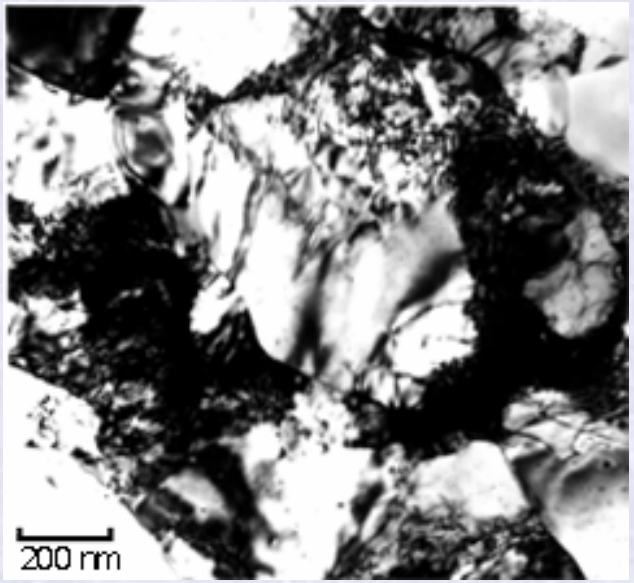

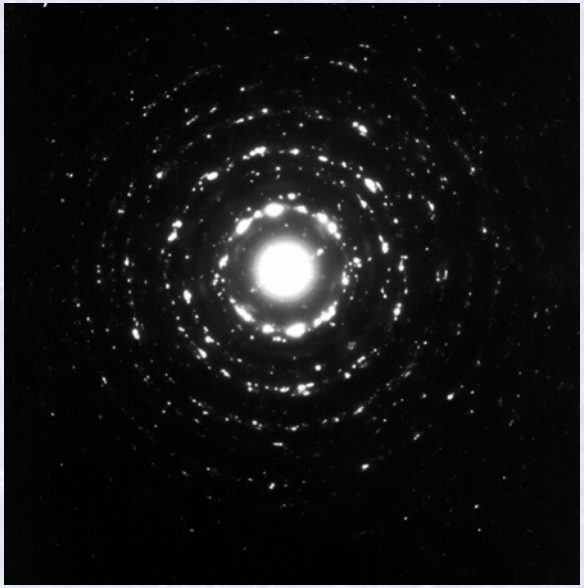

UFG Cu prepared by HPT, p = 6 GPa

- grain size 105(9) nm
- fragmented structure
- high-angle missorientation
- non-equilibrium GB's

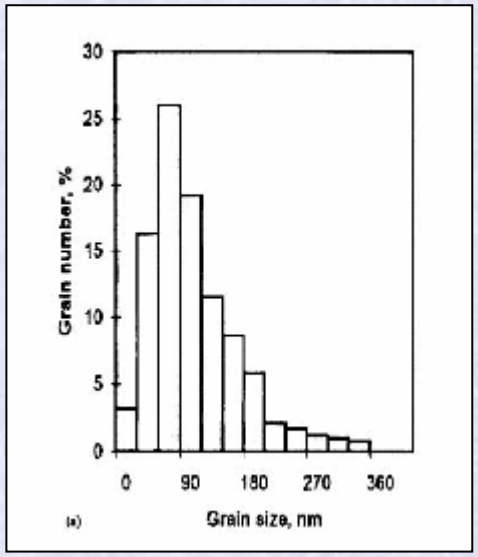

grain size distribution

Microstructure of UFG metals prepared by SPD

polycrystalline material

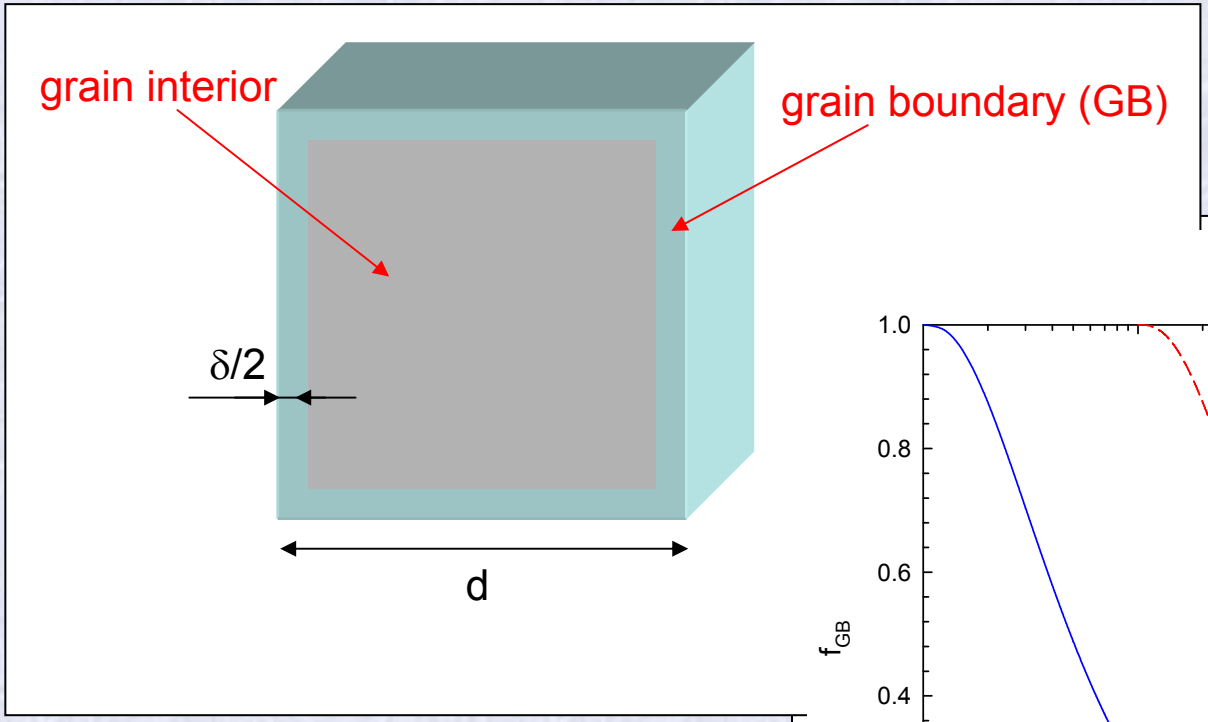

equilibrium GB: $\delta \approx 1$ nm
non-equilibrium GB: $\delta \approx 10$ nm

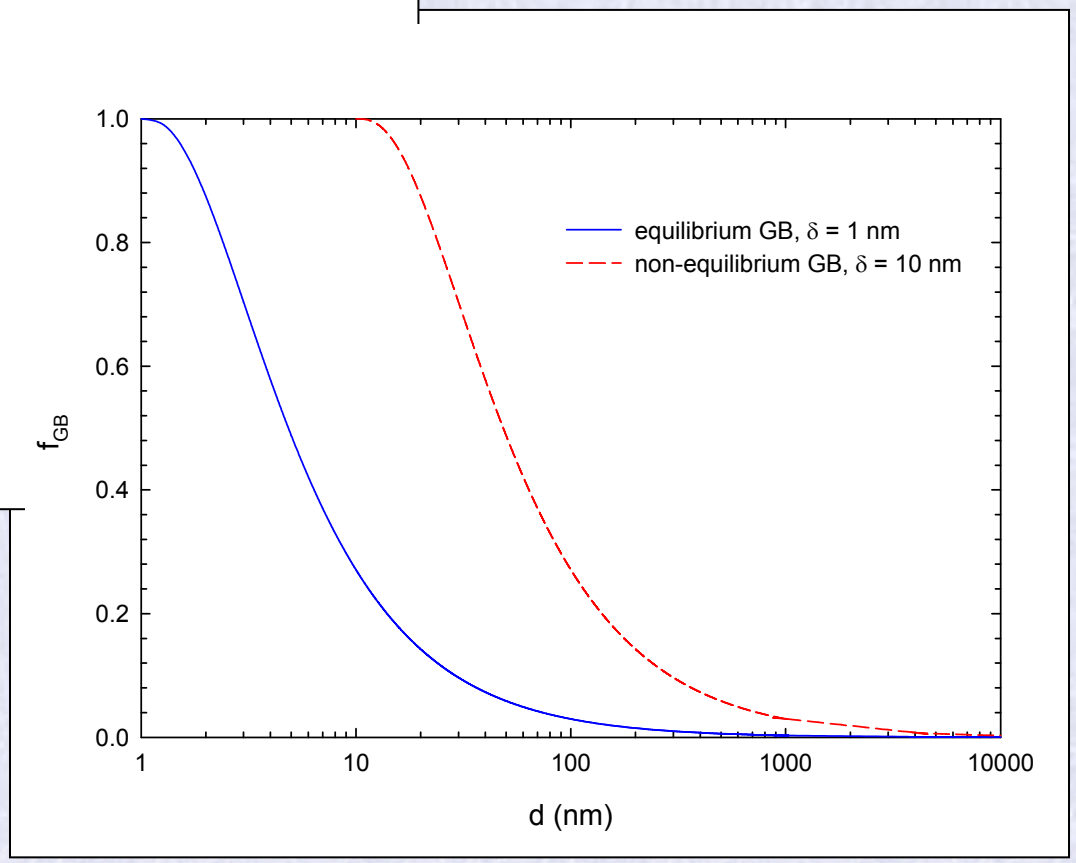

volume fraction of GB's

$$f_{GB} = 1 - \left(\frac{d - \delta}{d} \right)^3$$

Generation of vacacies during SPD

movement of dislocation with jogs

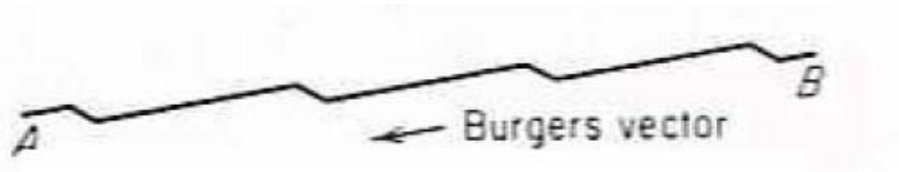

1. no stress

Generation of vacacies during SPD

movement of dislocation with jogs

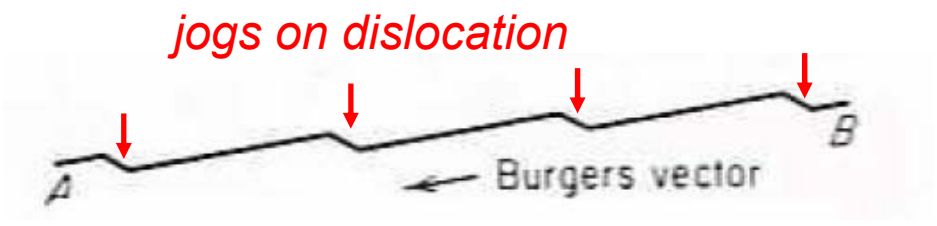

1. no stress

Generation of vacacies during SPD

movement of dislocation with jogs

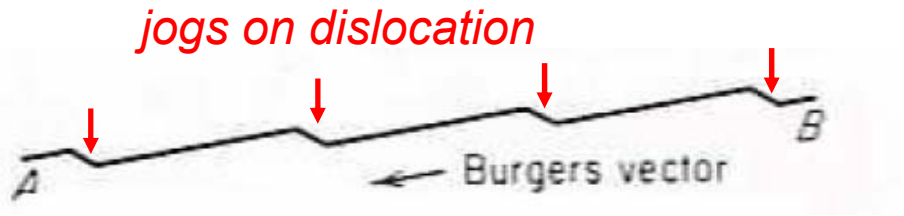

1. no stress

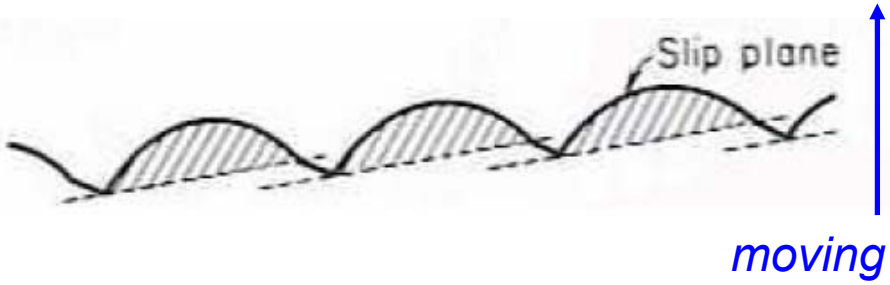

2. applied stress

moving direction

Generation of vacacies during SPD

movement of dislocation with jogs

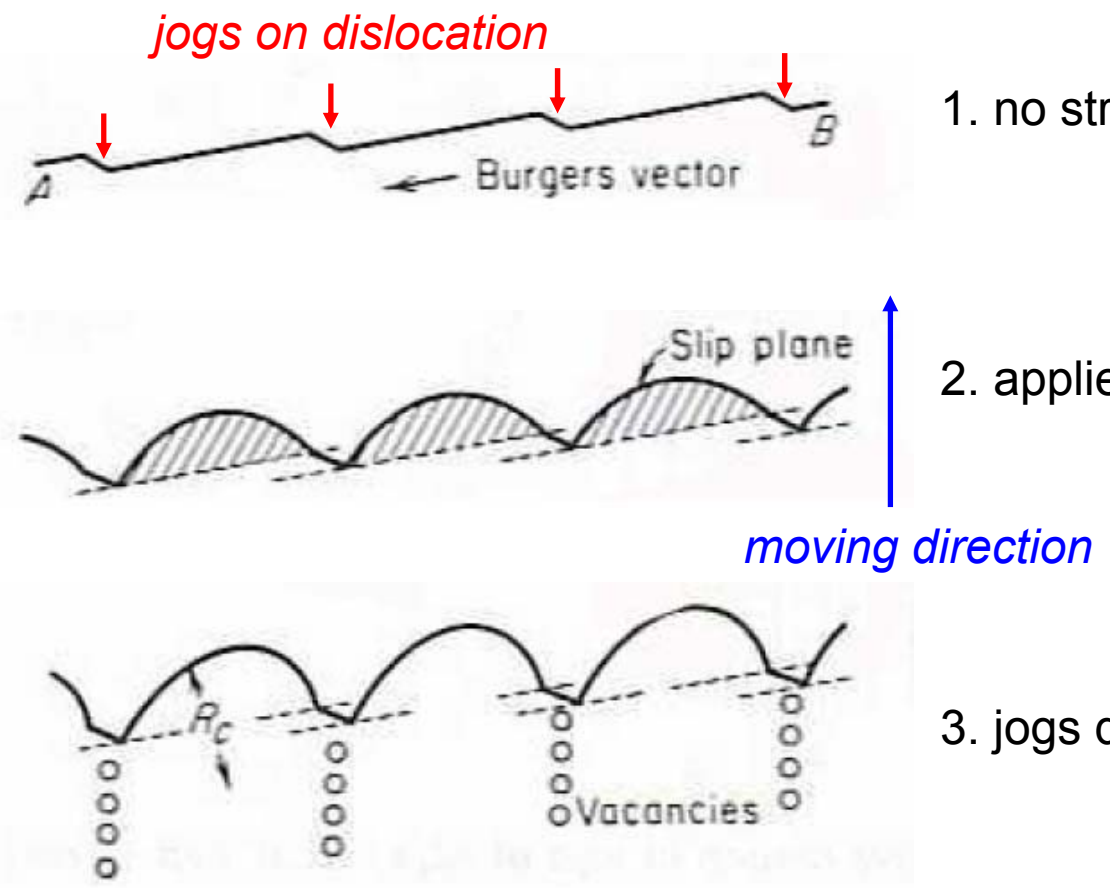

1. no stress

2. applied stress

3. jogs dragged by dislocation

Generation of vacacies during SPD

- **X-ray line profile analyzis:**
  - dislocation density $\rho_D \approx 10^{14} - 10^{15}$ m^{-2}

    T. Ungár et al. Mater. Sci. Eng. A 462, 398 (2007)

- **differential scanning calorimetry (DSC) & electrical resistivity**
  - dislocation density $\rho_D \approx 10^{15} - 10^{16}$ m^{-2}

    E. Schafler et al. Mater. Sci. Eng. A 410-411, 169 (2005)

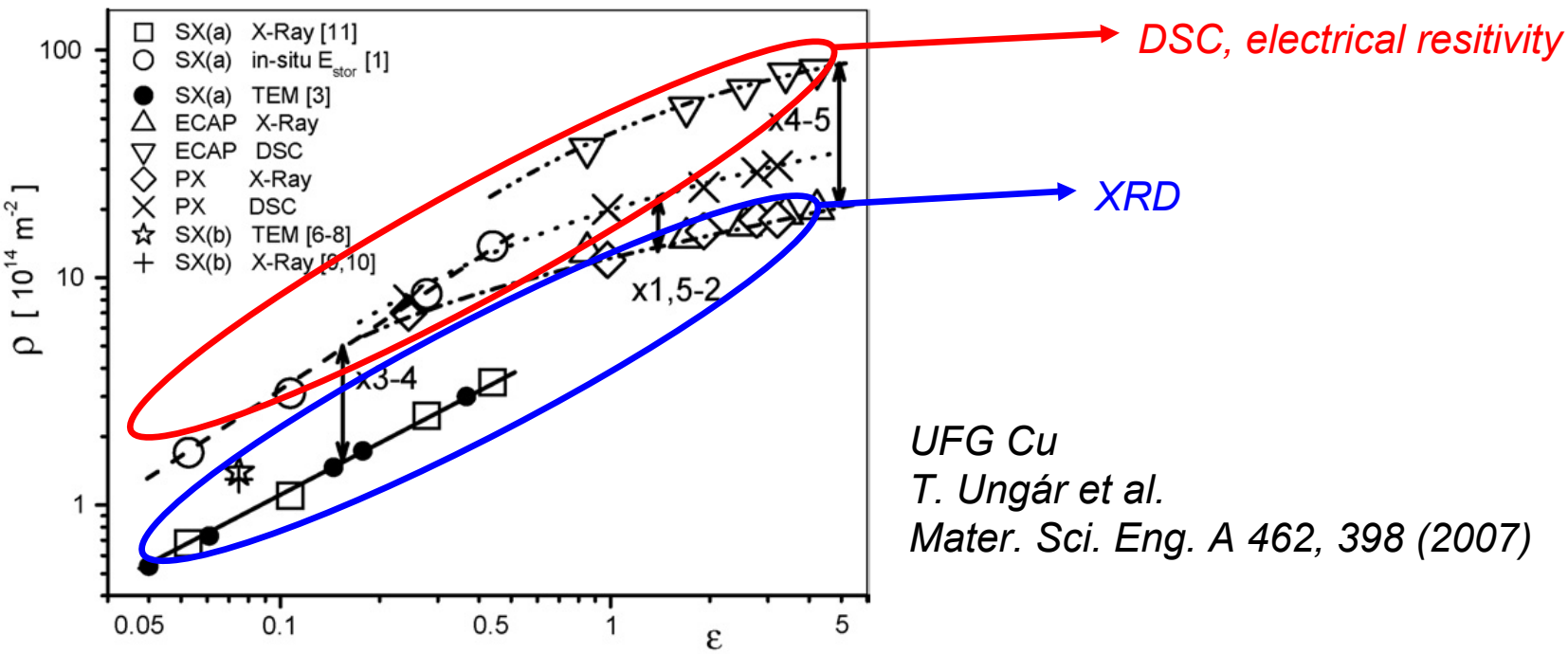

UFG Cu
T. Ungár et al.
Mater. Sci. Eng. A 462, 398 (2007)

Generation of vacacies during SPD

deformation-induced vacancies contribute to the total stored energy and electrical resitivity, but do not cause broadening of XRD profiles

- **indirect evidence for deformation-induced vacancies**

- **deformation-induced vacancies can be detected probed by positron annihilation**

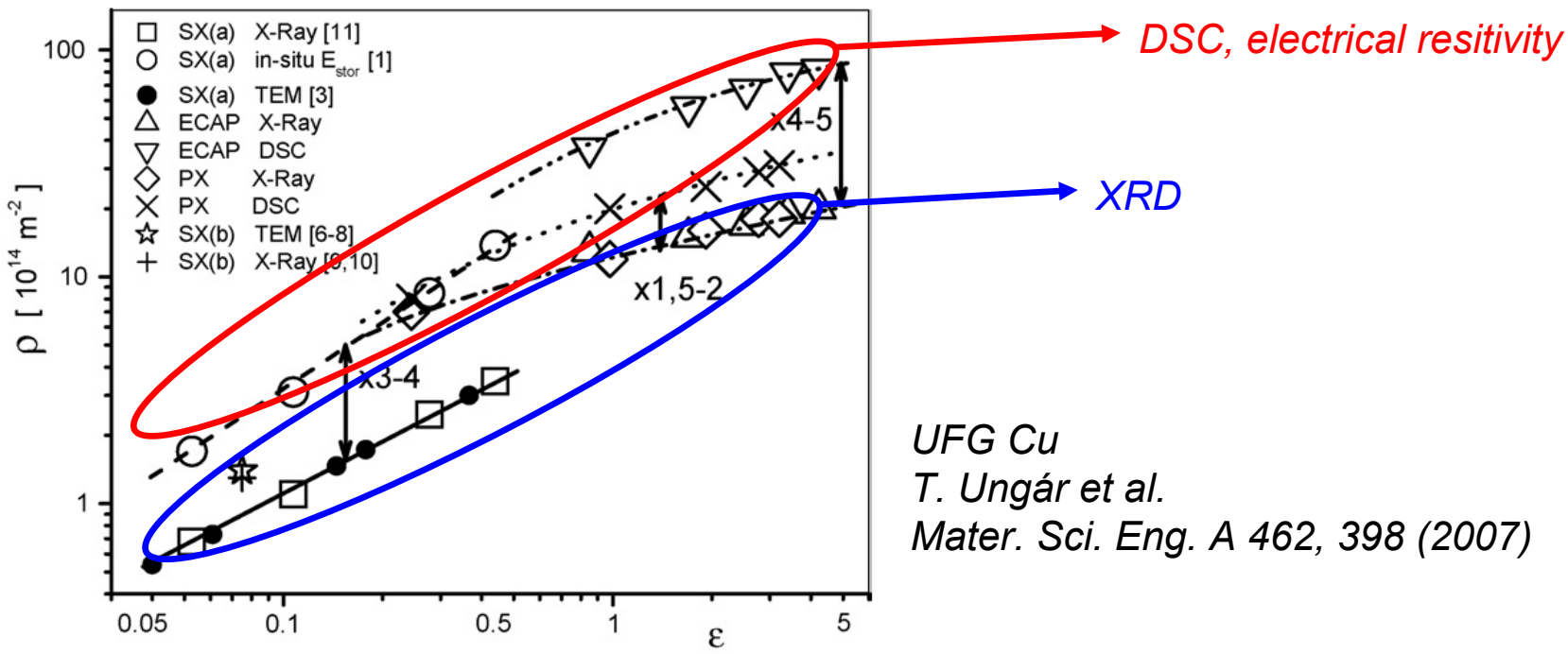

UFG Cu
T. Ungár et al.
Mater. Sci. Eng. A 462, 398 (2007)

LT spectroscopy

Digital LT spectrometer: *F. Bečvář et al., Nucl. Instr. Meth. A **539**, 372 (2005)*

- Two photomultipliers Hamamatsu H3378
- BaF_2 scintilators truncated cone (∅ 18-36 mm, thickness 12 mm)
- two 8-bit digitizers Acqiris DC211, sampling rate 4 GHz
- time resolution 145 ps (FWHM ^{22}Na)
- at least 10^7 annihilation events collected in each LT spectrum

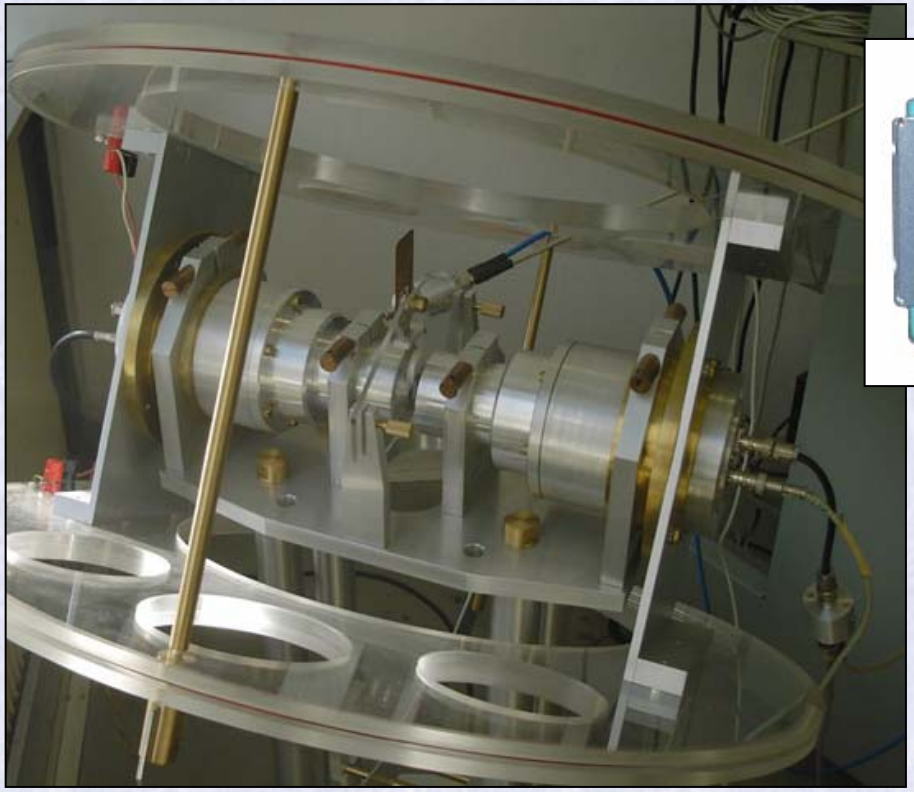

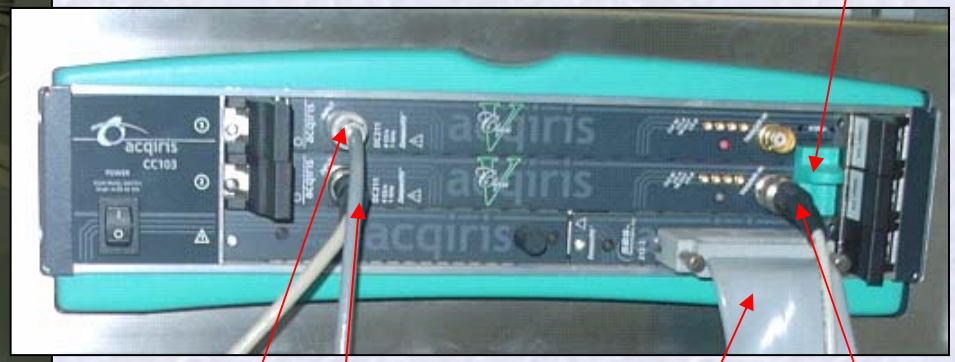

Positron lifetime studies of Cu

- pure Cu (99.99%)

sample	τ_1 (ps)	I_1 (%)	τ_2 (ps)	I_2 (%)	τ_3 (ps)	I_3 (%)
well annealed 800°C/1h	114.5(2)	100	-	-	-	-

free positrons

- theoretical calculations: Cu bulk lifetime
  - τ_B = 108 ps (ATSUP, LDA)
  - τ_B = 118 ps (LMTO, GGA)

Positron lifetime studies of Cu

- pure Cu (99.99%)

sample	τ_1 (ps)	I_1 (%)	τ_2 (ps)	I_2 (%)	τ_3 (ps)	I_3 (%)
well annealed 800°C/1h	114.5(2)	100	-	-	-	-
cold rolled, 20%, ε = 0.22	102(3)	71(2)	164(1)	29(1)	-	-
cold rolled, 50%, ε = 0.69	68(4)	31(2)	163(1)	69(1)	-	-

free positrons dislocations

Positron lifetime studies of Cu

- pure Cu (99.99%)

sample	τ_1 (ps)	I_1 (%)	τ_2 (ps)	I_2 (%)	τ_3 (ps)	I_3 (%)
well annealed 800°C/1h	114.5(2)	100	-	-	-	-
cold rolled, 20%, ε = 0.22	102(3)	71(2)	164(1)	29(1)	-	-
cold rolled, 50%, ε = 0.69	68(4)	31(2)	163(1)	69(1)	-	-
ECAP, N = 1, ε = 1	-	-	164(1)	88.9(6)	257(5)	11.1(5)
ECAP, B_c, N = 8, ε = 8	-	-	165(1)	84.7(4)	258(3)	15.3(4)

free positrons dislocations vacancy clusters

- theoretical calculations: Cu monovacancy
  - τ_V = 170 ps (ATSUP, LDA)
  - τ_V = 178 ps (LMTO, GGA)

Positron lifetime studies of UFG Cu prepared by ECAP

- pure Cu (99.99%), ECAP B_c route
- saturated trapping at dislocations and vacancy clusters
- fraction of e^+ trapped at vacancy clusters increases with number of passes

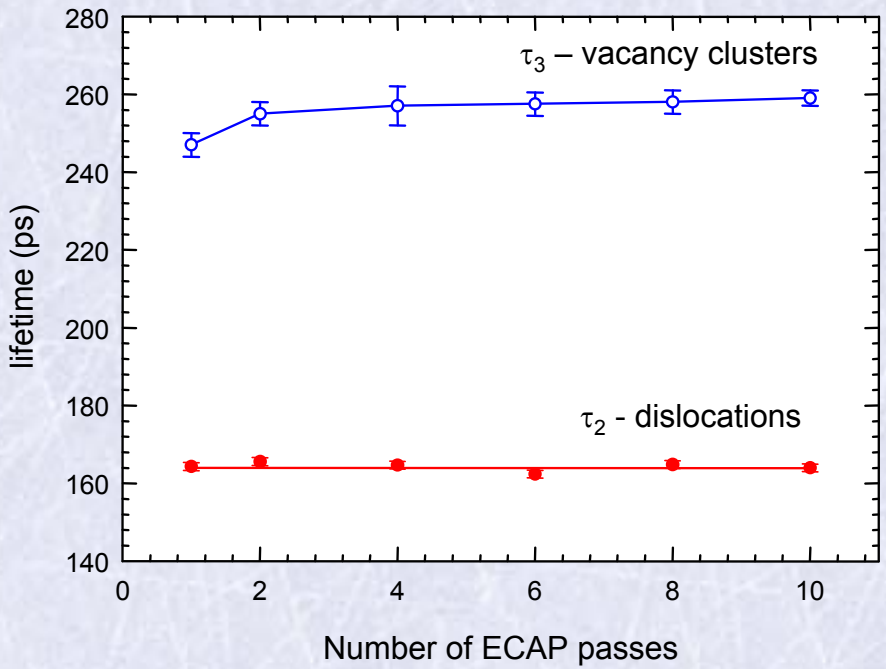

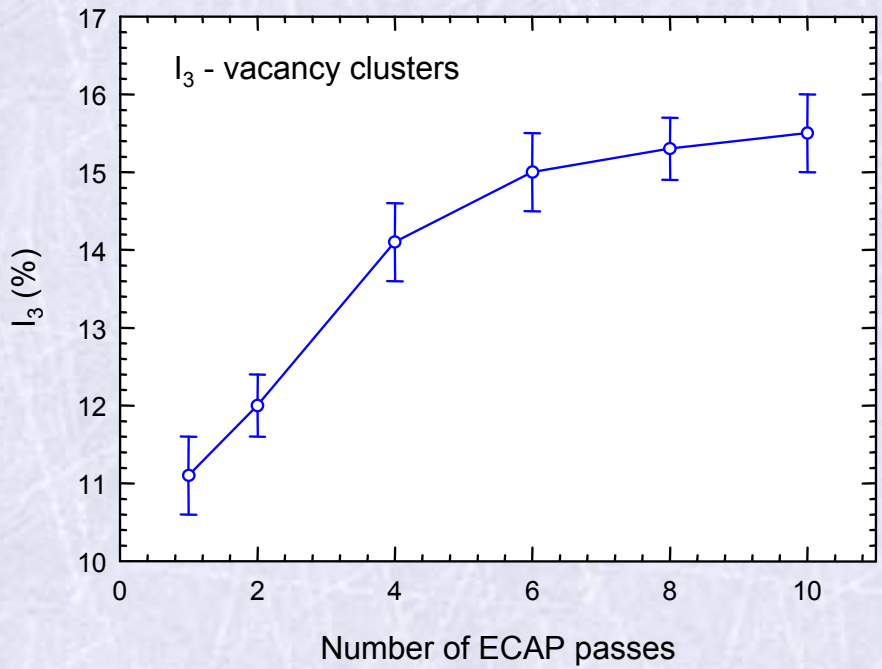

Positron lifetime studies of Cu

- pure Cu (99.99%)

sample	τ_1 (ps)	I_1 (%)	τ_2 (ps)	I_2 (%)	τ_3 (ps)	I_3 (%)
well annealed 800°C/1h	114.5(2)	100	-	-	-	-
cold rolled, 20%, ε = 0.22	102(3)	71(2)	164(1)	29(1)	-	-
cold rolled, 50%, ε = 0.69	68(4)	31(2)	163(1)	69(1)	-	-
ECAP, N = 1, ε = 1	-	-	164(1)	88.9(6)	257(5)	11.1(5)
ECAP, N = 8, ε = 8	-	-	165(1)	84.7(4)	258(3)	15.3(4)
HPT, N = 5, *r* = 0 mm, ε = 40	-	-	164(1)	82.0(8)	255(3)	18(1)
HPT, N = 5, *r* = 3 mm, ε = 180	-	-	163(1)	70.5(5)	310(3)	29.5(7)

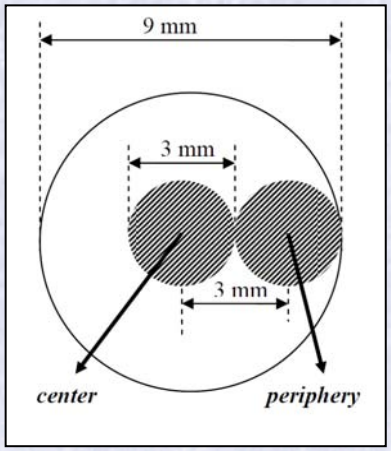

free positrons

dislocations

vacancy clusters

Positron lifetime studies of UFG Cu prepared by HPT

- pure Cu (99.99%), HPT p = 6GPa
- center *r* = 0
- intensity of the cluster component increases with the number of HPT revolutions

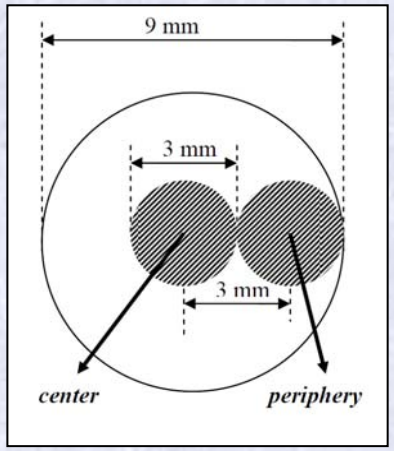

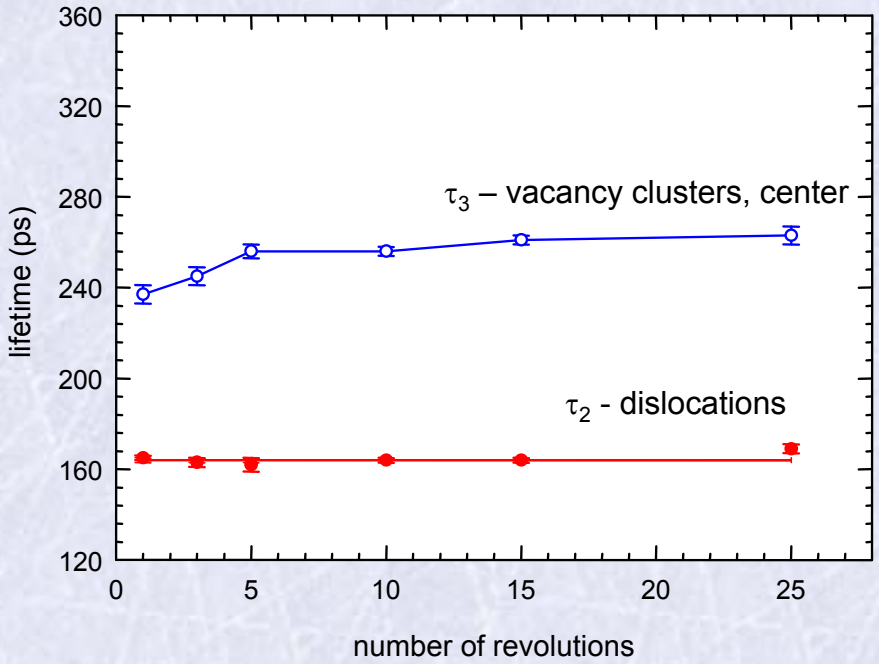

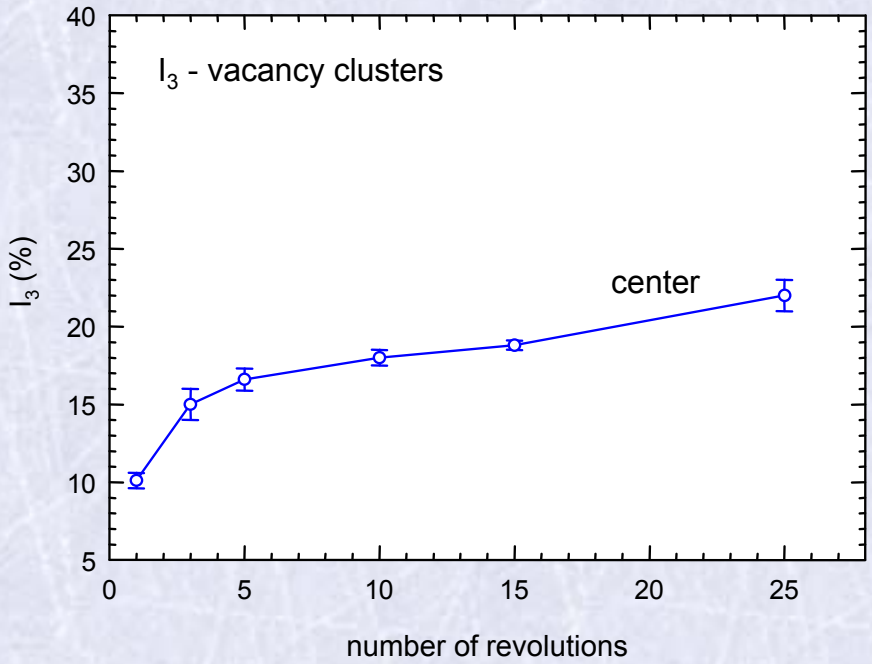

J. Čížek et al., Acta Mater. ***59****, 2322 (2011)*

Positron lifetime studies of UFG Cu prepared by HPT

- pure Cu (99.99%), HPT p = 6GPa
- center *r* = 0, periphery *r* = 3 mm
- diameter of positron source spot ≈ 3 mm
- vacancy clusters at periphery are larger

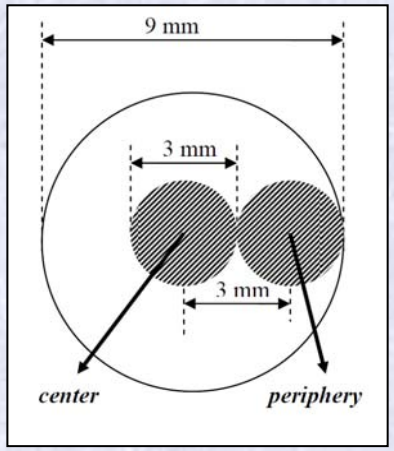

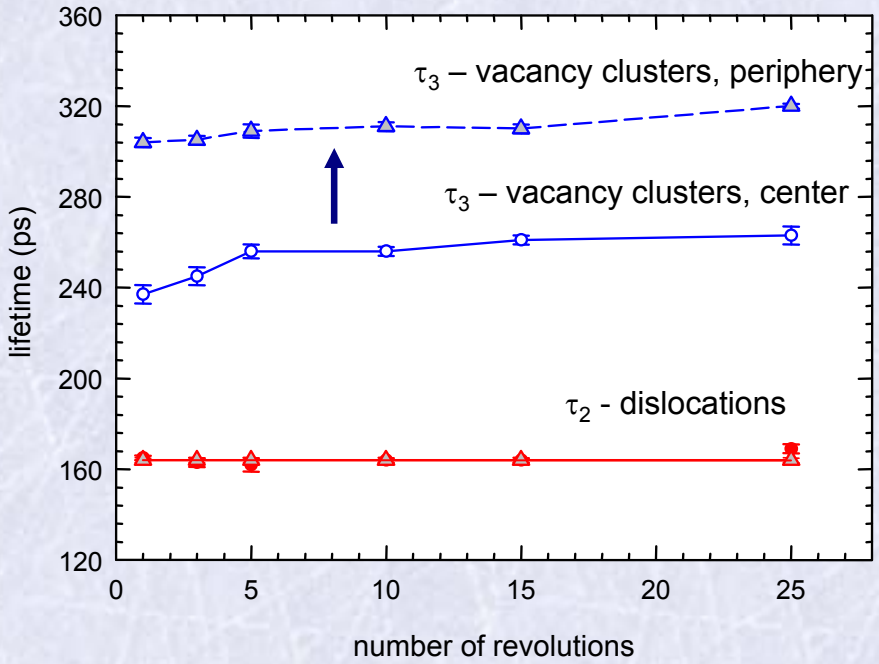

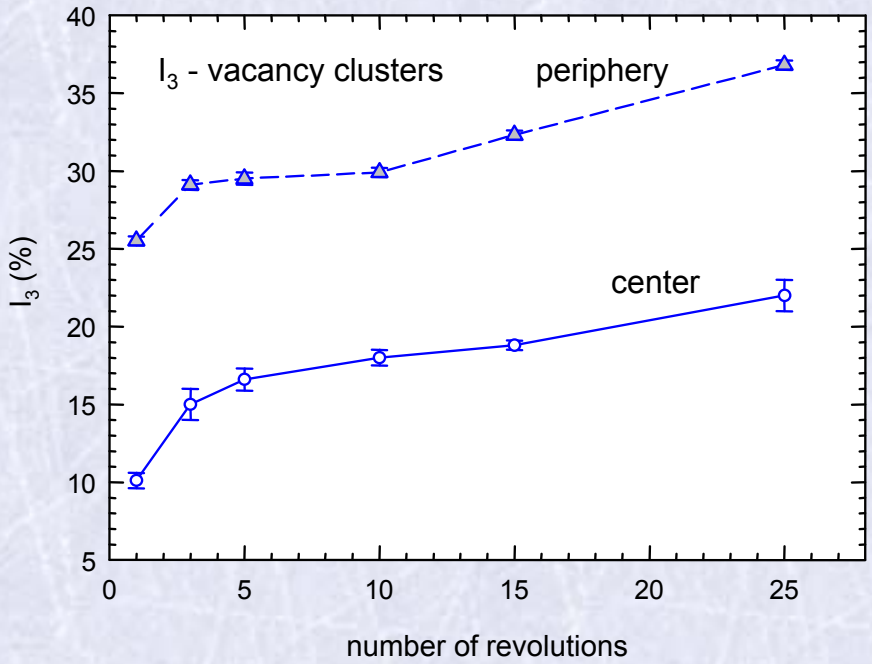

J. Čížek et al., Acta Mater. ***59****, 2322 (2011)*

Size distribution of vacancy clusters

- movement of dislocation with a jog

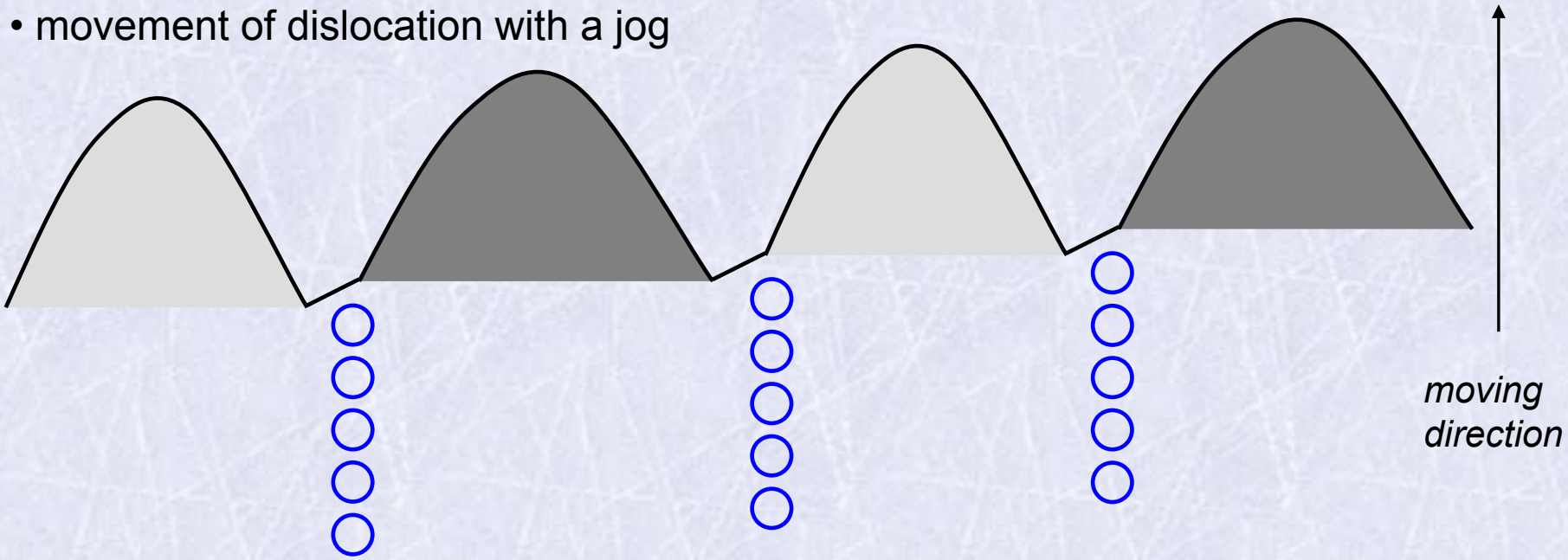

- monovacancies in Cu are mobile at room temperature

*S. Mantl and W. Trifthäuser, Phys. Rev. B **17**, 1645 (1978)*

Size distribution of vacancy clusters

- movement of dislocation with a jog

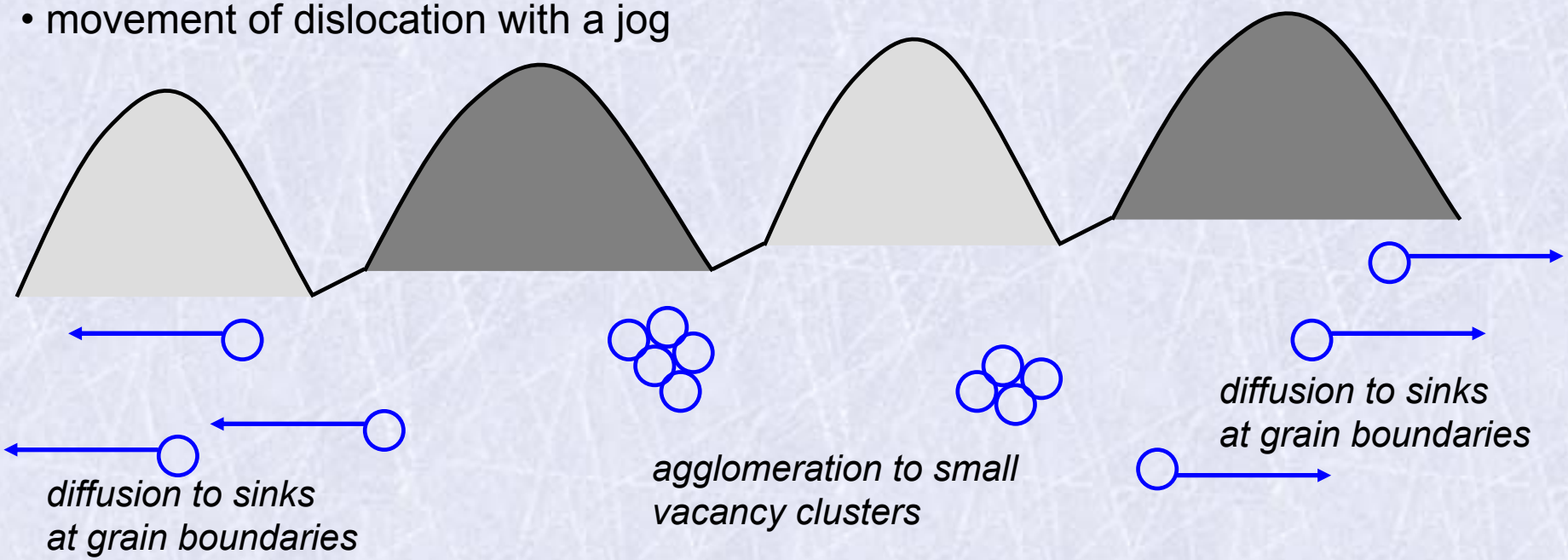

- monovacancies in Cu are mobile at room temperature

*S. Mantl and W. Trifthäuser, Phys. Rev. B **17**, 1645 (1978)*

- some fraction of vacancies disappear by diffusion to sinks at grain boundaries

- remaining vacancies agglomerate to small vacancy clusters

UFG microstructure

UFG Cu prepared by HPT, p = 6 GPa, N = 5

- dislocations are located mainly in distorted layers along GB's
- vacancy clusters are located predominantly inside grains

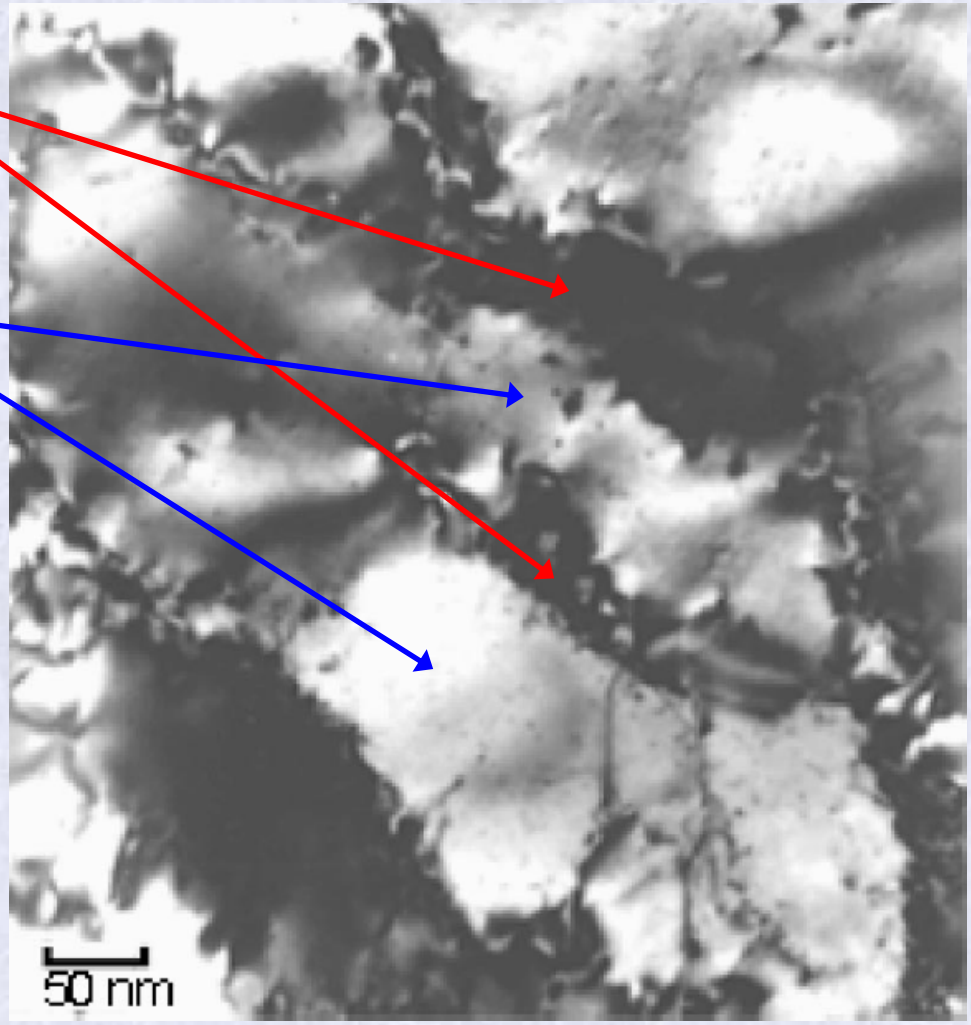

*J. Čížek et al., Phys. Rev. B **65**, 0944106 (2002)*

Size of vacancy clusters

- *ab-initio* calculations of positron lifetimes for vacancy clusters of various size
- ECAP Cu: clusters consist on average of 4 vacancies

experiment:
ECAP Cu

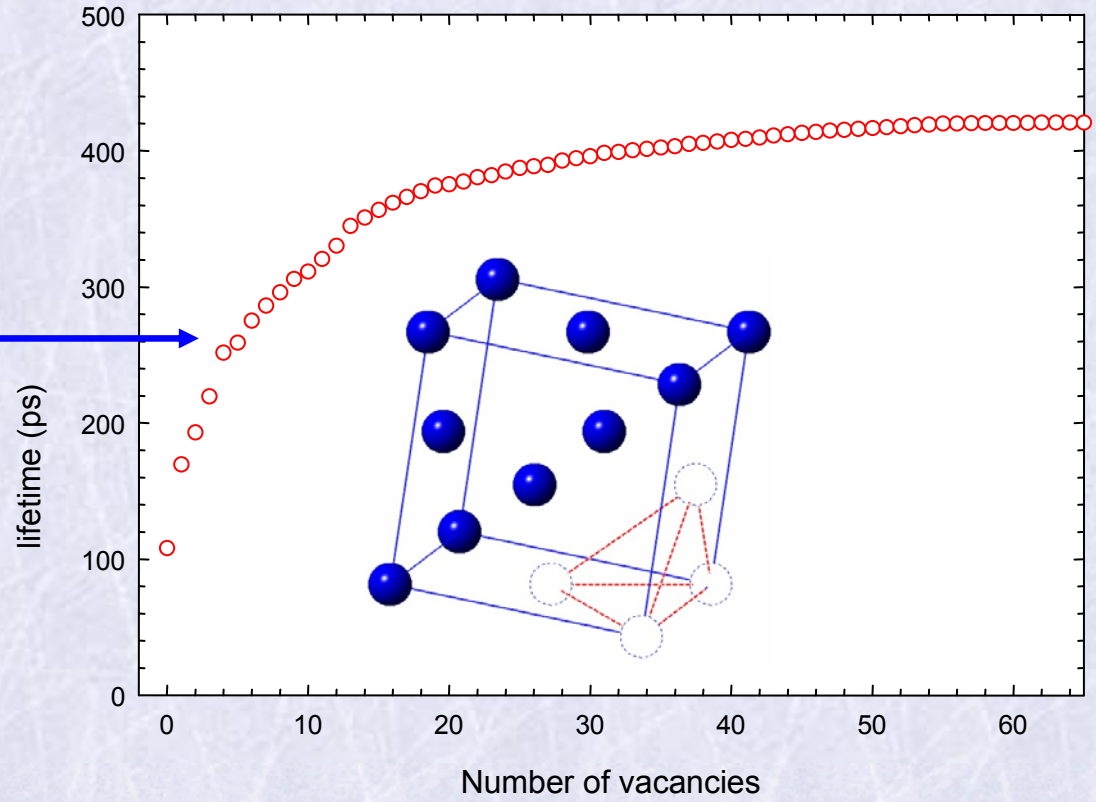

Size of vacancy clusters

- *ab-initio* calculations of positron lifetimes for vacancy clusters of various size
- HPT Cu: cluster size increases with radial distance *r* from the center
- HPT Cu: clusters in the center consist of 4 vacancies
- HPT Cu: clusters at the periphery consist of 6 vacancies

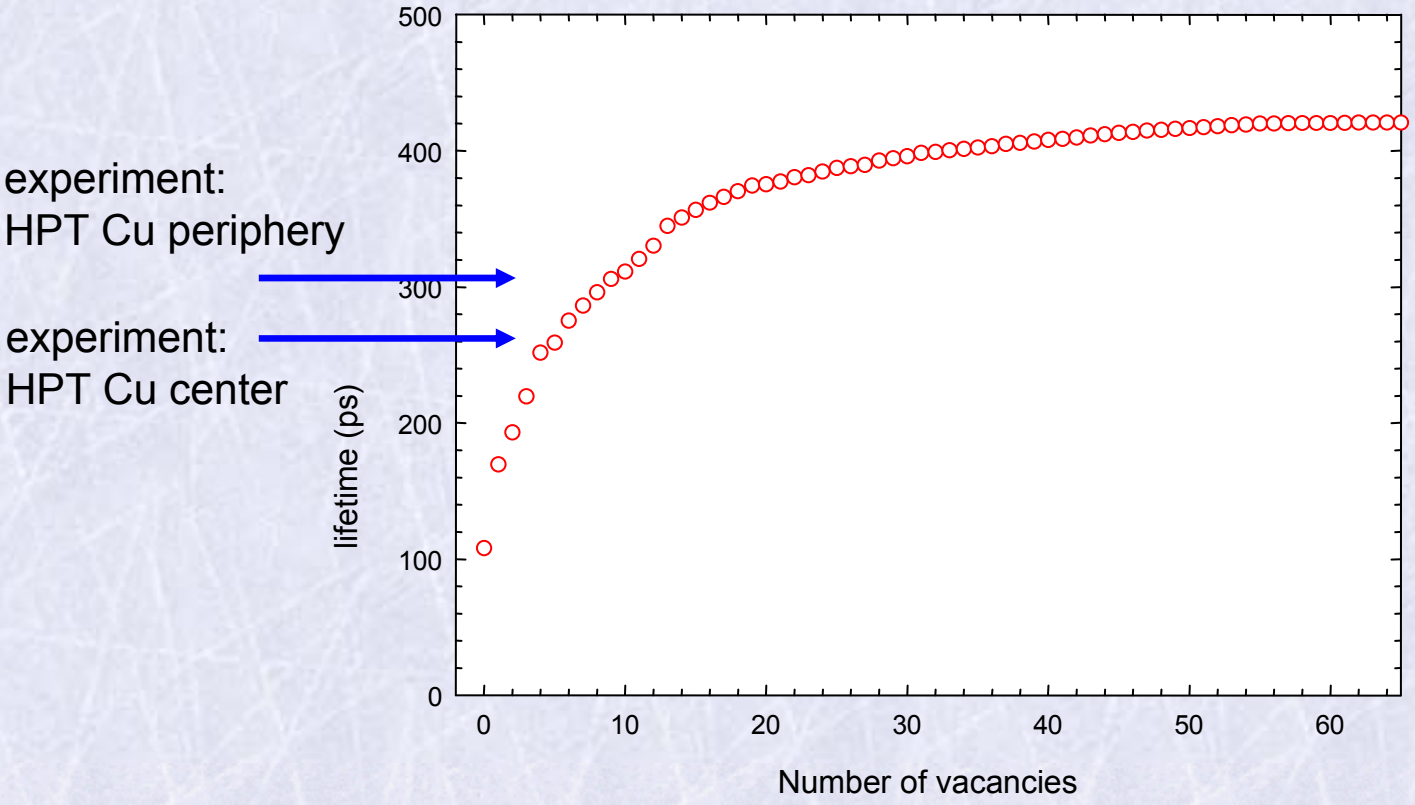

Size distribution of vacancy clusters

*J. Čížek et al., J. Phys.: Conf. Series **443**, 012008 (2013)*

- decomposition of LT spectrum: discreet components + cluster distribution

$$S(t)=\left(\sum_{i=1}^{n-1}\frac{I_i}{\tau_i}e^{-\frac{t}{\tau_i}}+I_d\left(\sum_{N=1}^{N_{\max}}P(N)\nu_N\right)^{-1}\sum_{N=1}^{N_{\max}}\frac{P(N)\nu_N}{\tau_N}e^{-\frac{t}{\tau_N}}\right)\otimes R(t)+B \qquad \sum_{i=1}^{n-1}I_i+I_d=1$$

discreet components
- dislocations,
- free positrons (if any)

cluster contribution

resolution function

random background

τ_N - positron lifetimes for clusters consting of *N* vacancies

- obtained from theoretical calculations

ν_N - the specific positron trapping rates for a clusters of various sizes

$P(N)$ - the relative population of clusters consting of *N* vacancies

- Poisson distribution

$$P(N)=\frac{\nu_d^{\,N}e^{-\nu_d}}{N!} \qquad \sum_{N=1}^{N_{\max}}P(N)=1$$

Development of deformation-induced vacancy clusters

- **HPT-deformed Cu, *p* = 6 GPa**
- comparison of centre and periphery of the sample disk
- periphery of the sample

  ↓
- **higher vacancy concentration**
- **bigger vacancy clusters**

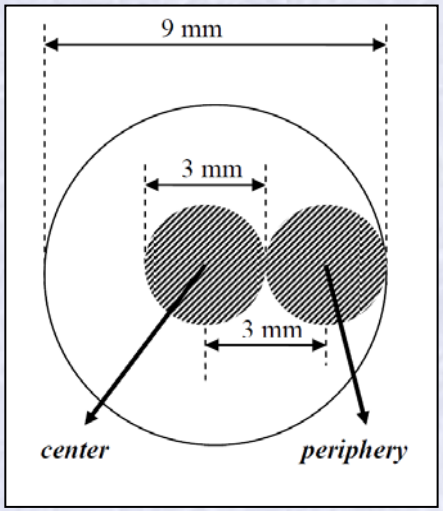

1 HPT revolution

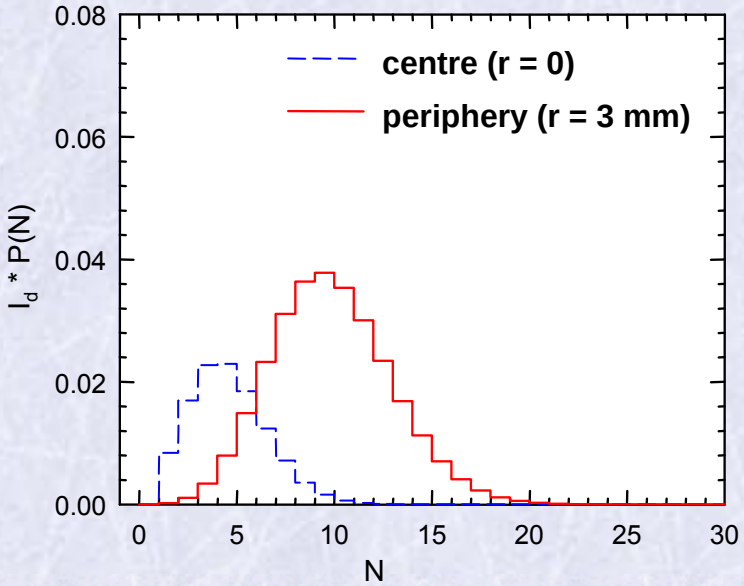

25 HPT revolutions

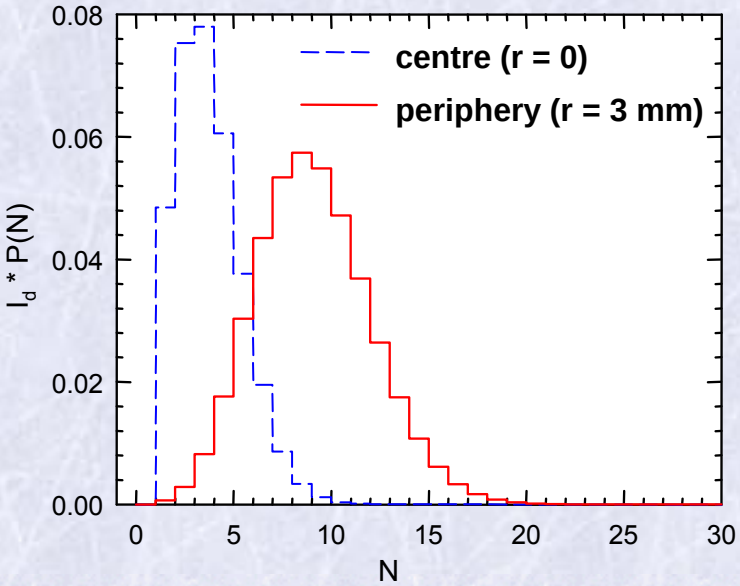

Development of deformation-induced vacancy clusters

- **HPT-deformed Cu, *p* = 6 GPa**
- comparison of centre and periphery of the sample disk
- periphery: higher vacancy concentration, bigger clusters
- increasing number of HPT revolutions:
  - **concentration of vacancies increases**
  - **size distribution remains constant**

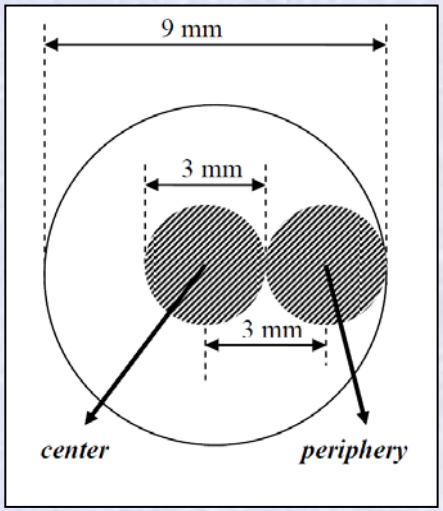

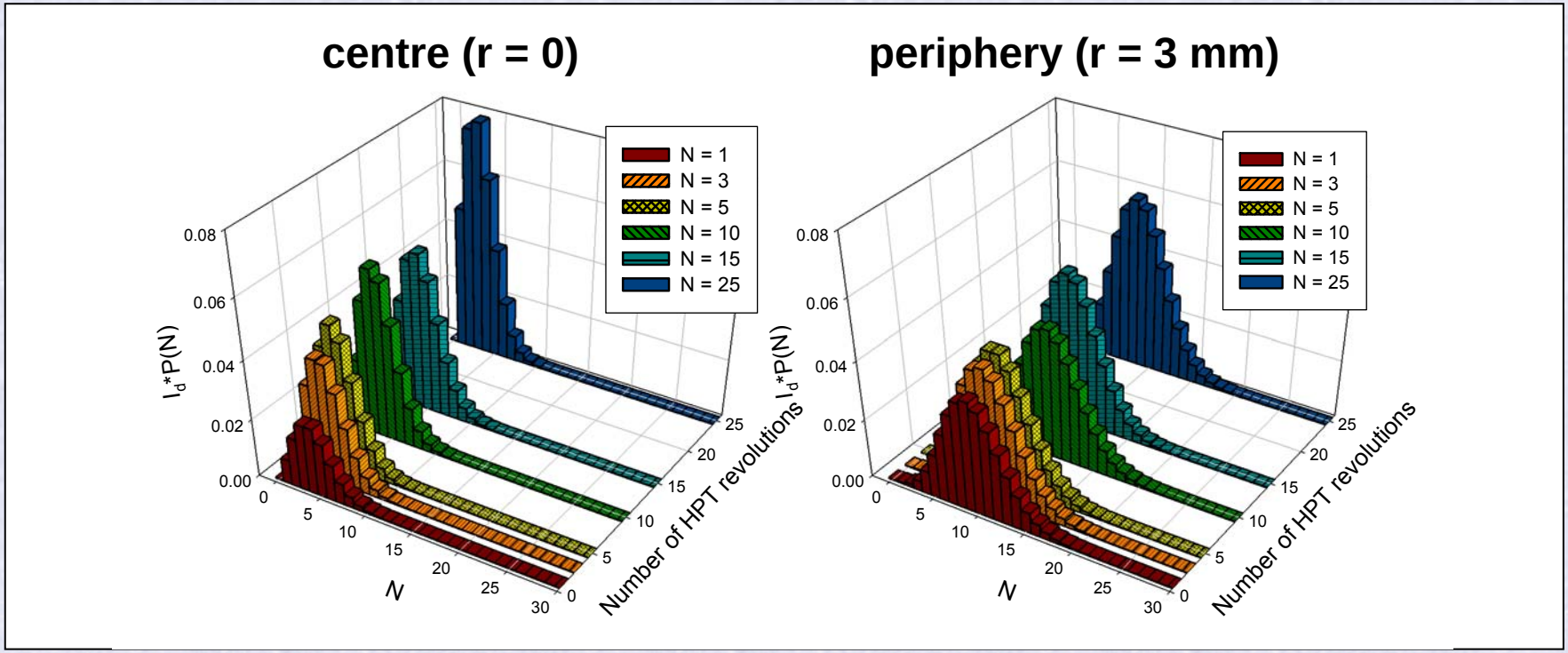

Production of deformation-induced vacancies

- production rate of deformation-induced vacancies

$$\Pi = \alpha \frac{\sigma \Omega_0}{E_f} \dot{\varepsilon}$$

strain rate

- coefficient $\alpha \approx 0.1$ *G. Gottstein et al. Acta Mater.* ***23****, 641 (1975*)
- σ: applied stress
- Ω_0 : atomic volume
- E_f : vacancy formation energy
- $\dot{\varepsilon}$: strain rate

HPT deformation

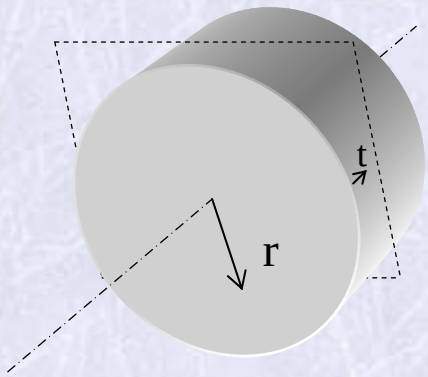

- strain rate increases with r

Mapping of spatial distribution of defects

- spatially resolved LT investigations (1 point ≈ 1 day)
- diameter of positron source spot < 1 mm
- spatial resolution ≈ 0.5 mm

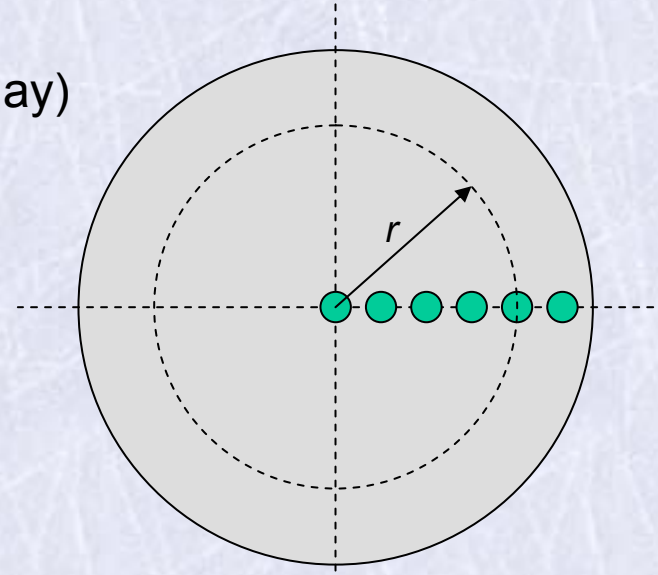

- spatially resolved DB mapping (1 point ≈ 30 min)
- diameter of positron source spot < 1 mm
- spatial resolution ≈ 0.5 mm

J. Čížek et al., Scripta Mater. ***65****, 171 (2011)*

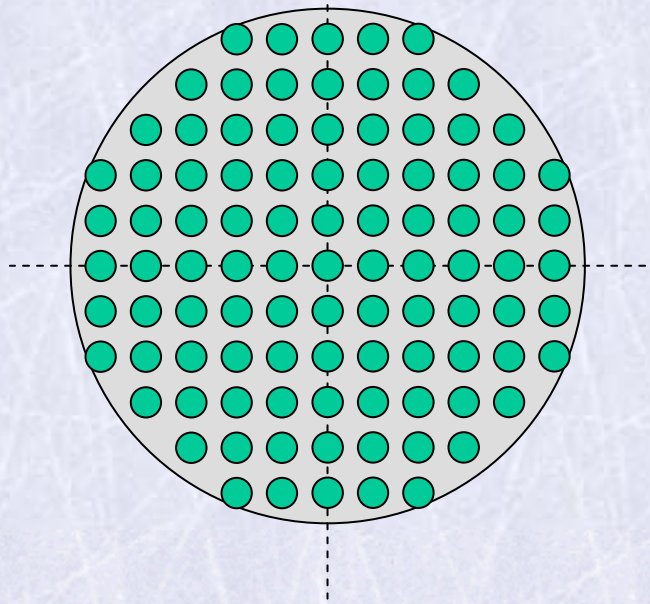

Mapping of spatial distribution of defects

- Vickers microhardness mapping
- automatic hardness tester Struers Durascan
- loading force 1 N applied for 10 s
- spatial resolution ≈ 50 μm

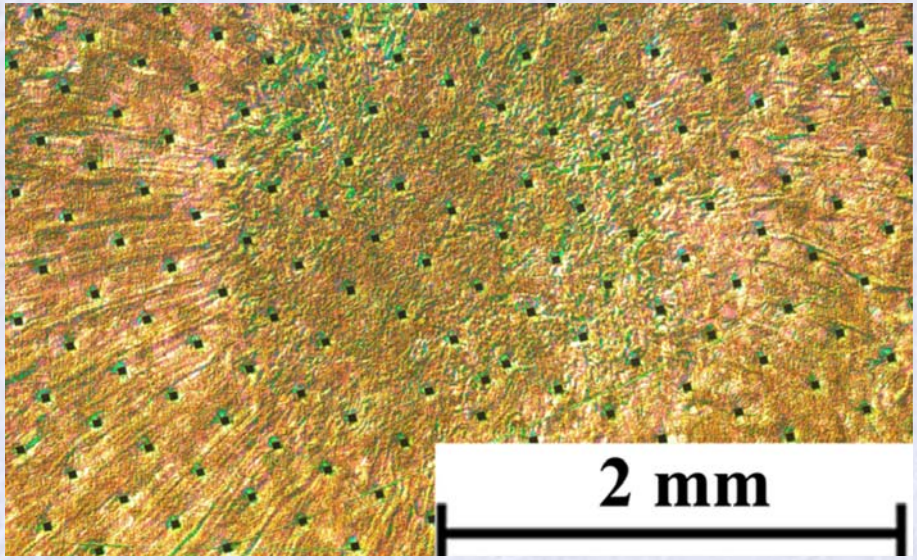

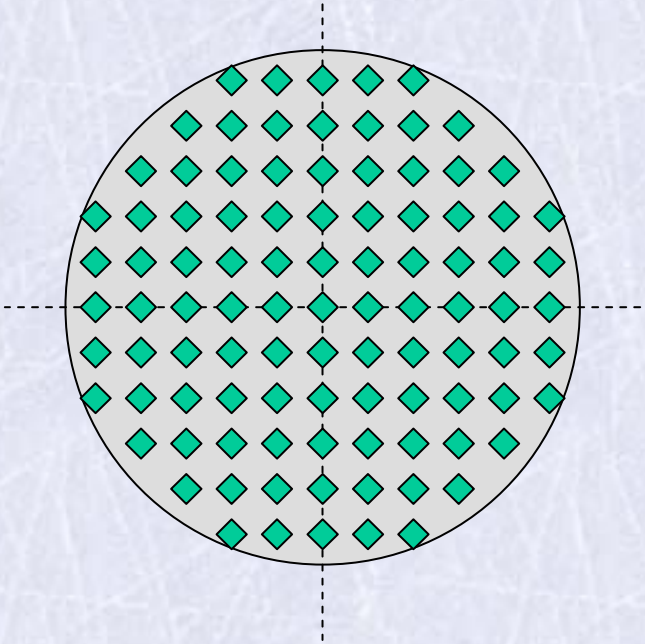

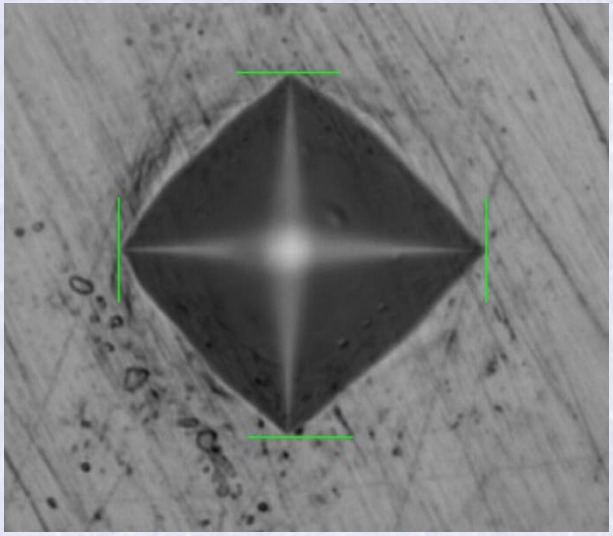

Spatial distribution of defects - microhardness (HV)

UFG Cu, HPT deformed, p = 6 GPa

- HV is influenced

  - by dislocations

$$HV \approx \sqrt{\rho_D}$$

(strain hardening)

  - by grain size

$$HV \approx d^{-1/2}$$

(Hall-Petch relation)

  - but not by vacancies

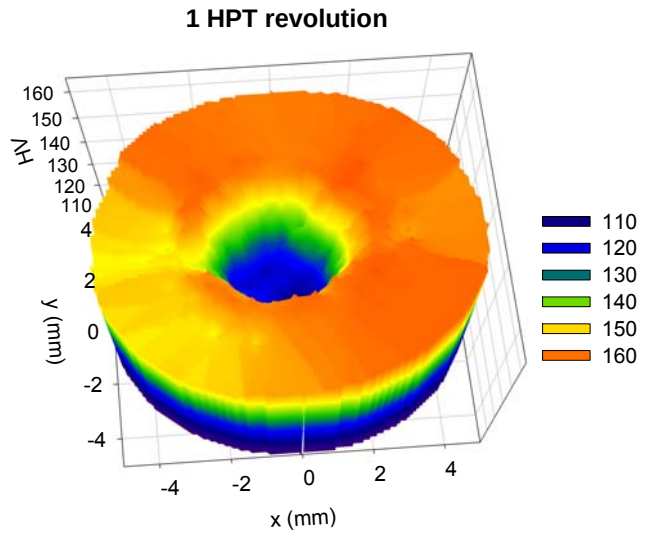

Spatial distribution of defects - microhardness (HV)

UFG Cu, HPT deformed, p = 6 GPa

- HV is influenced
  - by dislocations

    $$HV \approx \sqrt{\rho_D}$$

    (strain hardening)
  - by grain size

    $$HV \approx d^{-1/2}$$

    (Hall-Petch relation)
  - but not by vacancies

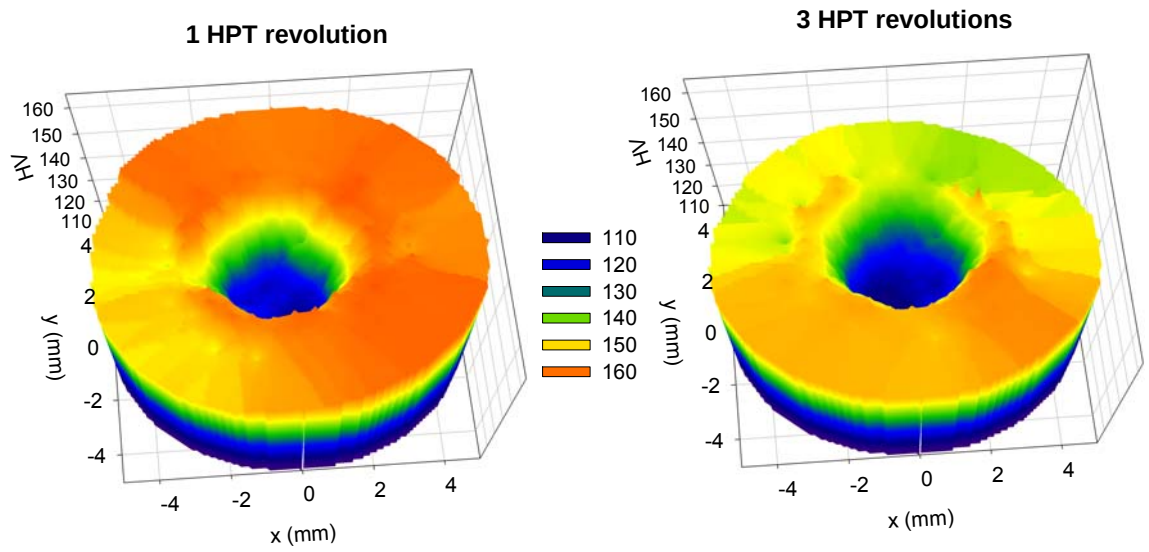

Spatial distribution of defects - microhardness (HV)

UFG Cu, HPT deformed, p = 6 GPa

- HV is influenced
  - by dislocations

$$HV \approx \sqrt{\rho_D}$$

(strain hardening)

  - by grain size

$$HV \approx d^{-1/2}$$

(Hall-Petch relation)

  - but not by vacancies

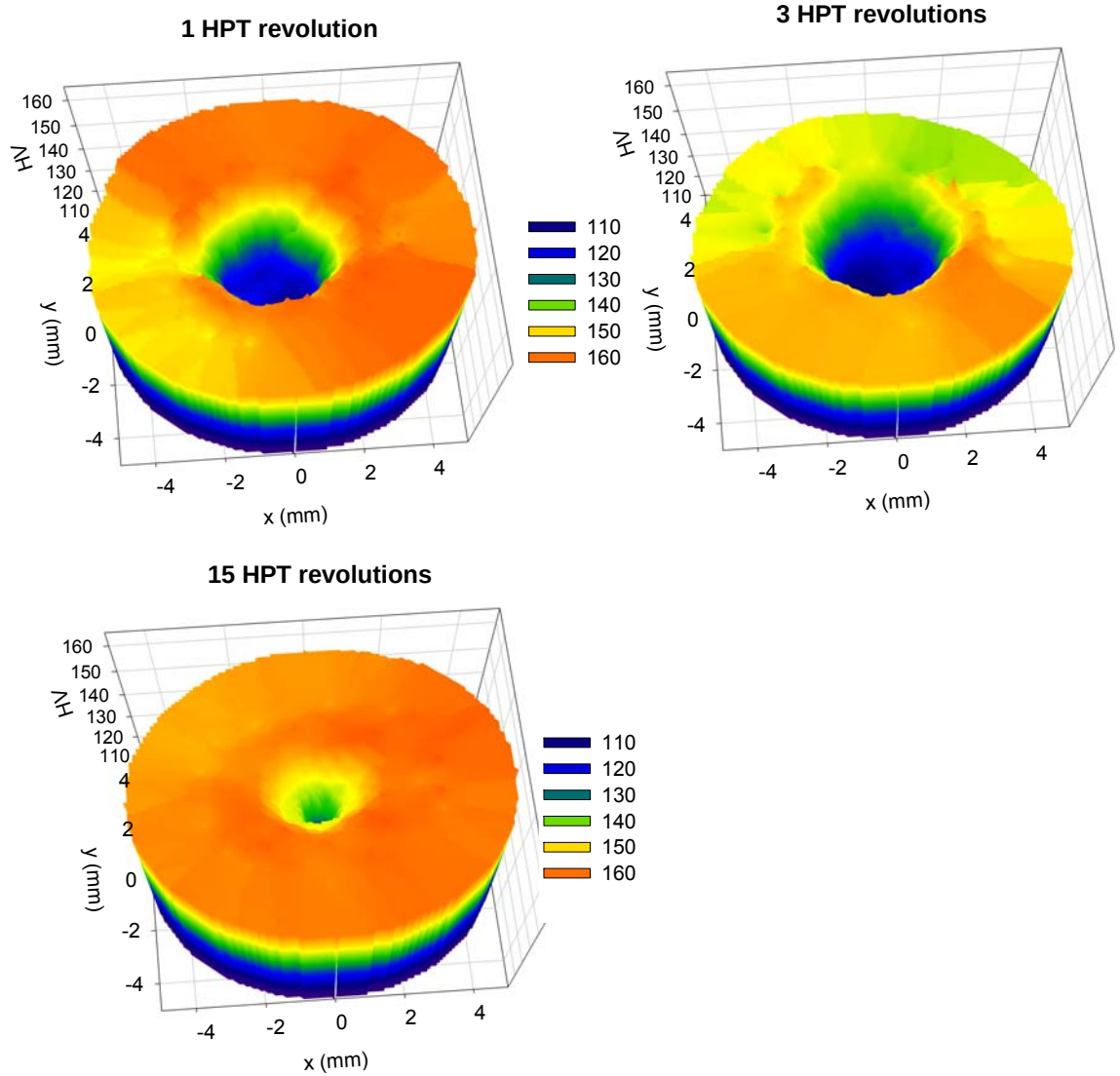

Spatial distribution of defects - microhardness (HV)

UFG Cu, HPT deformed, p = 6 GPa

- HV is influenced
  - by dislocations

$$HV \approx \sqrt{\rho_D}$$

(strain hardening)

  - by grain size

$$HV \approx d^{-1/2}$$

(Hall-Petch relation)

  - but not by vacancies

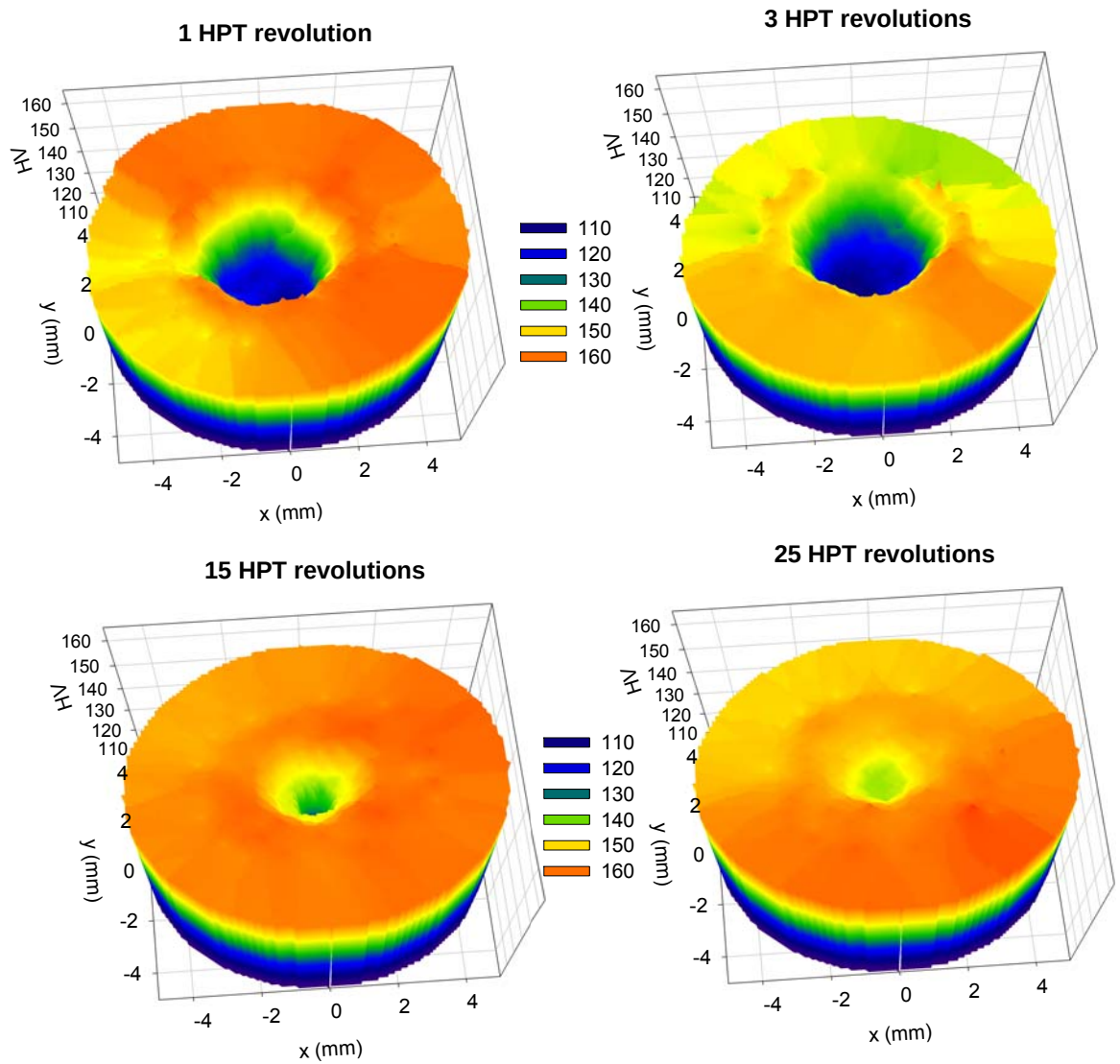

Spatial distribution of defects - microhardness (HV)

UFG Cu, HPT deformed, p = 6 GPa

- HV is almost uniform after 15 HPT revolutions
- except of a small region just in the center

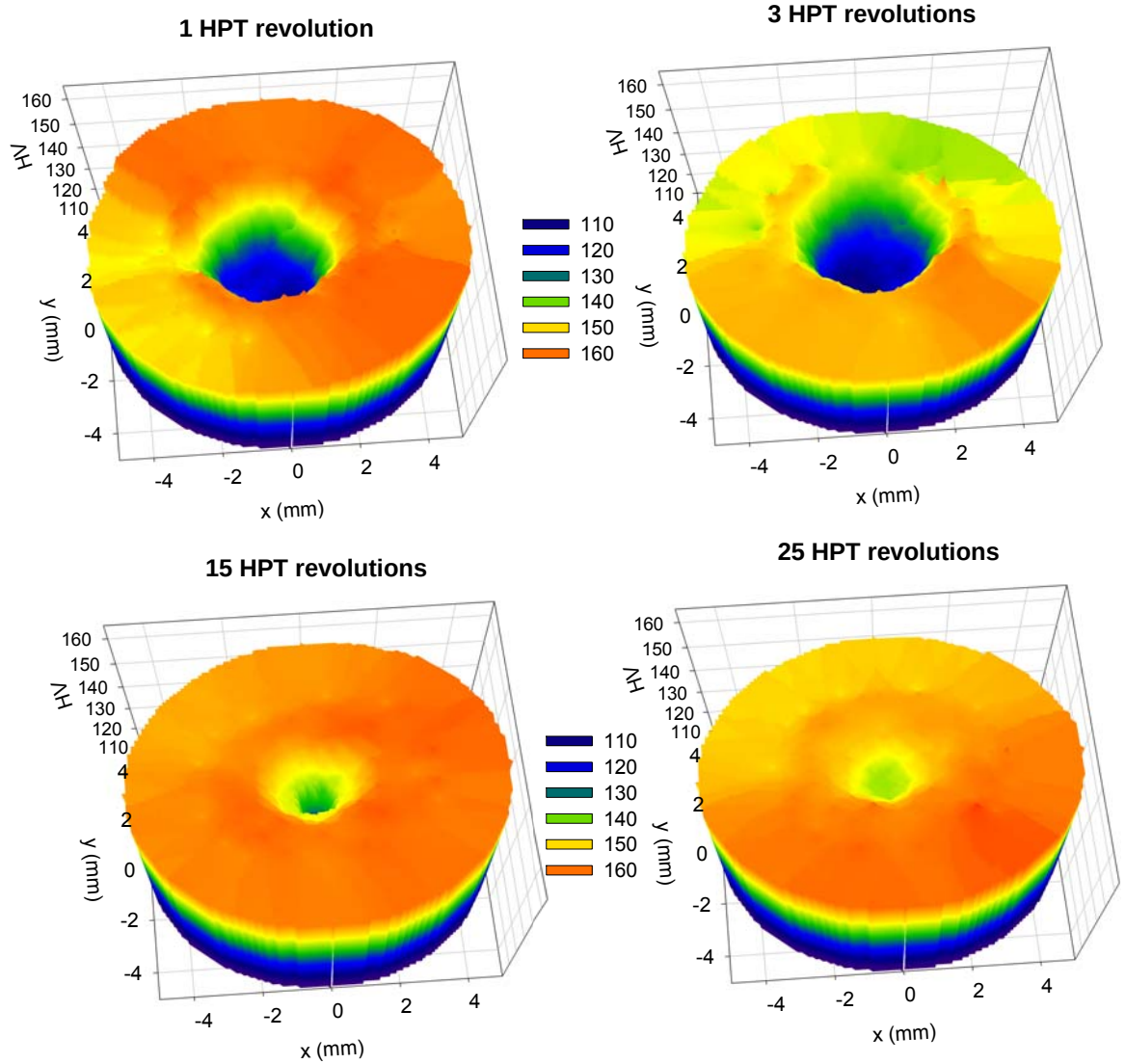

Homogeneity of microstructure - TEM

- **HPT deformed Cu, p = 6 GPa, N = 15**

center (r = 0)

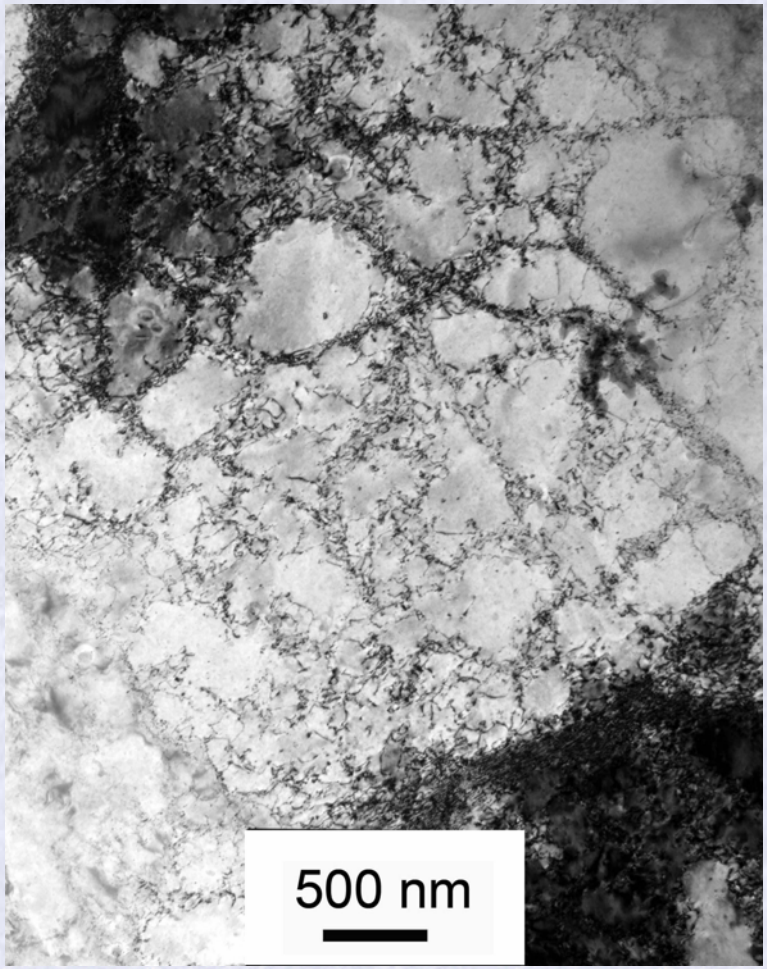

periphery (r = 3.5 mm)

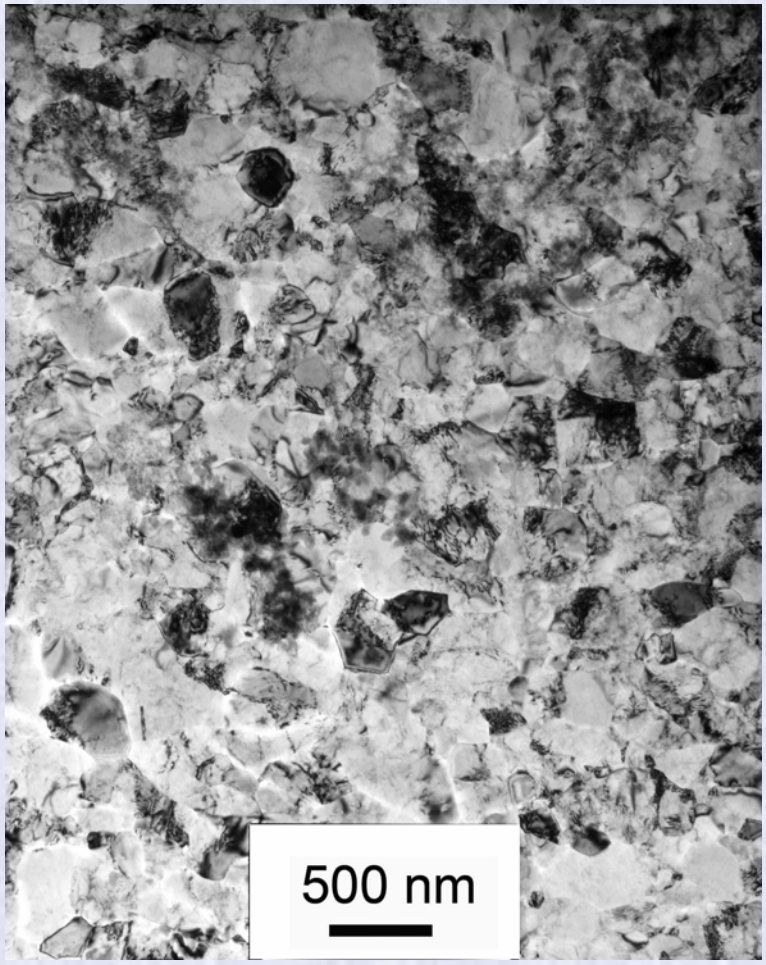

Spatial distribution of defects – *S* parameter

UFG Cu, HPT deformed, p = 6 GPa

- *S* parameter is sensitive to
  - dislocation density
  - size and concentration of vacancy clusters

1 HPT revolution

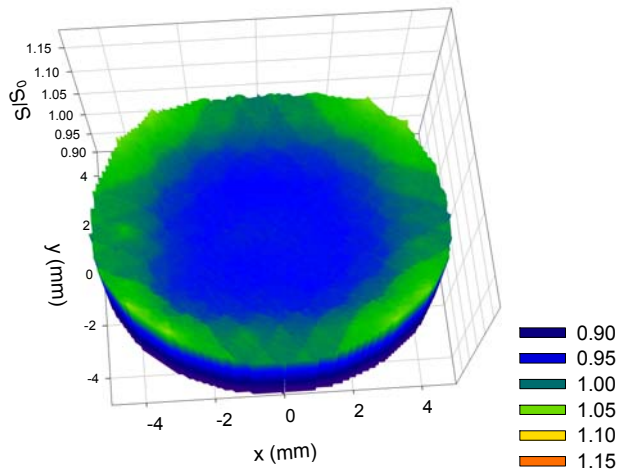

Spatial distribution of defects – *S* parameter

UFG Cu, HPT deformed, p = 6 GPa

- *S* parameter is sensitive to
  - dislocation density
  - size and concentration of vacancy clusters

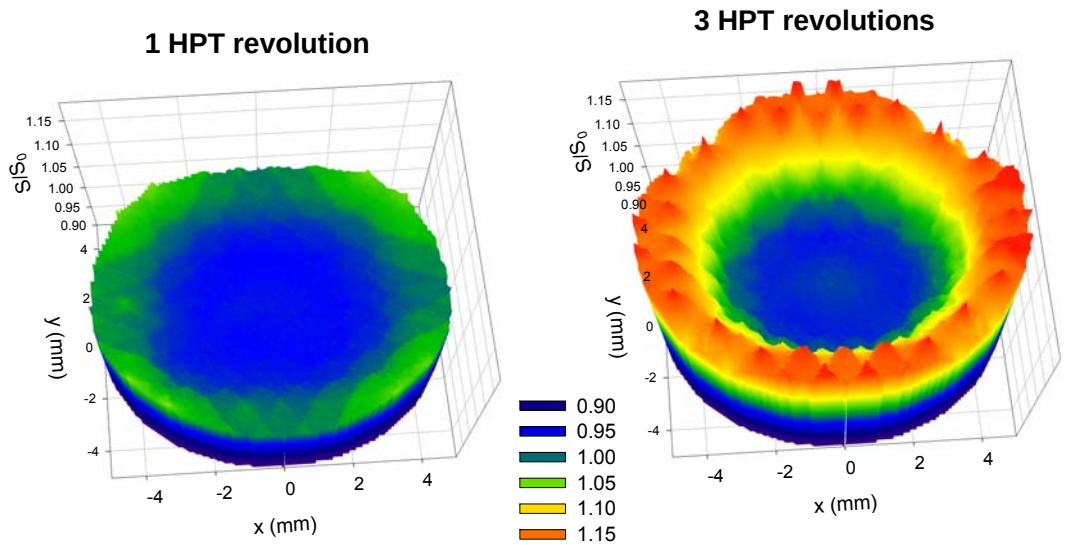

Spatial distribution of defects – *S* parameter

UFG Cu, HPT deformed, p = 6 GPa

- *S* parameter is sensitive to
  - dislocation density
  - size and concentration of vacancy clusters

1 HPT revolution

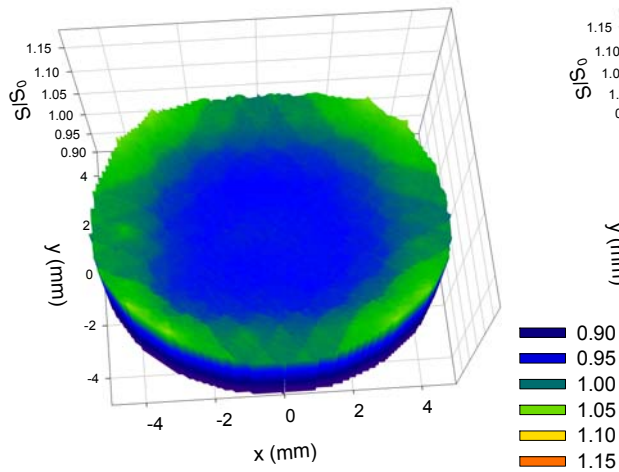

3 HPT revolutions

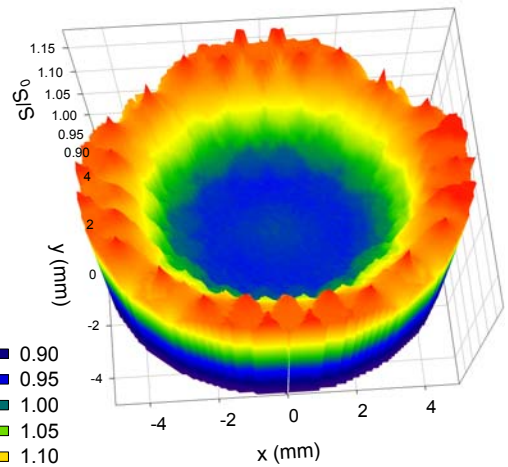

15 HPT revolutions

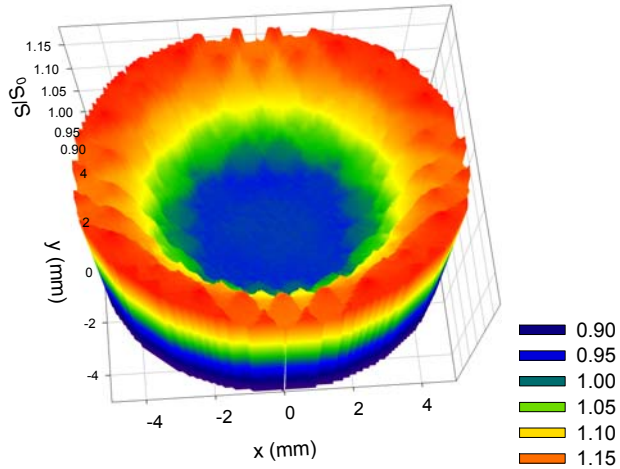

Spatial distribution of defects – *S* parameter

UFG Cu, HPT deformed, p = 6 GPa

- *S* parameter is sensitive to
  - dislocation density
  - size and concentration of vacancy clusters

- *S* parameter increases with *r*

↓

- increasing size of vacancy clusters

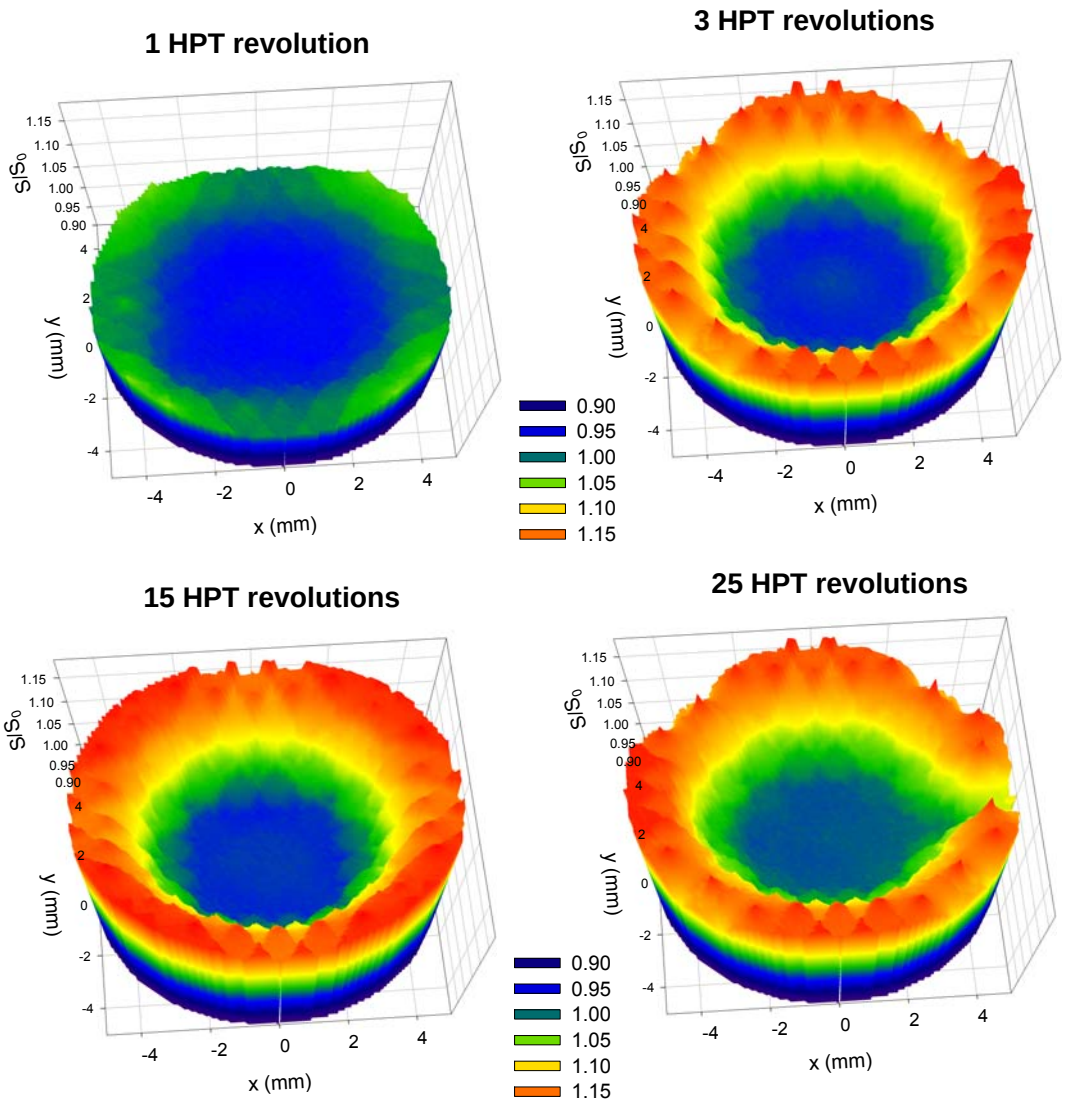

Spatial distribution of defects - comparison of HV and *S* parameter

UFG Cu, HPT deformed, p = 6 GPa, 25 HPT revolutions

microhardness

- **microhardness (HV)** is influenced by
  - grain size
  - dislocation density

for more than 25 HPT revolutions HV becomes uniform

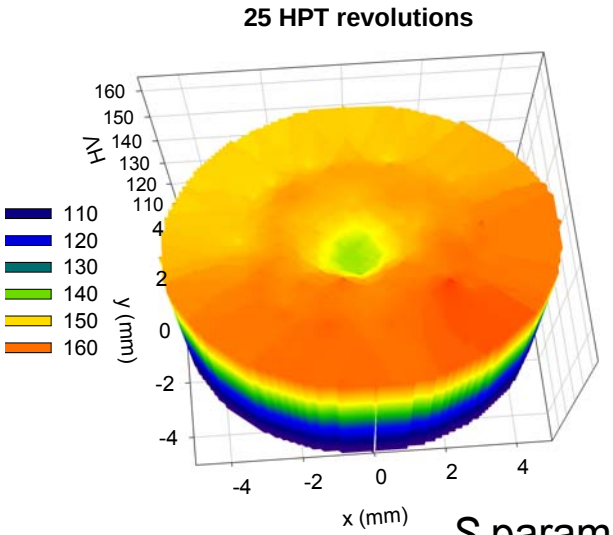

S parameter

- **S parameter** is influenced by
  - dislocation density
  - cocentration and size of vacancy clusters

after 25 HPT revolutions S is still higher at the periphery

- **spatial distribution of vacancy clusters is far from being uniform even after 25 HPT rotations**

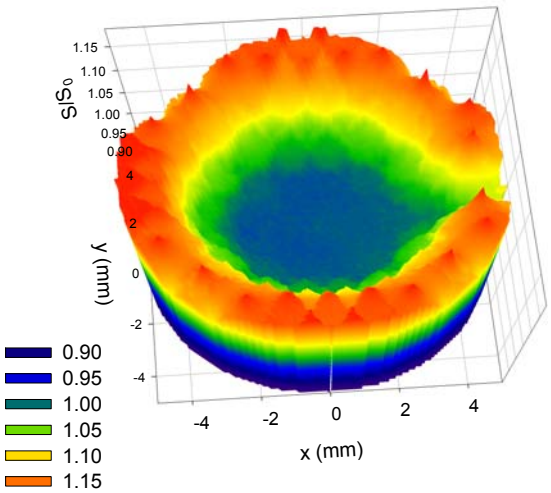

Spatial distribution of defects – LT spectroscopy

- HPT deformed Cu, p = 6 GPa, N = 2
- size & concentration of vacancy clusters increase with *r*

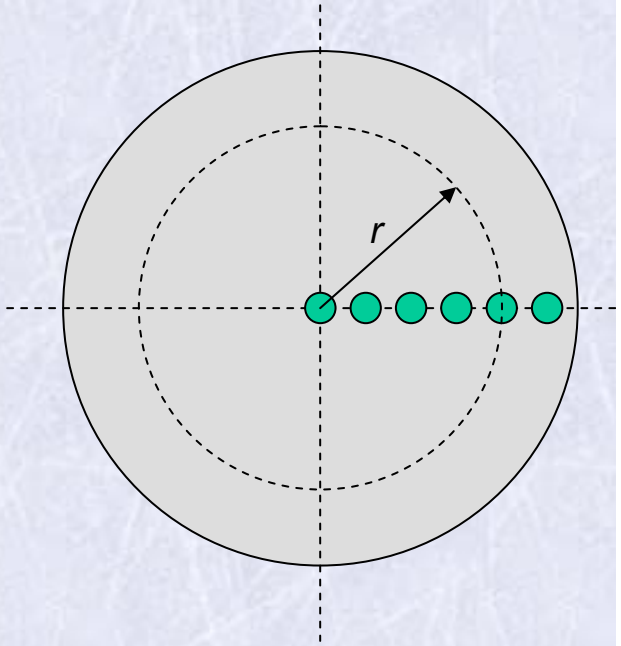

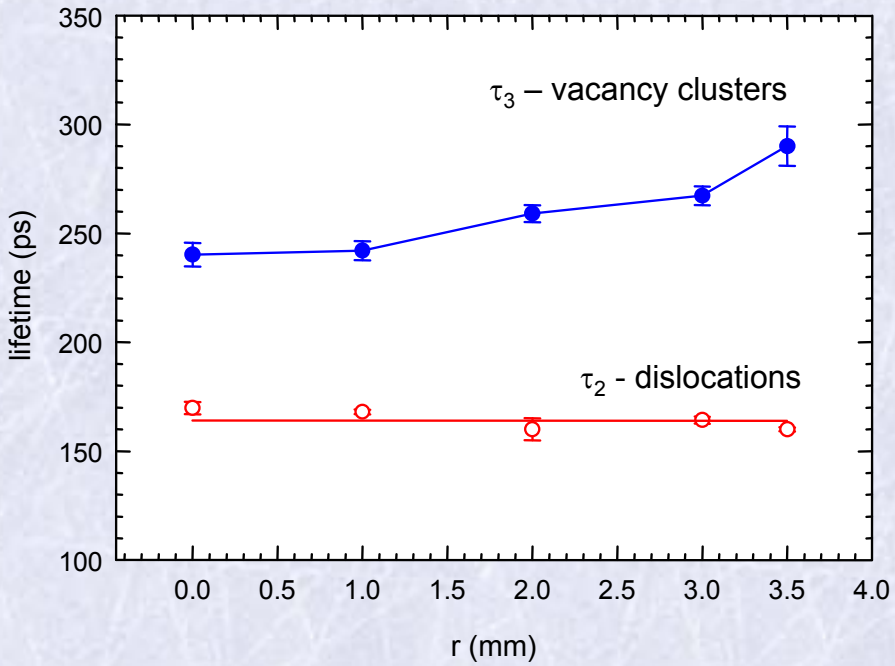

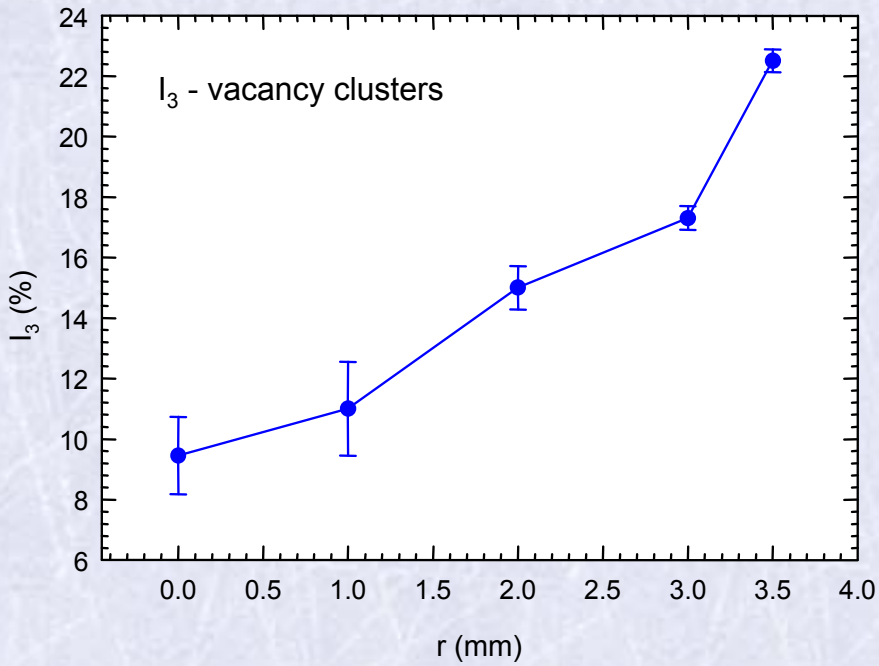

Thermal stability of UFG structure – HV mapping

- HPT deformed Cu, p = 6 GPa, N = 2
- isochronnal annealing 20°C/20 min

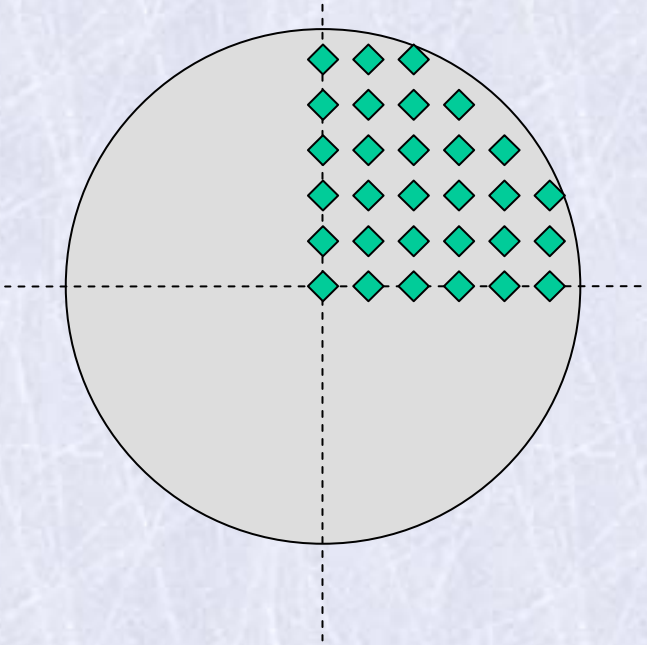

Thermal stability of UFG structure – HV mapping

- HPT deformed Cu, p = 6 GPa, N = 2
- isochronnal annealing 20°C/20 min

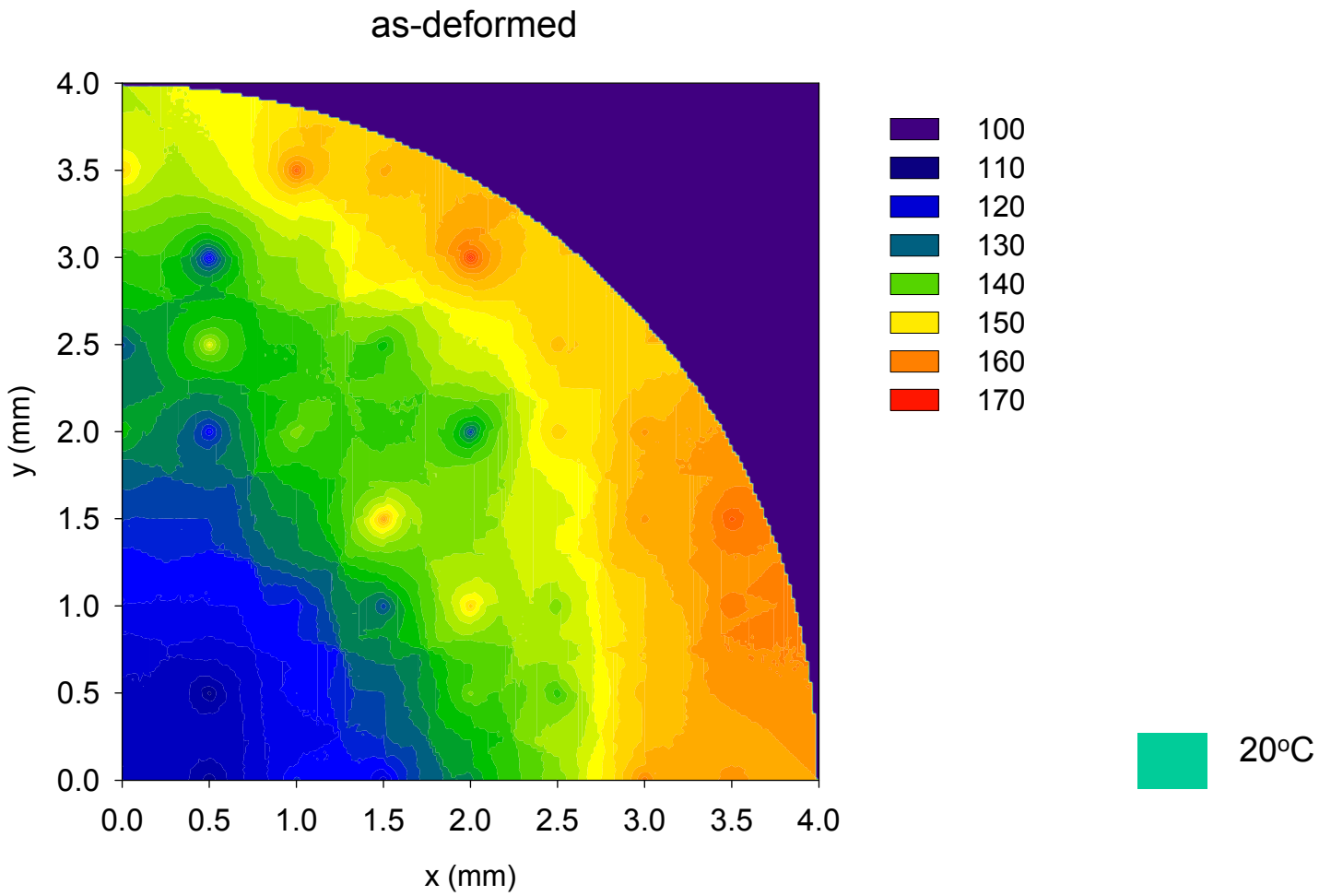

Thermal stability of UFG structure – HV mapping

- HPT deformed Cu, p = 6 GPa, N = 2
- isochronnal annealing 20°C/20 min

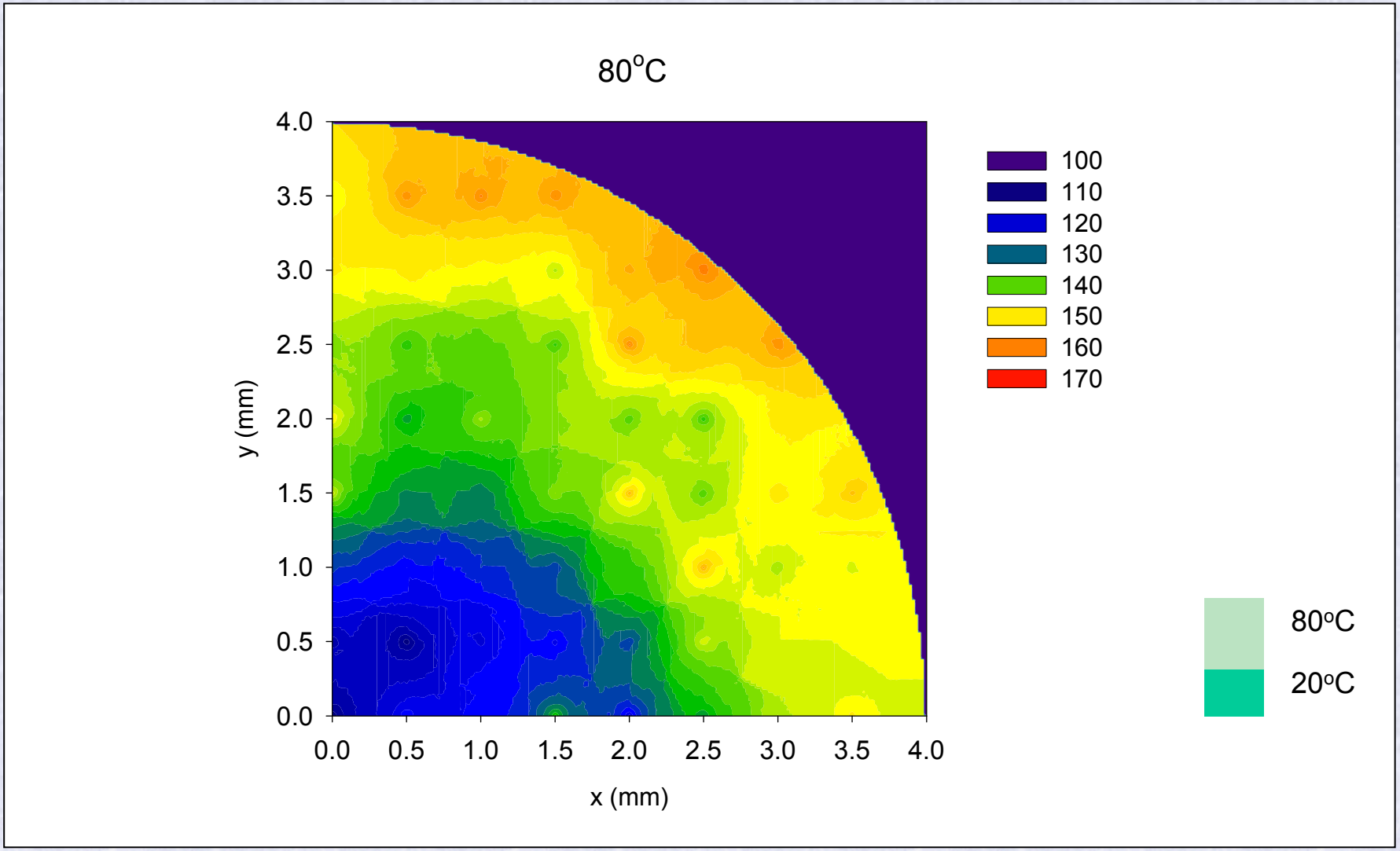

Thermal stability of UFG structure – HV mapping

- HPT deformed Cu, p = 6 GPa, N = 2
- isochronnal annealing 20°C/20 min

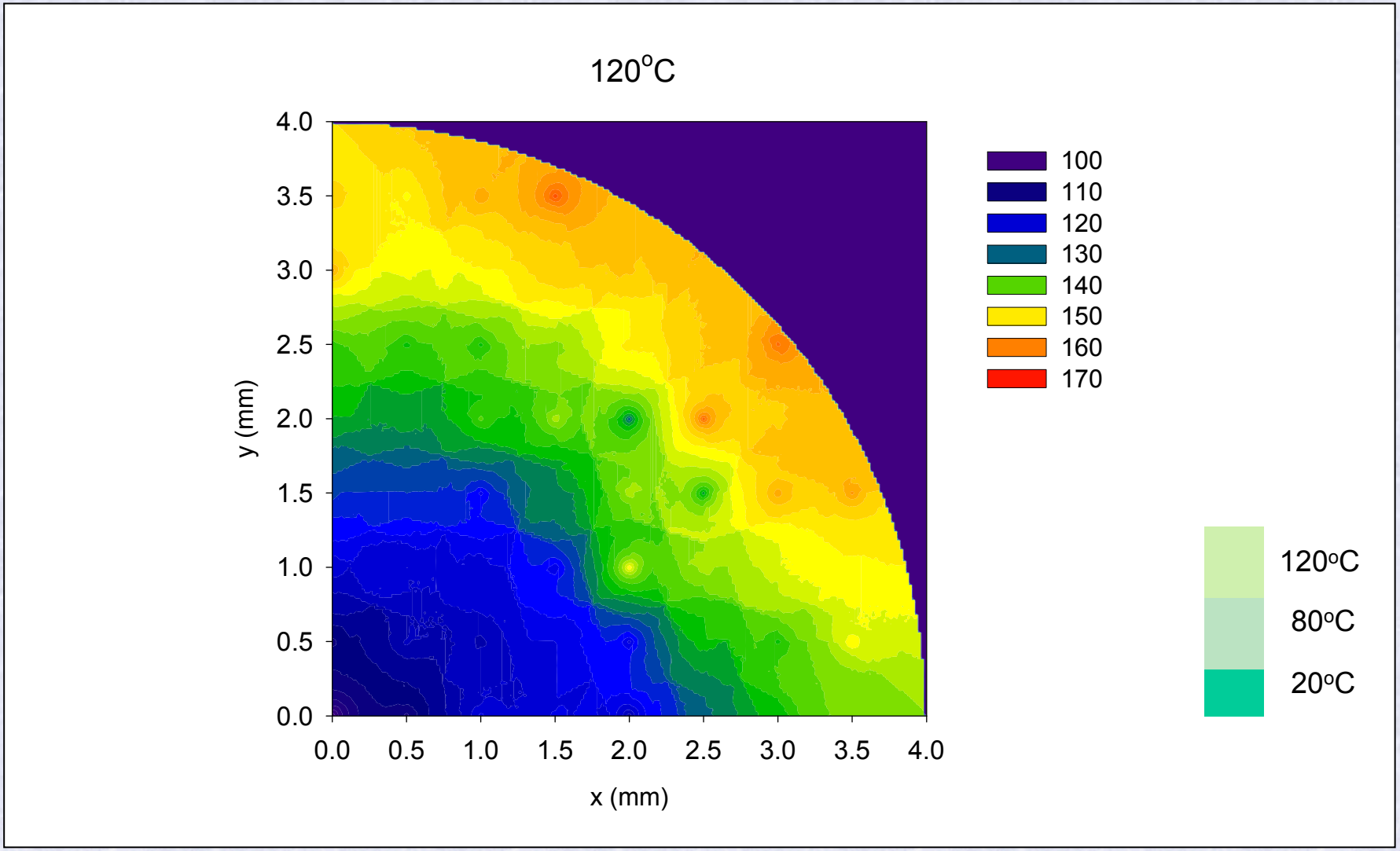

Thermal stability of UFG structure – HV mapping

- HPT deformed Cu, p = 6 GPa, N = 2
- isochronnal annealing 20°C/20 min

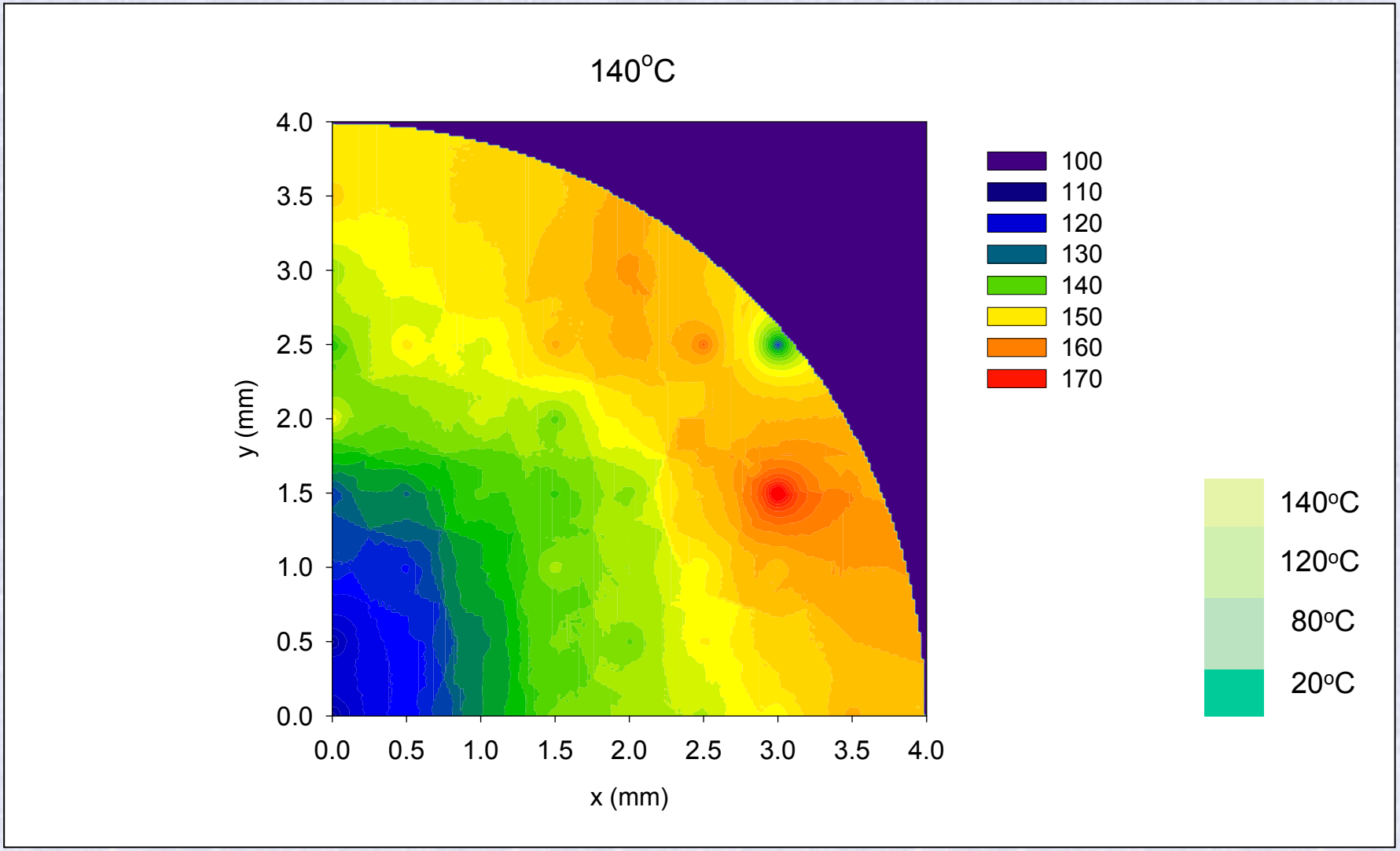

Thermal stability of UFG structure – HV mapping

- HPT deformed Cu, p = 6 GPa, N = 2
- isochronnal annealing 20°C/20 min

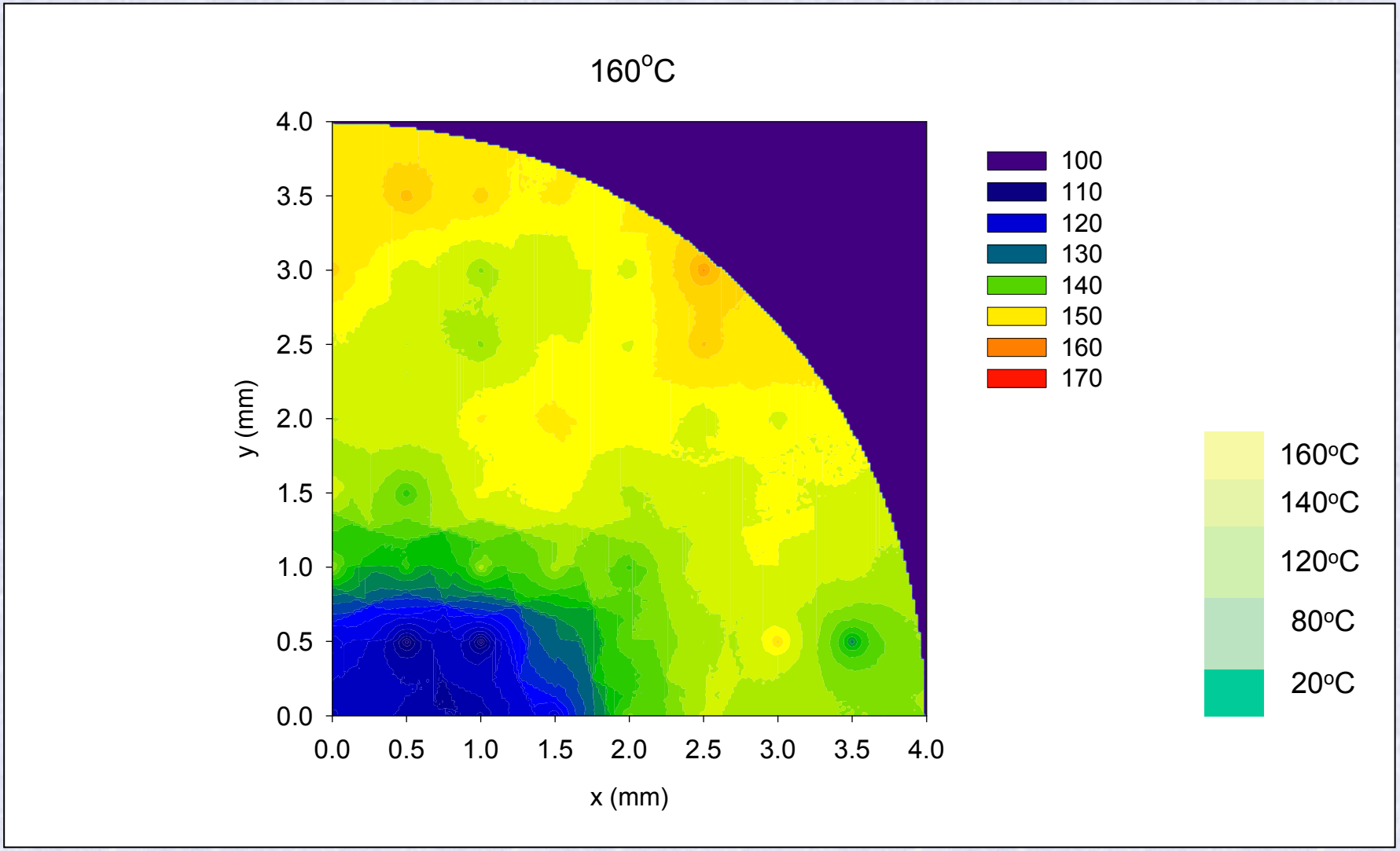

Thermal stability of UFG structure – HV mapping

- HPT deformed Cu, p = 6 GPa, N = 2
- isochronnal annealing 20°C/20 min

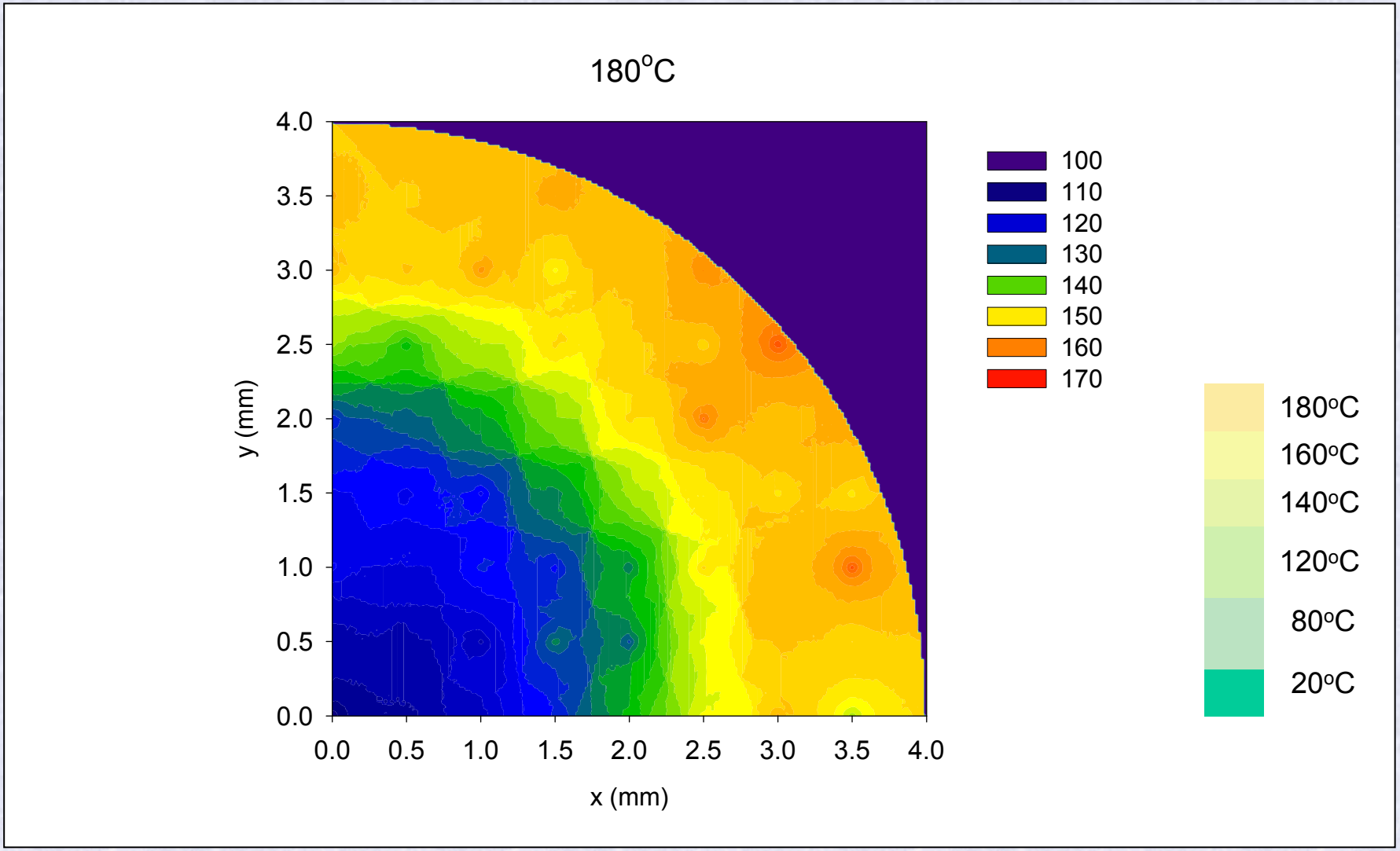

Thermal stability of UFG structure – HV mapping

- HPT deformed Cu, p = 6 GPa, N = 2
- isochronnal annealing 20°C/20 min

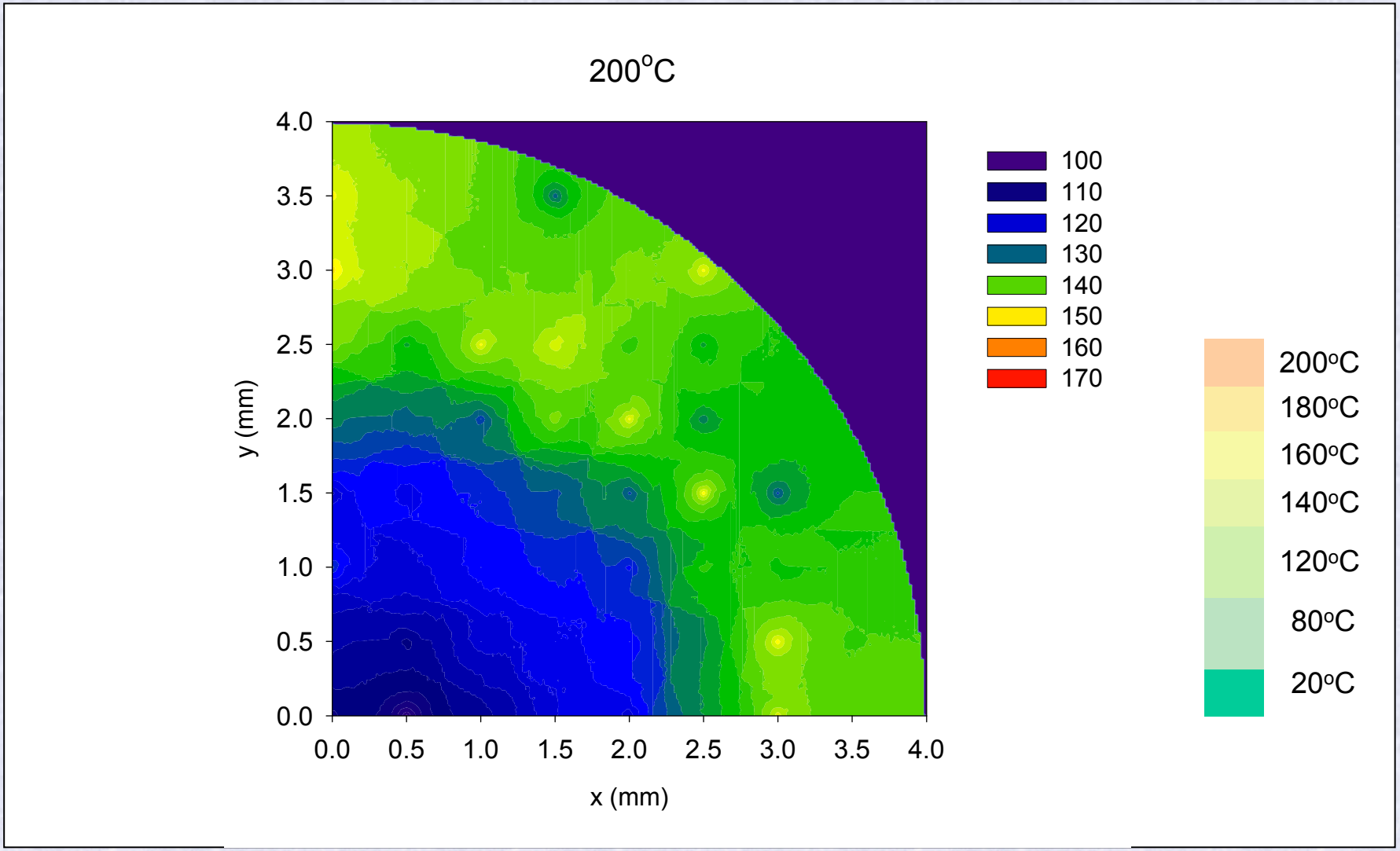

Thermal stability of UFG structure – HV mapping

- HPT deformed Cu, p = 6 GPa, N = 2
- isochronnal annealing 20°C/20 min

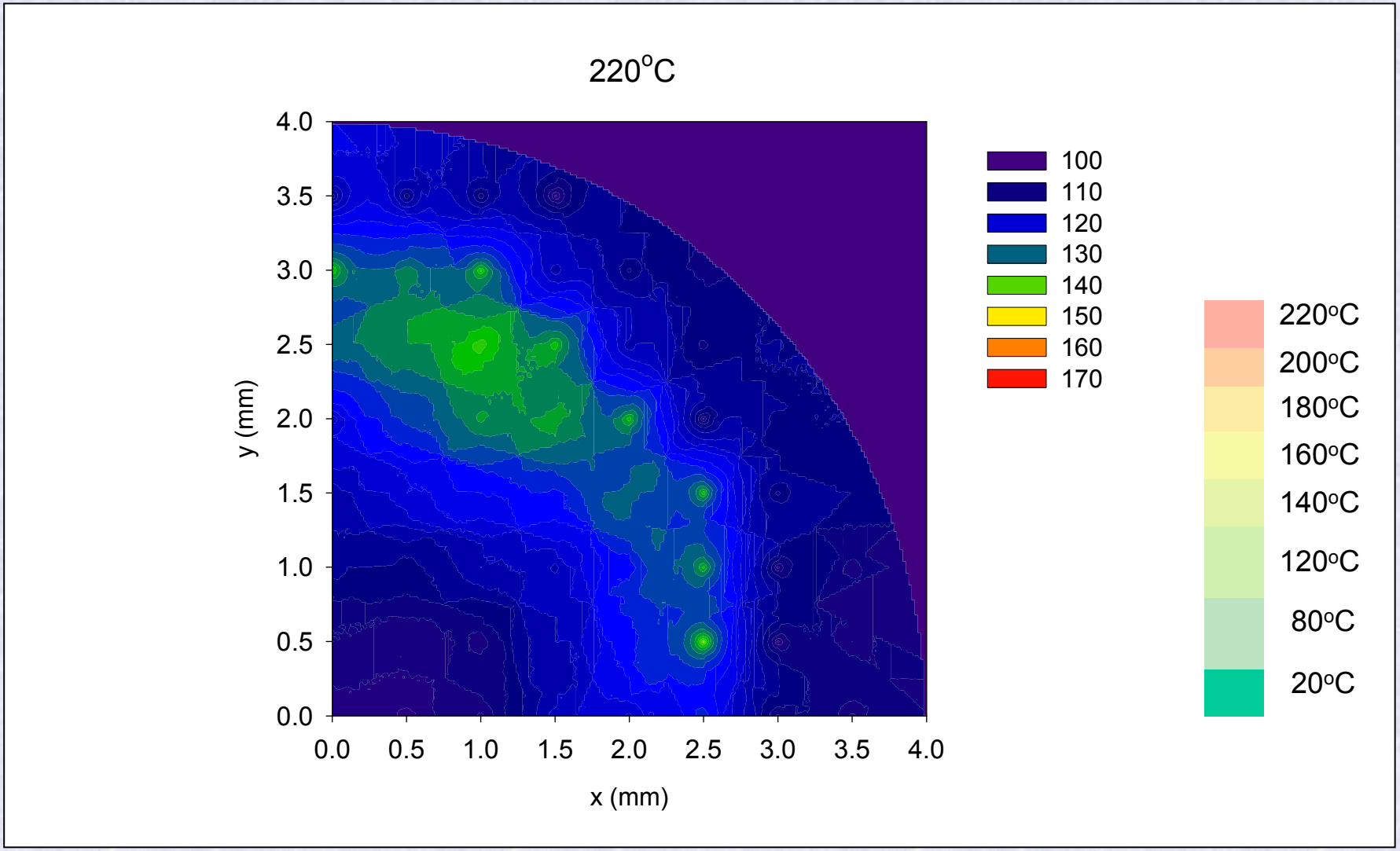

Thermal stability of UFG structure – HV mapping

- HPT deformed Cu, p = 6 GPa, N = 2
- isochronnal annealing 20°C/20 min

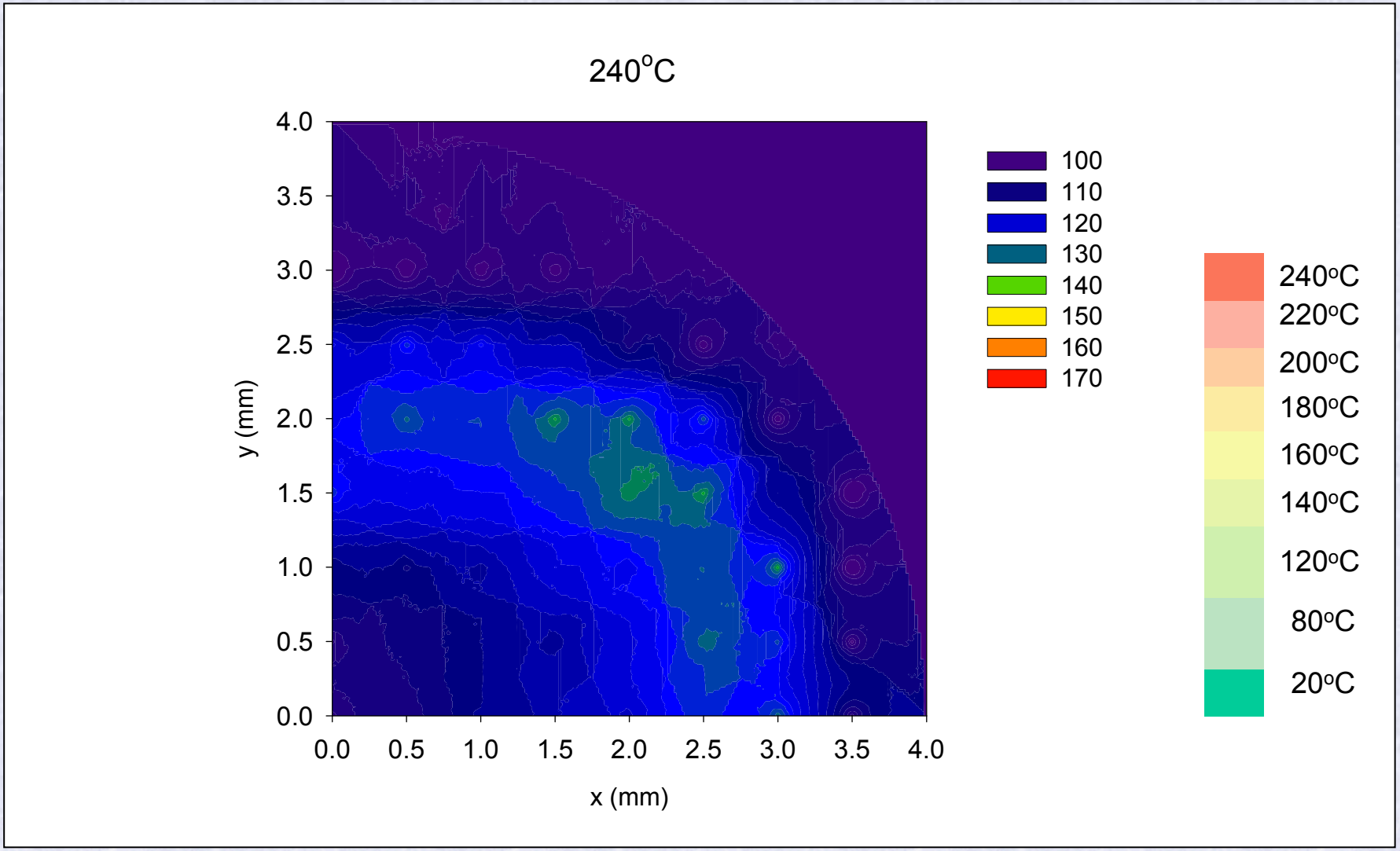

Thermal stability of UFG structure – HV mapping

- HPT deformed Cu, p = 6 GPa, N = 2
- isochronnal annealing 20°C/20 min

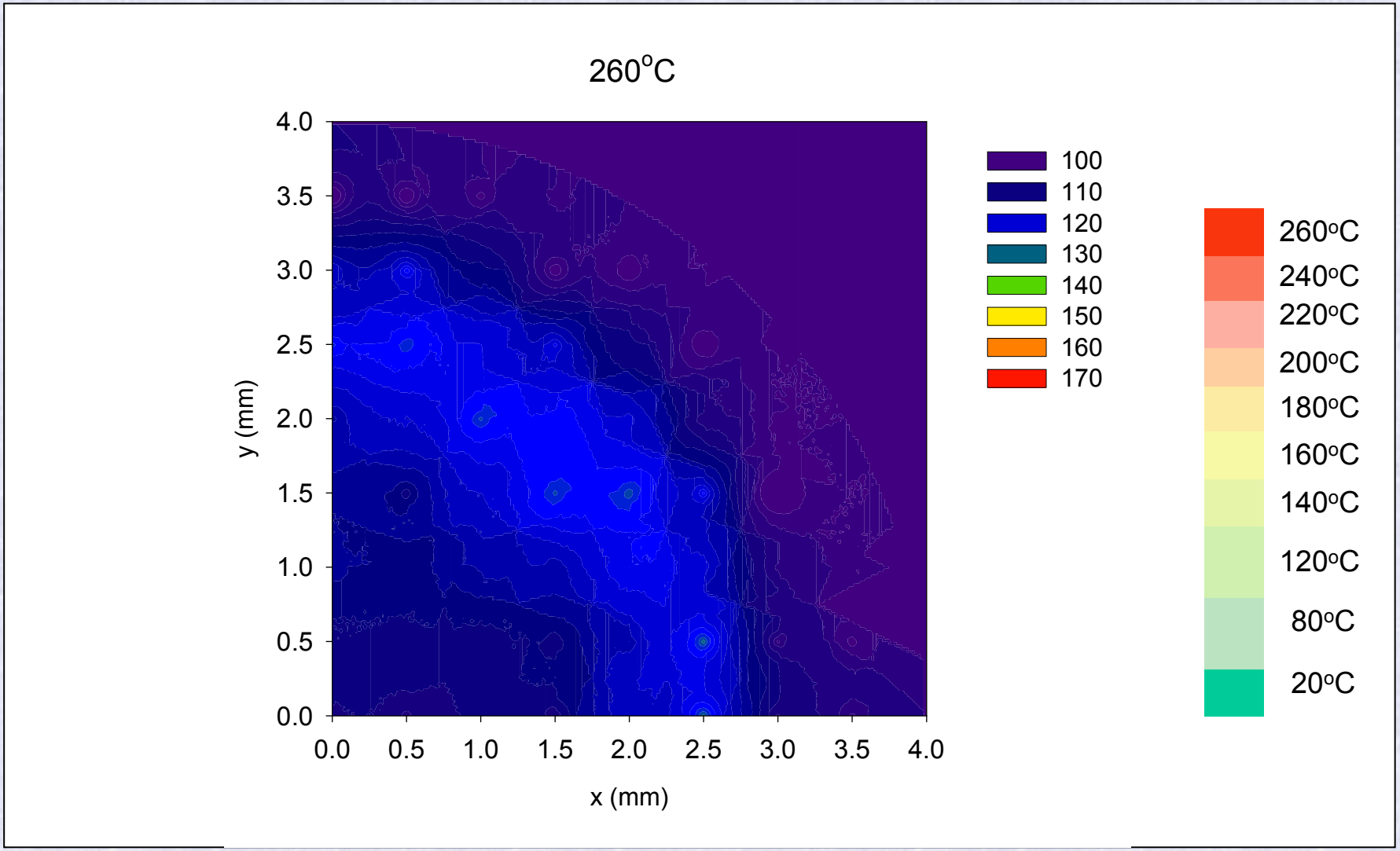

Thermal stability of UFG structure – HV mapping

- HPT deformed Cu, p = 6 GPa, N = 2
- isochronnal annealing 20°C/20 min

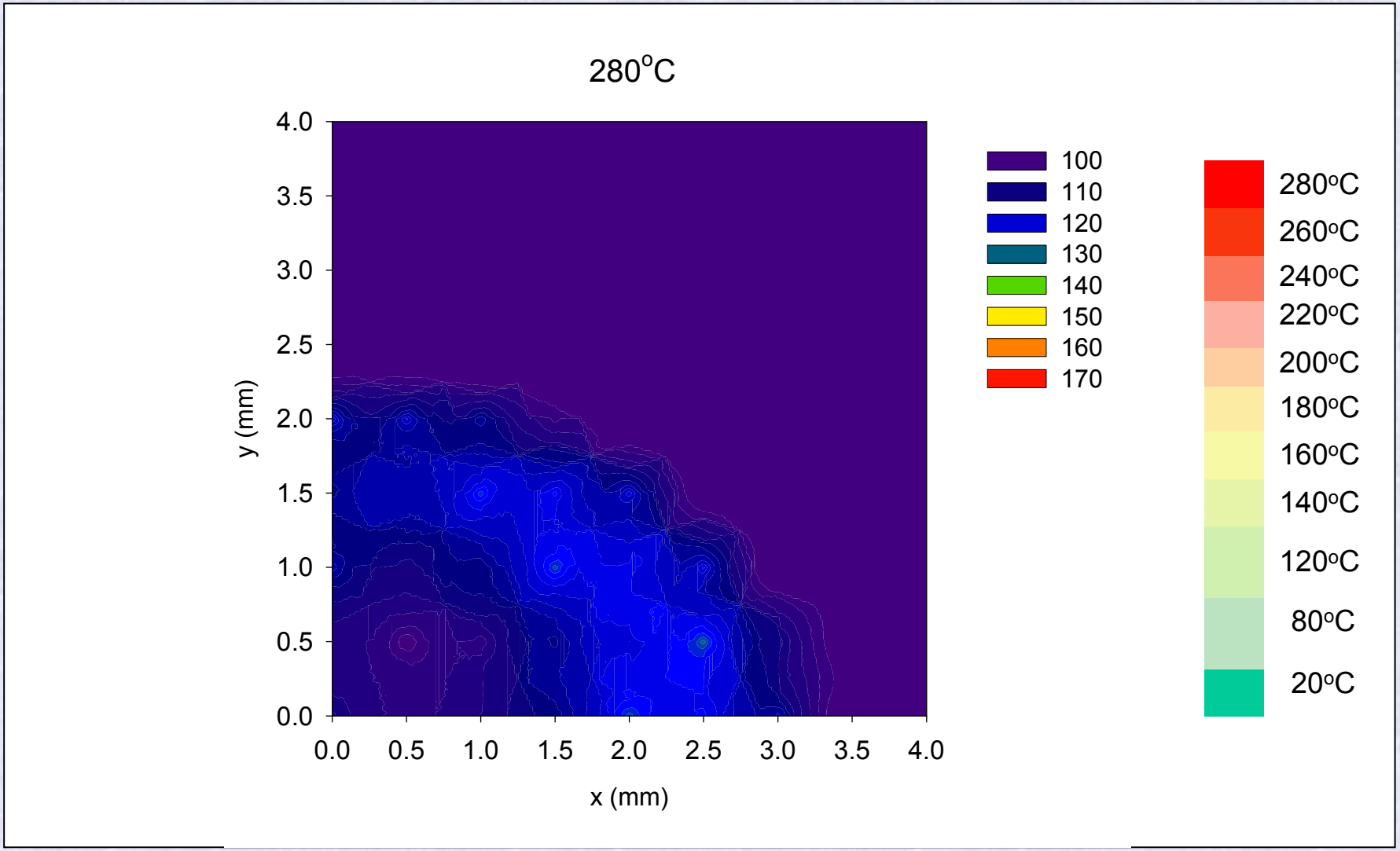

Thermal stability of UFG structure – HV mapping

- HPT deformed Cu, p = 6 GPa, N = 2
- isochronnal annealing 20°C/20 min

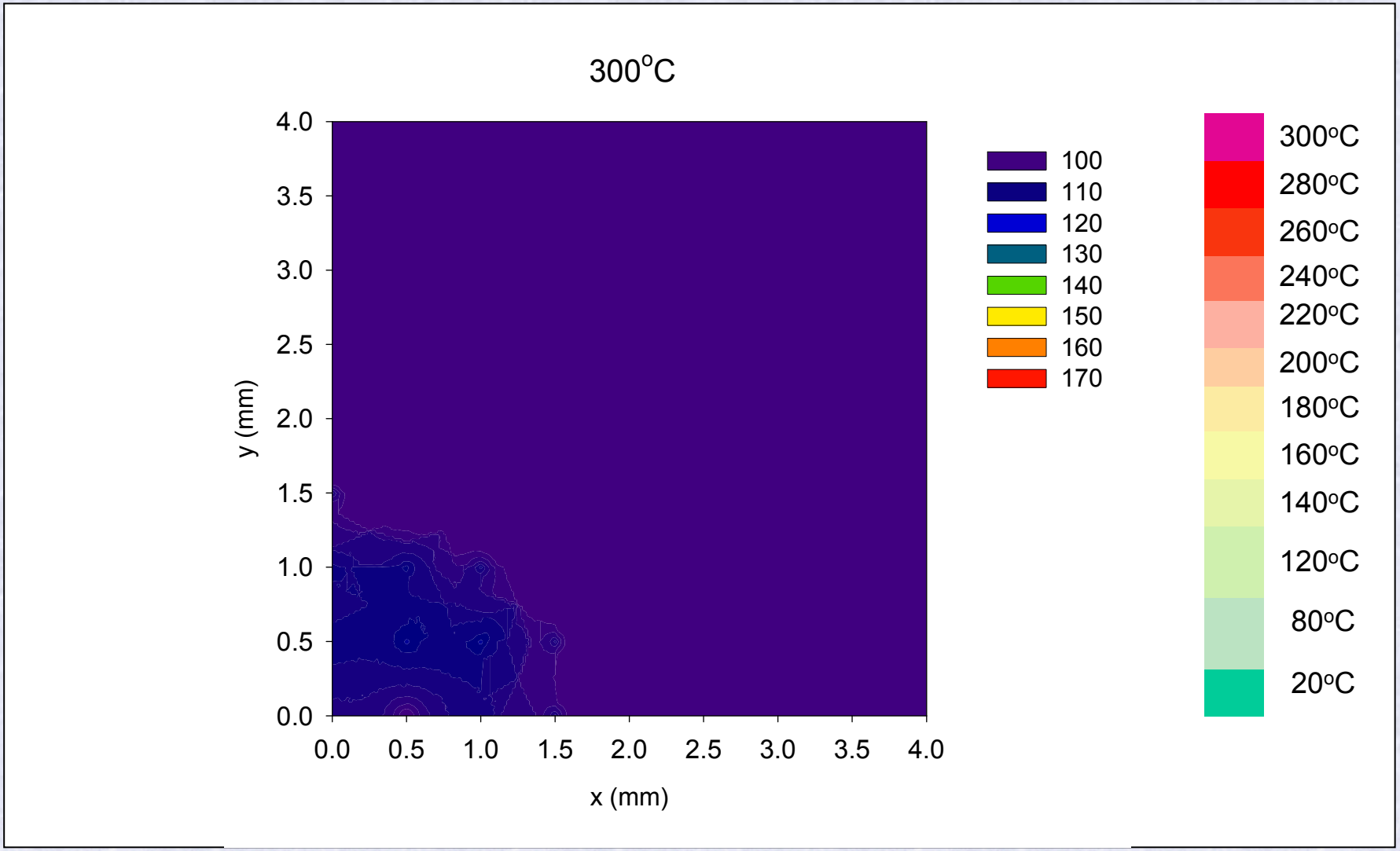

Thermal stability of UFG structure – HV mapping

- HPT deformed Cu, p = 6 GPa, N = 2
- isochronnal annealing 20°C/20 min
- radial dependence of microhardness

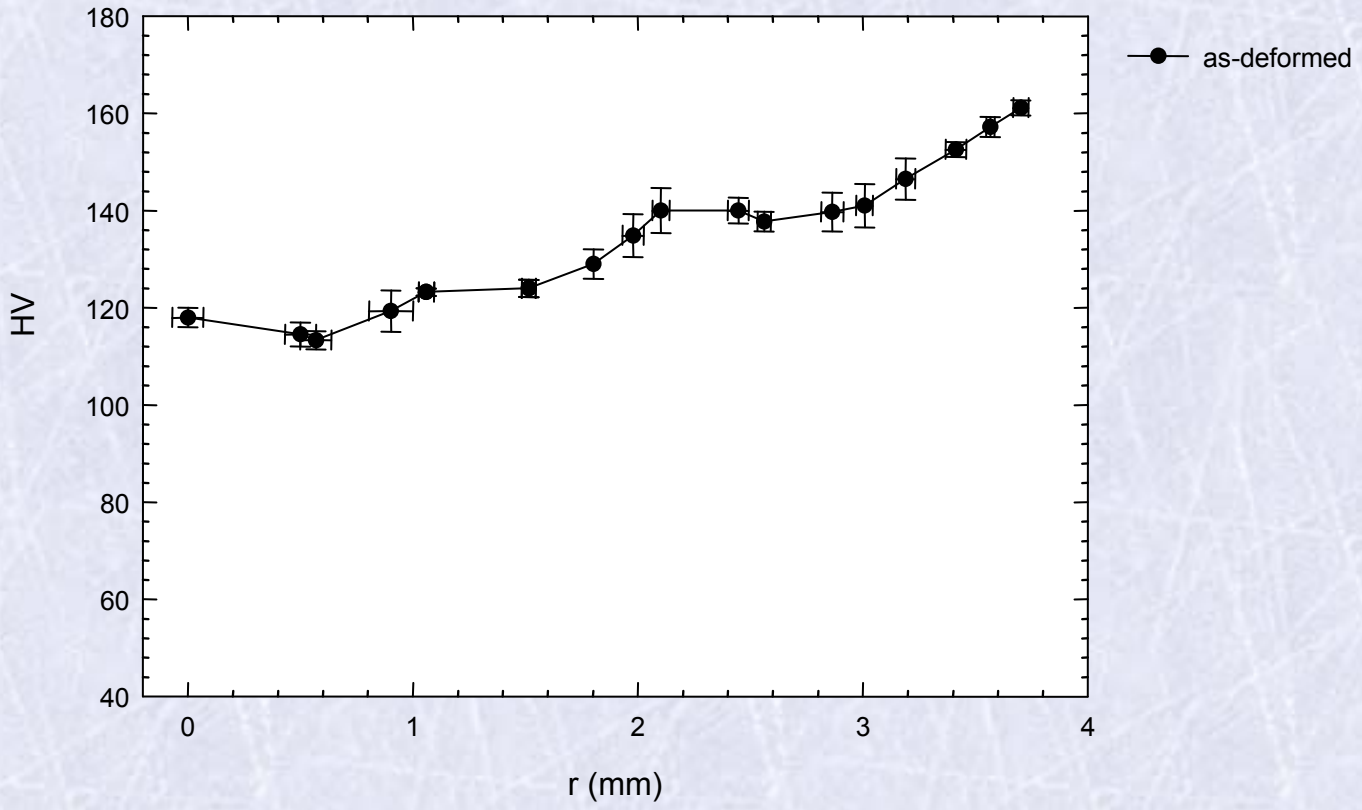

Thermal stability of UFG structure – HV mapping

- HPT deformed Cu, p = 6 GPa, N = 2
- isochronnal annealing 20°C/20 min
- radial dependence of microhardness

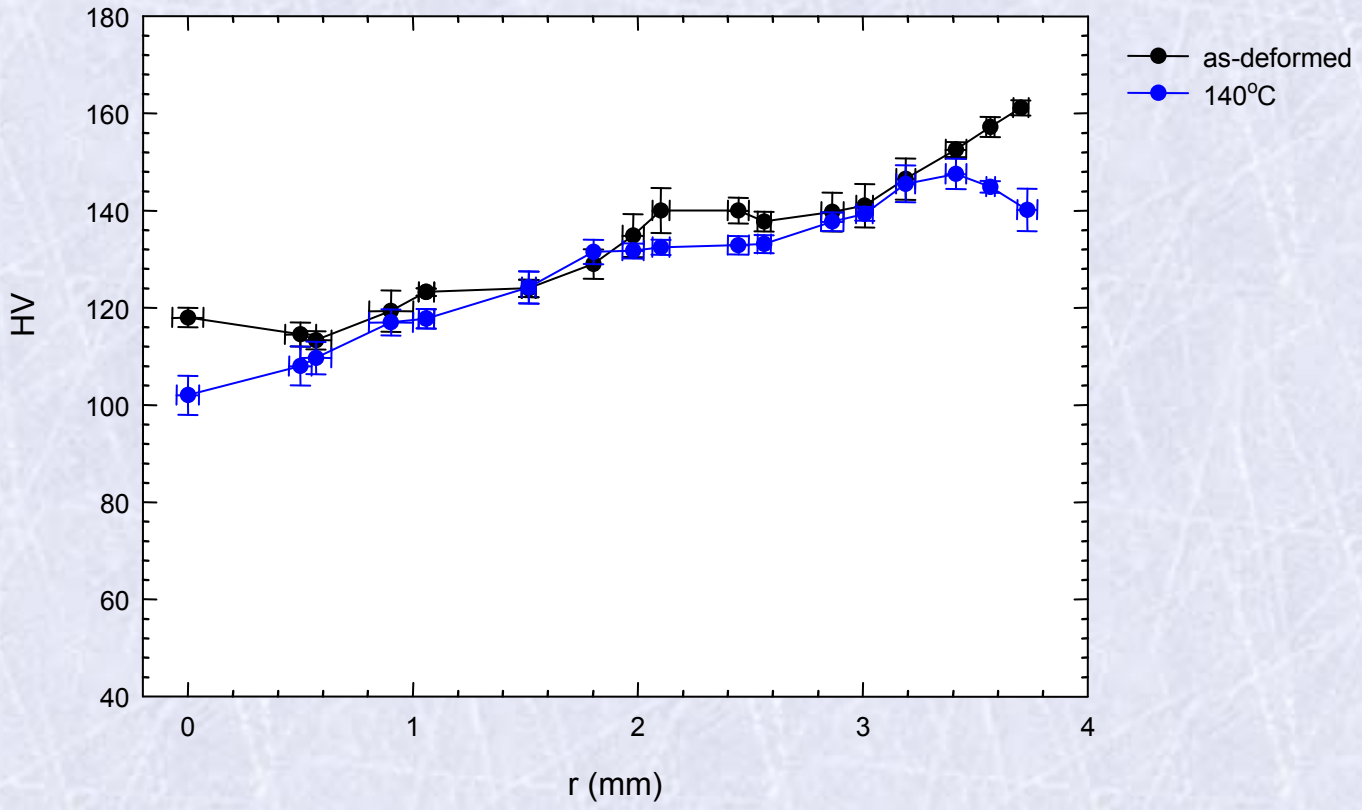

Thermal stability of UFG structure – HV mapping

- HPT deformed Cu, p = 6 GPa, N = 2
- isochronnal annealing 20°C/20 min
- radial dependence of microhardness

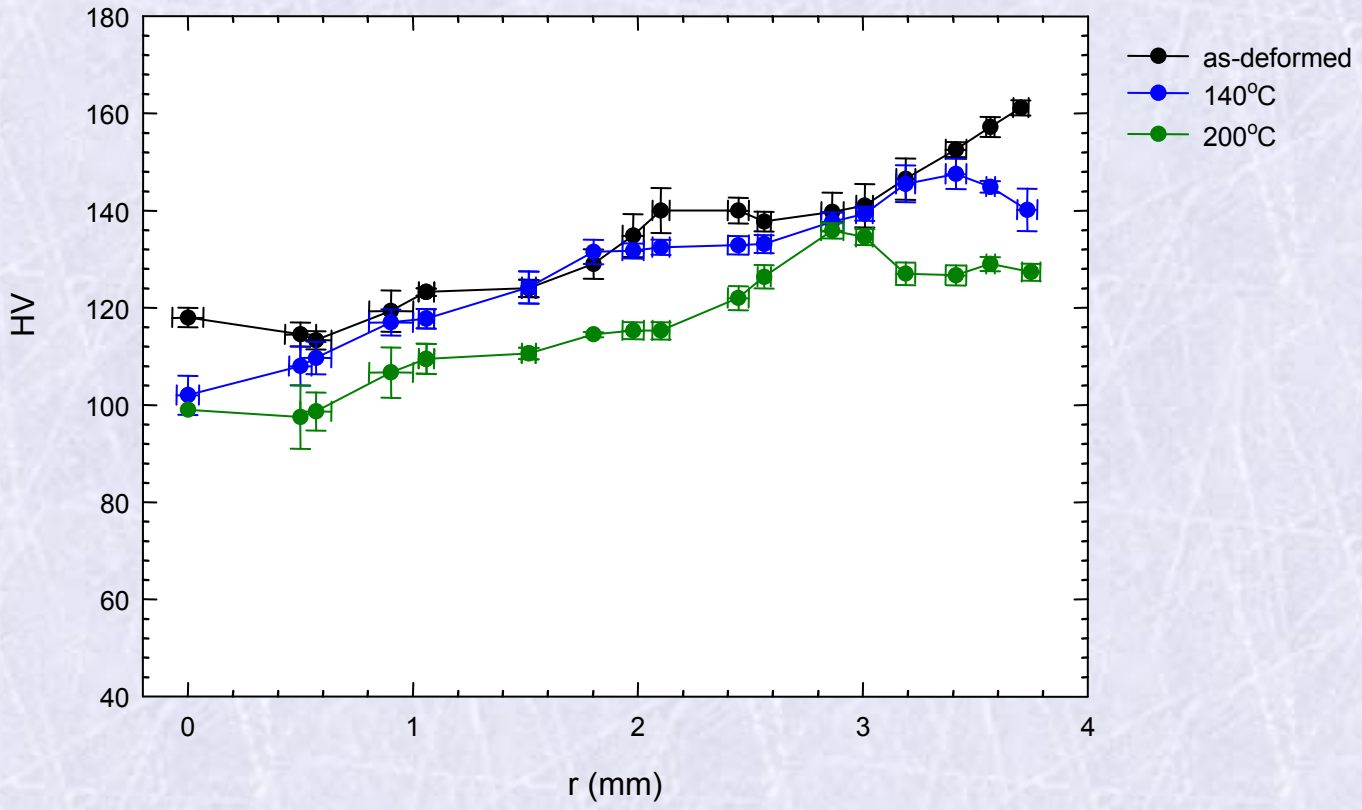

Thermal stability of UFG structure – HV mapping

- HPT deformed Cu, p = 6 GPa, N = 2
- isochronnal annealing 20°C/20 min
- radial dependence of microhardness

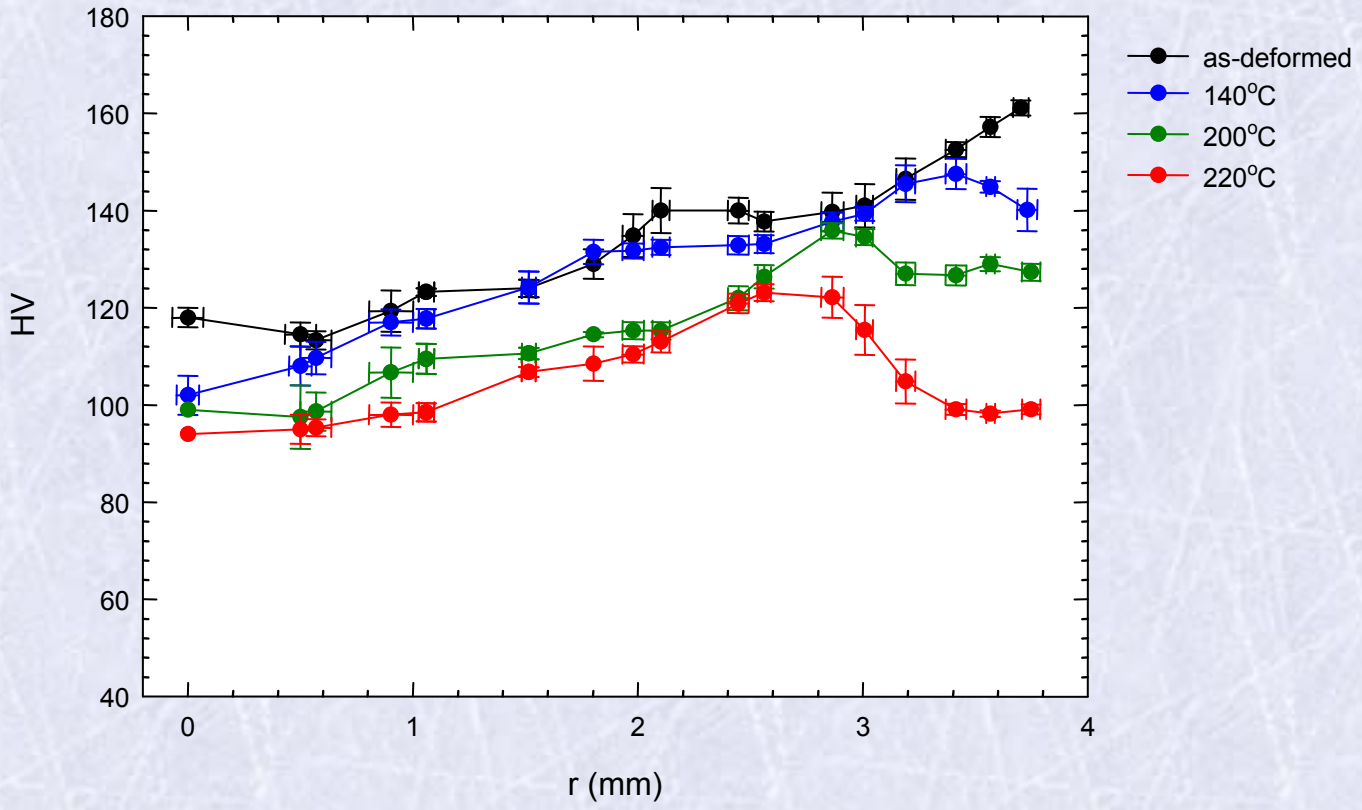

Thermal stability of UFG structure – HV mapping

- HPT deformed Cu, p = 6 GPa, N = 2
- isochronnal annealing 20°C/20 min
- radial dependence of microhardness

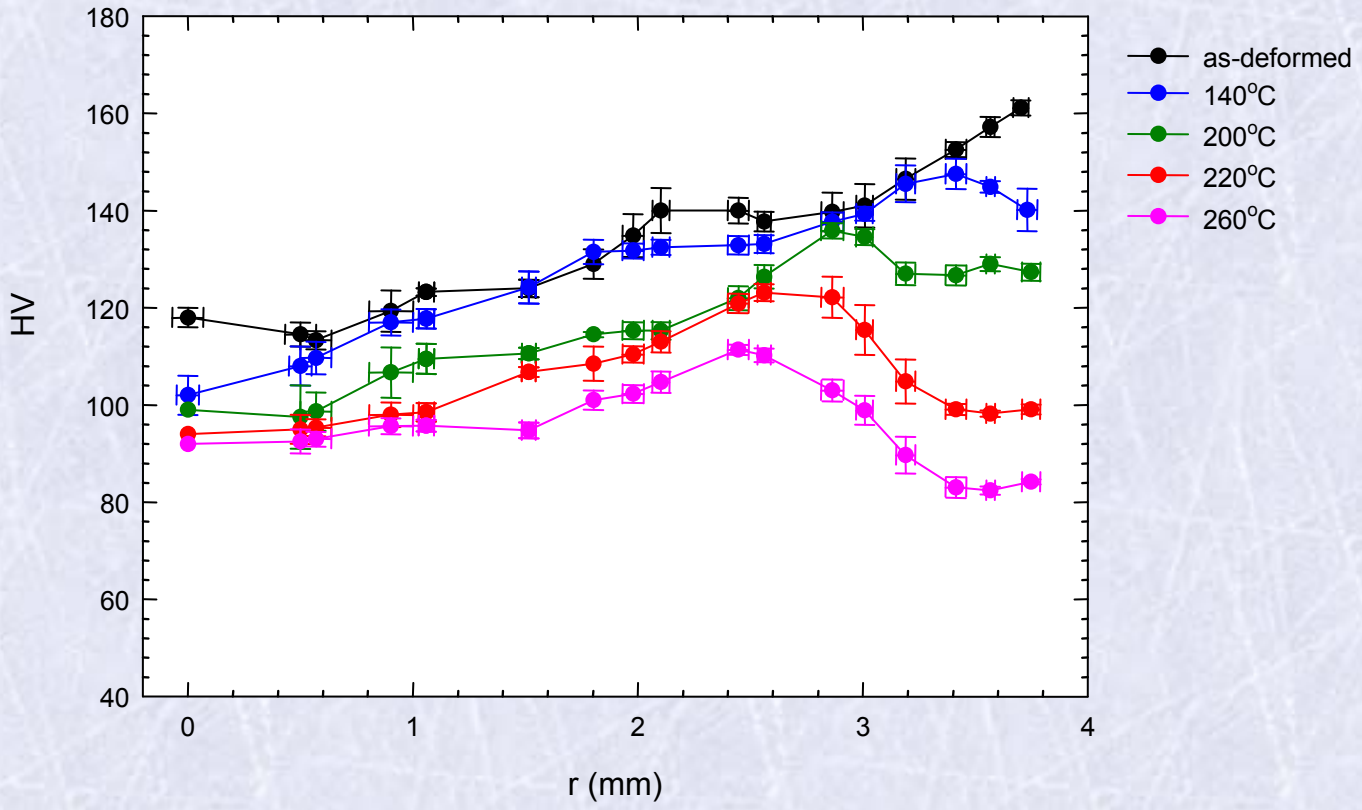

Thermal stability of UFG structure – HV mapping

- HPT deformed Cu, p = 6 GPa, N = 2
- isochronnal annealing 20°C/20 min
- radial dependence of microhardness

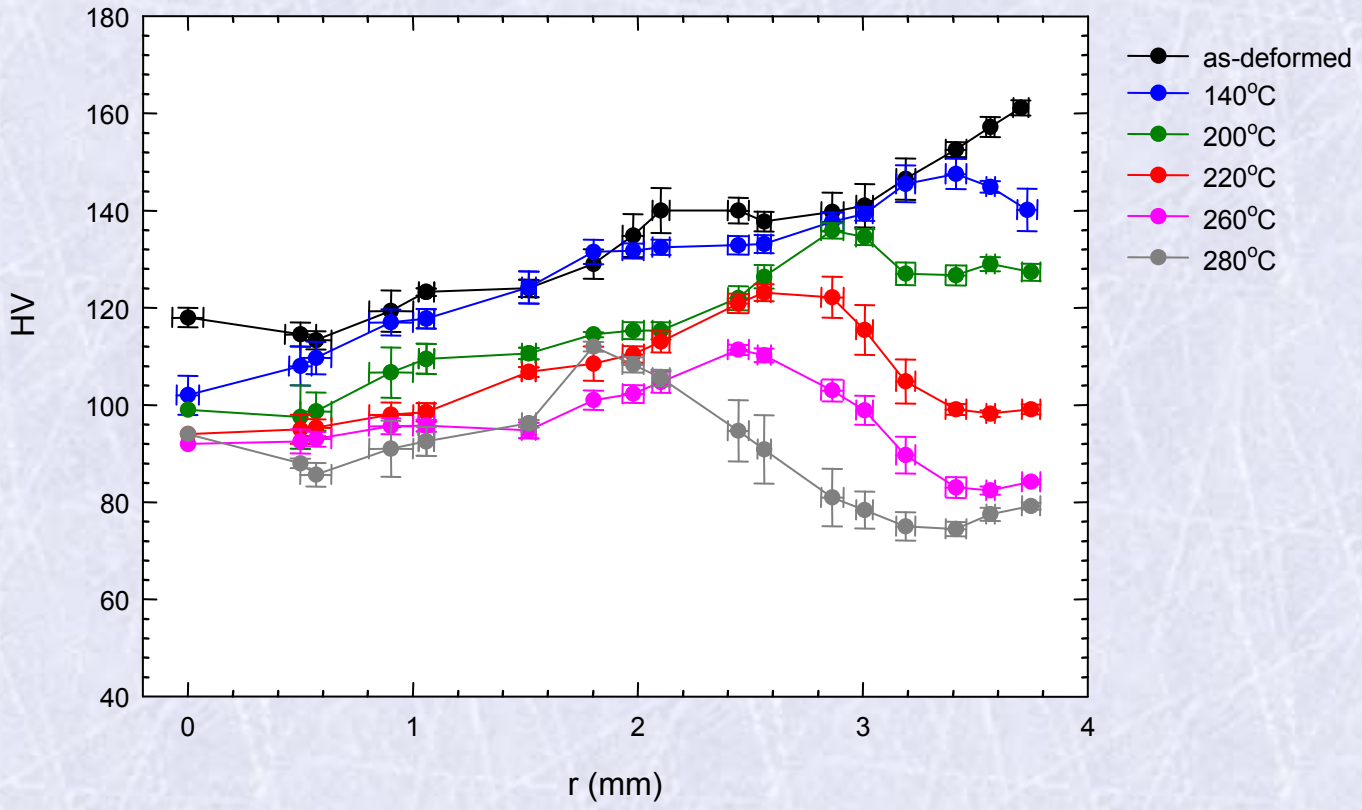

Thermal stability of UFG structure – HV mapping

- HPT deformed Cu, p = 6 GPa, N = 2
- isochronnal annealing 20°C/20 min
- radial dependence of microhardness

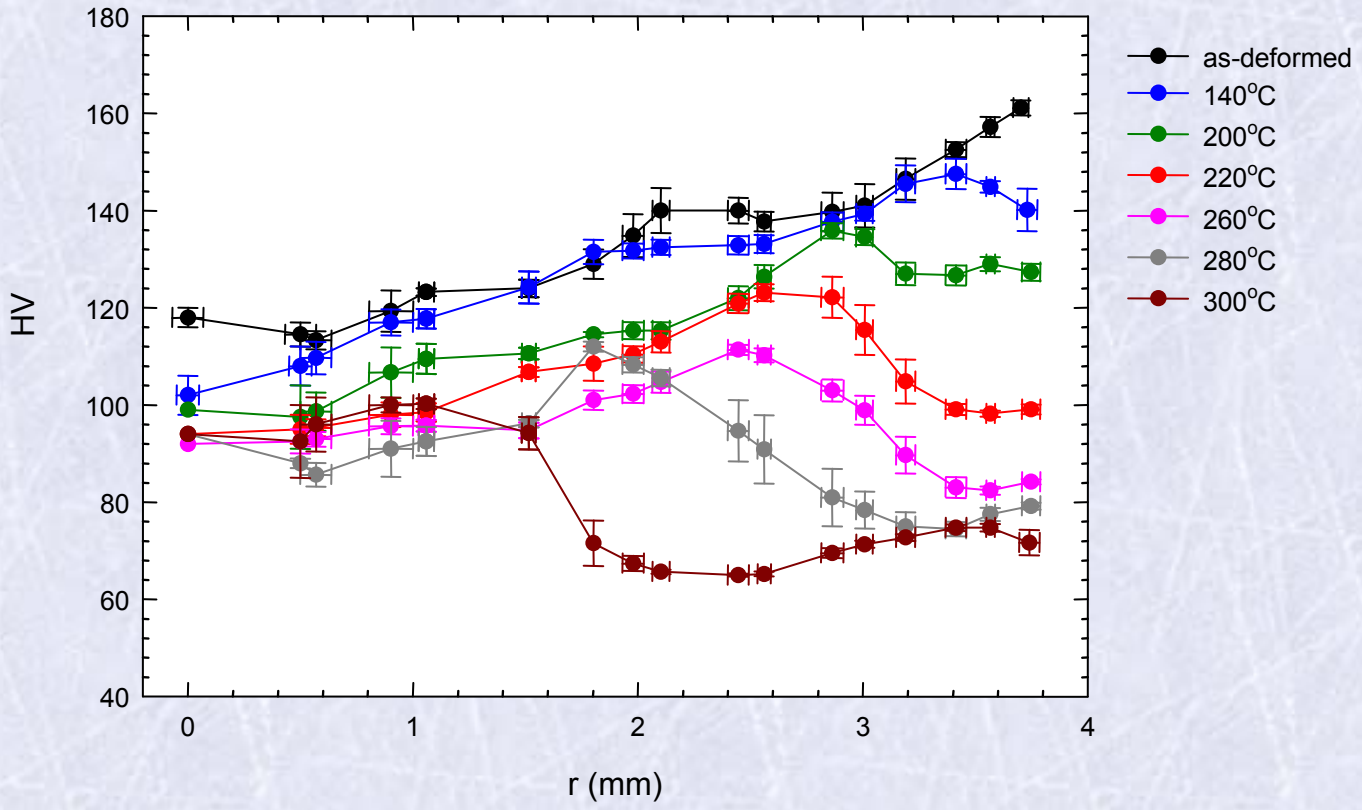

Thermal stability of UFG structure – HV mapping

- HPT deformed Cu, p = 6 GPa, N = 2
- isochronnal annealing 20°C/20 min
- radial dependence of microhardness

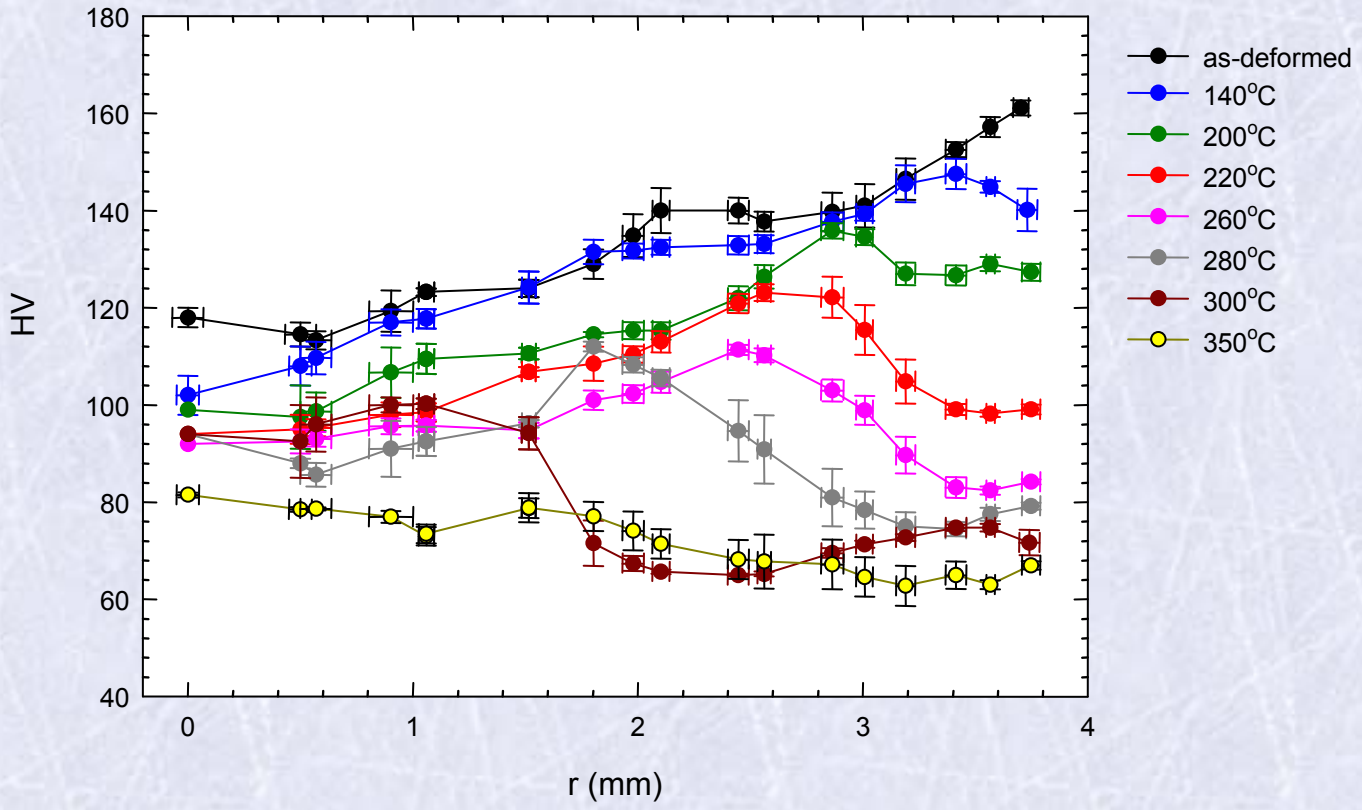

Thermal stability of UFG structure – HV mapping

- HPT deformed Cu, p = 6 GPa, N = 2
- isochronnal annealing 20°C/20 min
- recovery of UFG structure starts at the periphery → higher stored deformation energy

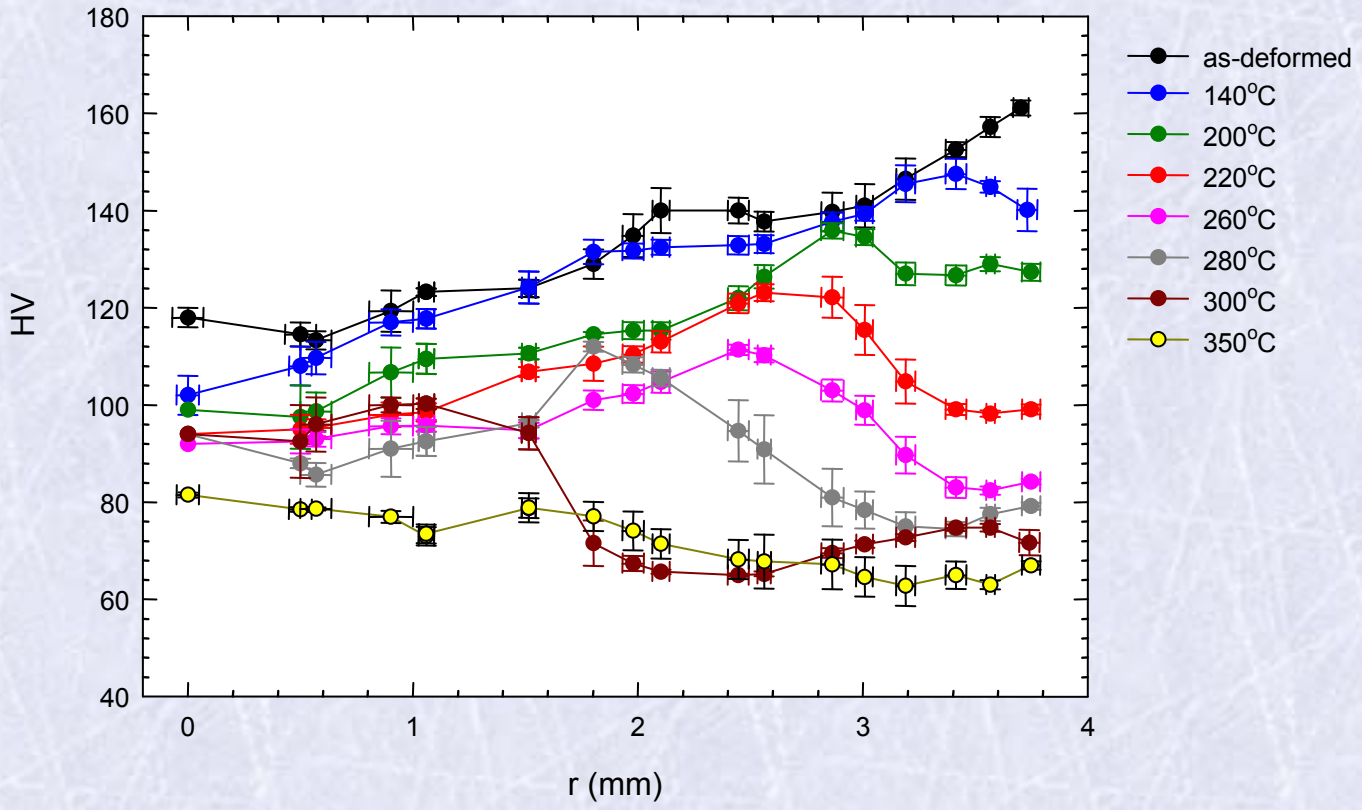

Thermal stability of UFG structure – HV mapping

- HPT deformed Cu, p = 6 GPa, N = 2
- isochronnal annealing 20°C/20 min
- averaged hardness

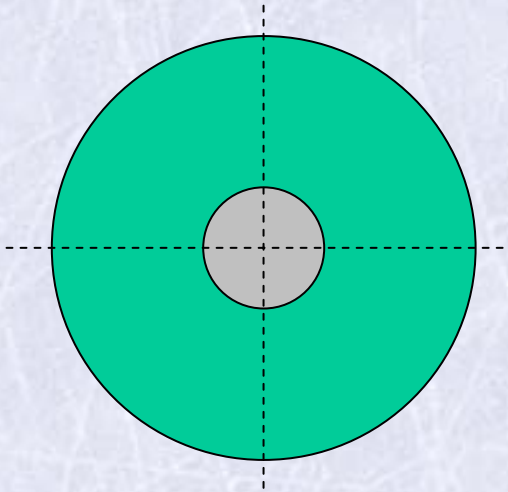

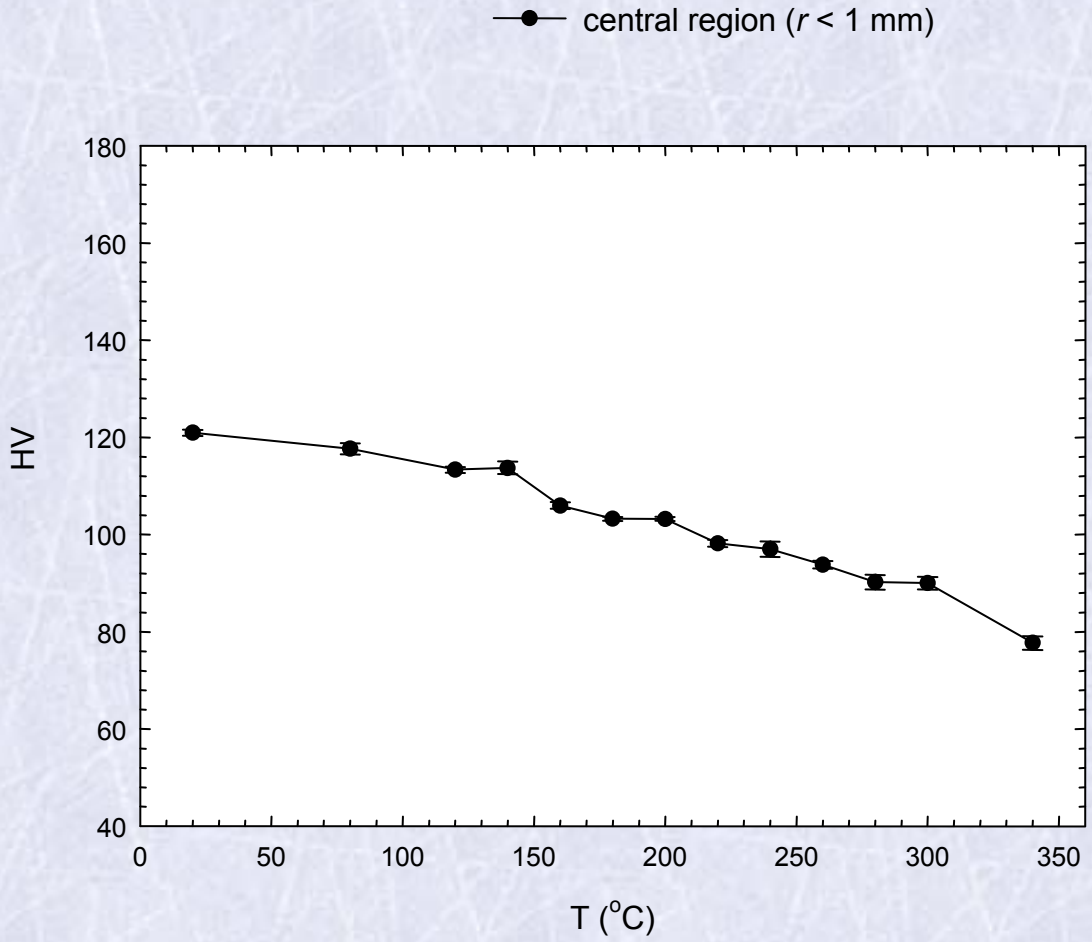

Thermal stability of UFG structure – HV mapping

- HPT deformed Cu, p = 6 GPa, N = 2
- isochronnal annealing 20°C/20 min
- averaged hardness

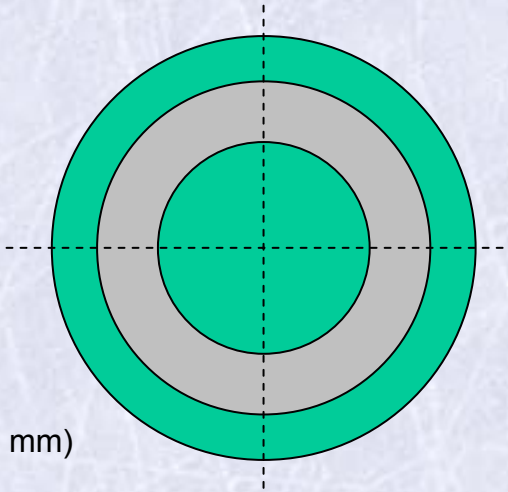

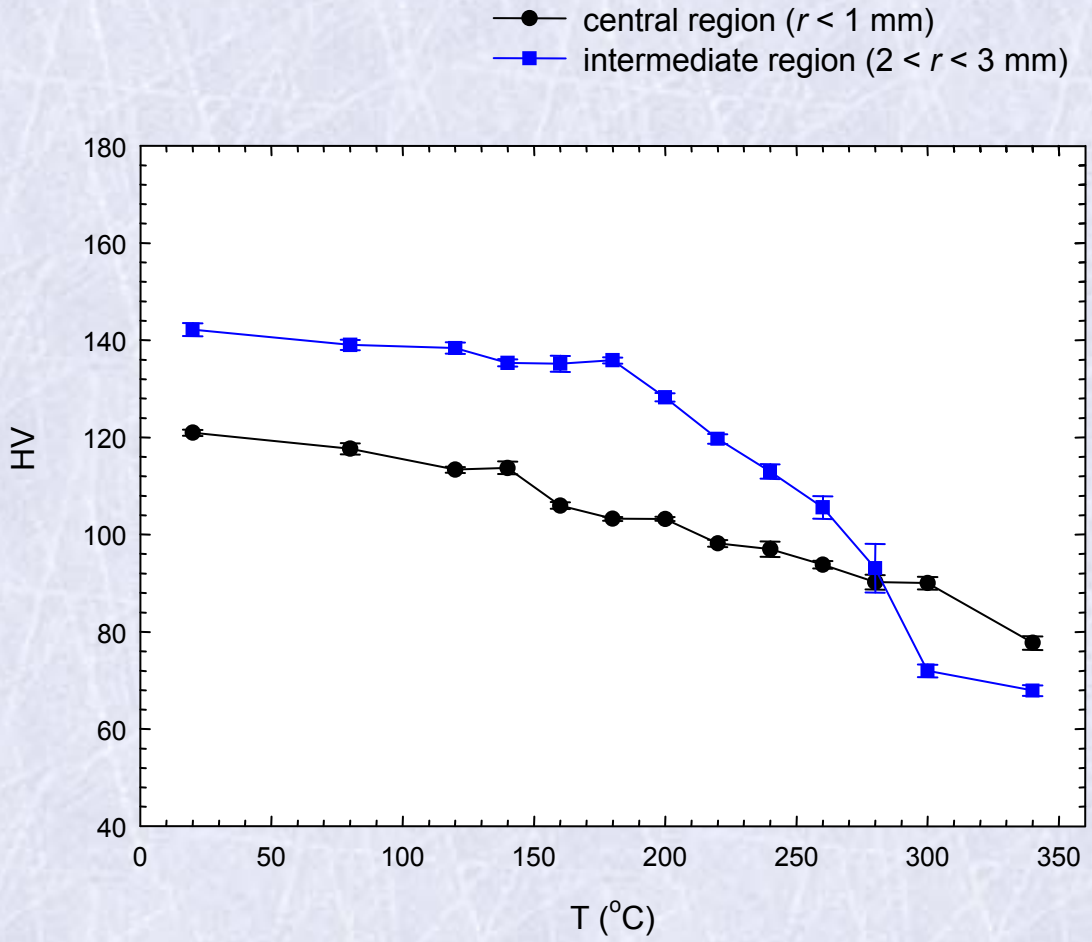

Thermal stability of UFG structure – HV mapping

- HPT deformed Cu, p = 6 GPa, N = 2
- isochronnal annealing 20°C/20 min
- averaged hardness

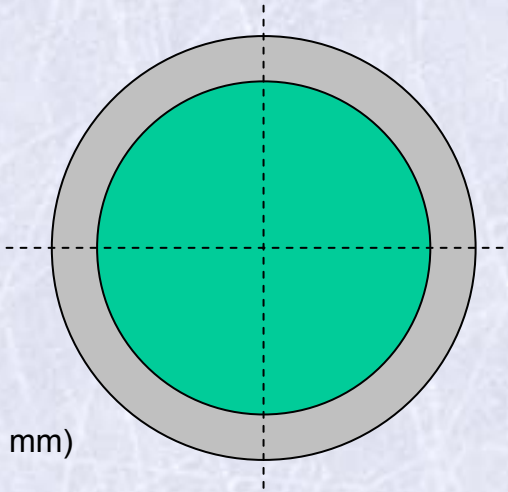

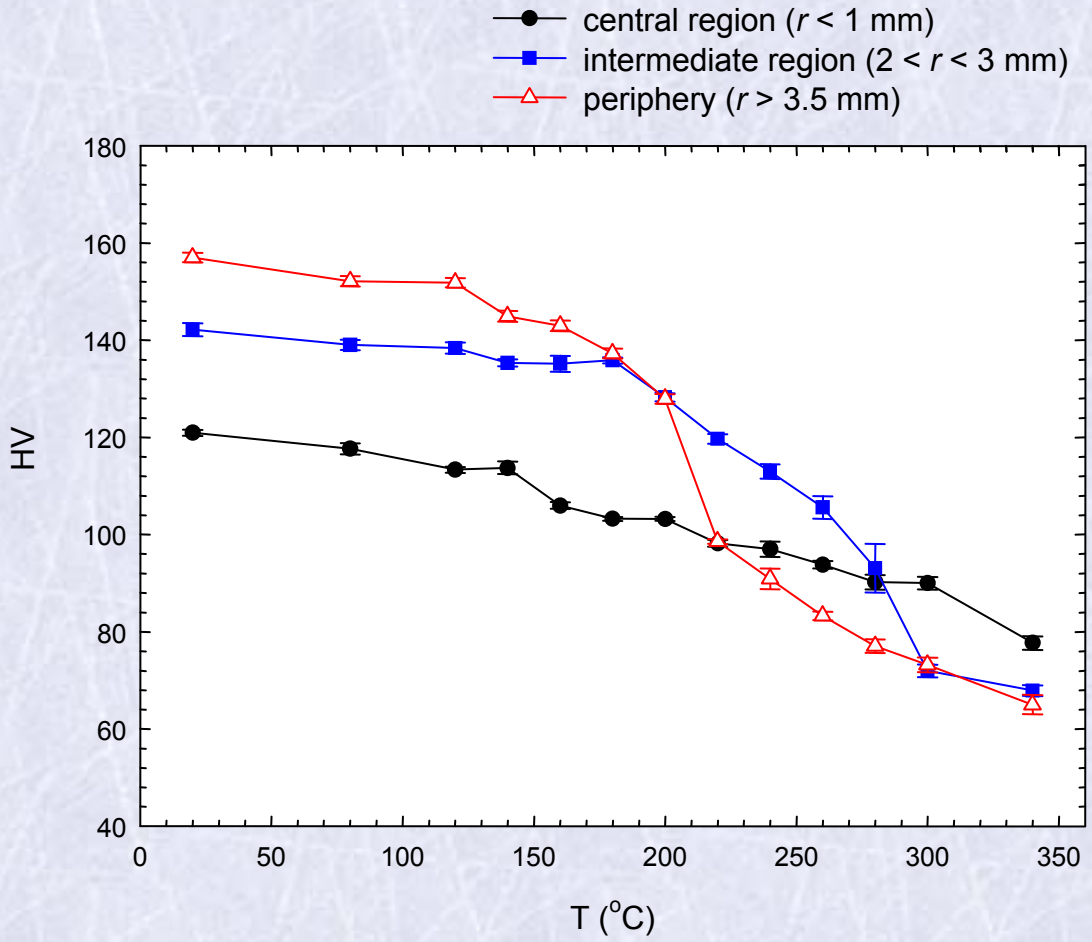

Thermal stability of UFG structure – *S* parameter

UFG Cu, HPT deformed, p = 6 GPa, N = 2

- recovery of UFG structure
  - annealing of vacancy clusters
  - recovery of dislocations
- recovery starts at the periphery

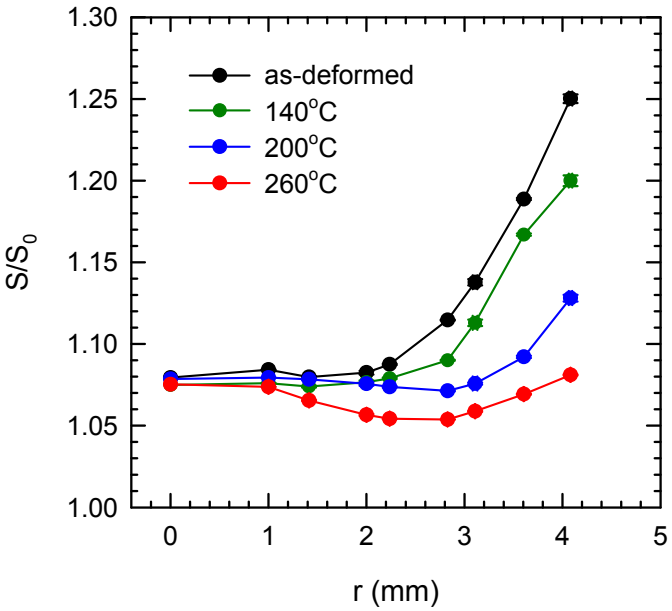

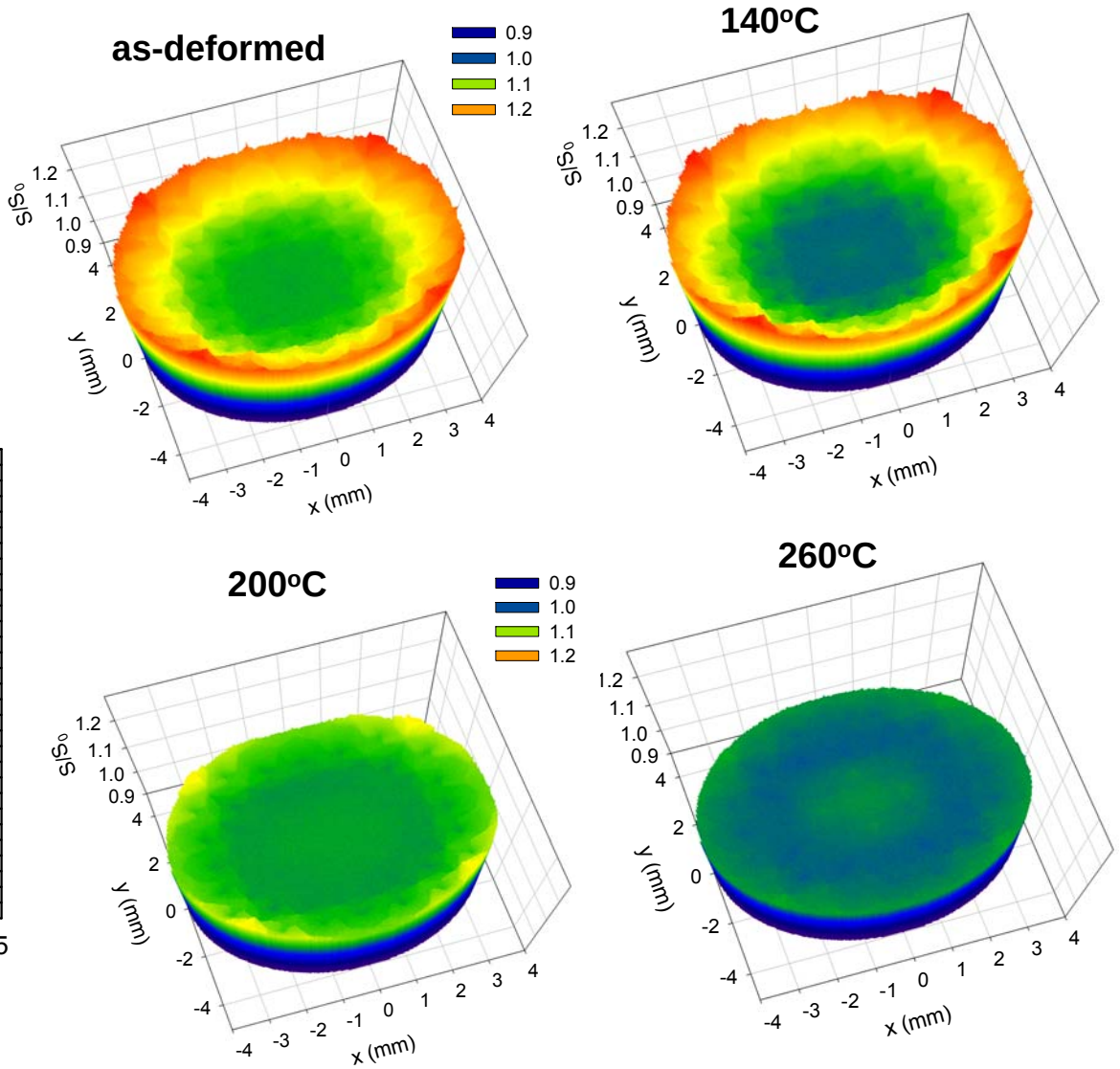

Thermal stability of UFG structure – LT mapping

- HPT deformed Cu, p = 6 GPa, N = 2
- isochronnal annealing 20°C/20 min
- recovery of vacancy clusters starts at the periphery
- free positron component appears firstly at the periphery (200°C)

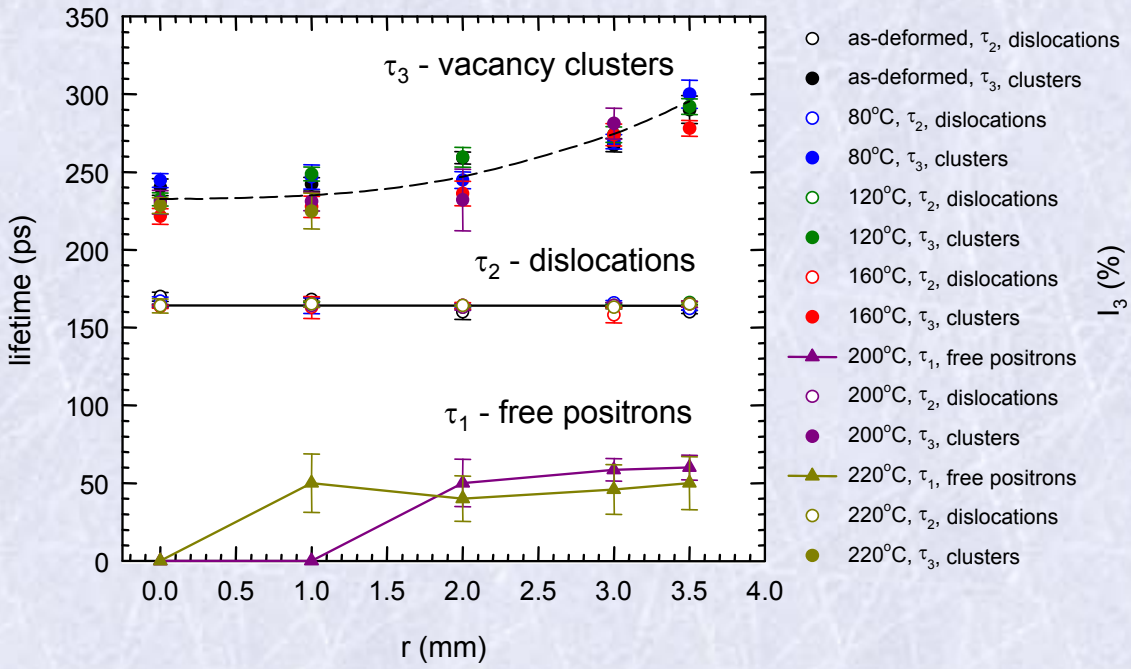

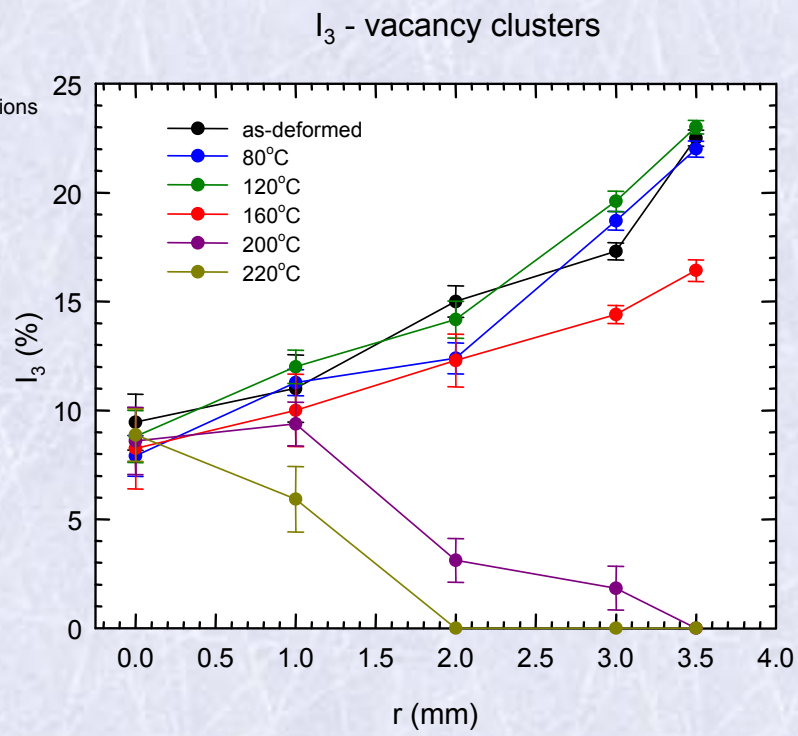

Conclusions

- Severe plastic deformation introduces dislocations and vacancies which subsequently agglomerate and form small vacancy clusters
- Size distribution of vacancy clusters was determined. In UFG Cu vacancy clusters consist of 4-6 vacancies.
- Size of vacancy clusters increases with the strain rate due to higher production rate of vacancies → size of vacancy clusters in HPT-deformed sample increases from center towards periphery
- Spatial distribution of defects was maped by microhardness and *S*-parameter
  - microhardness is sensitive to dislocation density and grain size
  - S-parameter is influenced by dislocations and vacancy clusters
- Recovery of UFG structure starts at the periphery of HPT-deformed sample due to higher stored deformation energy